PhD Thesis

Effects of Confinement on Conventional Spin Problems

- Spin-orbit Coupling in Two-Dimensional Systems
- State Transfer in Spin Chains

Oleksandr Marchukov

Department of Physics and Astronomy

Aarhus University, Denmark

2015

Oleksandr Marchukov
Department of Physics and Astronomy
Aarhus University
Ny Munkegade, Bldg. 1520
8000 Aarhus C
Denmark
E-mail: ovm@phys.au.dk

This dissertation has been submitted to the Faculty of Science and Technology at Aarhus University, Denmark, in partial fulfillment of the requirements for the PhD degree in physics. The work presented has been performed in the period from September 2012 to August 2015 under the supervision of Dmitri V. Fedorov, Aksel S. Jensen and Nikolaj T. Zinner. The work was carried out at the Department of Physics and Astronomy in Aarhus.

Summary

In recent years quantum simulations in cold-atom set-ups has attracted a lot of interest both from experimental and theoretical research groups around the world. Unprecedented level of control over physical systems allowed one to investigate rather peculiar models, such as artificial gauge fields, Hubbard model, etc., which are nevertheless used to describe physical phenomena in various fields, such as condensed matter physics, nuclear physics, etc. This dissertation discusses the effects of the external confinement on some conventional spin problems. It consists of two parts: In the first part the effects of spin-orbit coupling on particles trapped in a two-dimensional harmonic oscillator are considered. The influences of the deformation of the trap, interparticle interaction and external magnetic field are analyzed. The statistical analysis of the single-particle energy spectrum and its relation to the quantum signatures of chaos are discussed. The second part of the dissertation is concerned with quantum state transfer in one-dimensional spin chains. The properties required to achieve conditional state transfer, i.e. “allowing” or “blocking” of state transfer depending on the parameters of the spin chain, are discussed.

Resumé

I de seneste år er kvante simuleringer i opstillinger med kolde atomer blevet et felt som tiltrækker sig meget interesse både fra eksperimentelle og teoretiske forskningsgrupper rundt om i verden. En hidtil uset grad af kontrol over sådanne fysiske systemer gør det i dag muligt at undersøge yderst specielle modeller, set i forhold til et konventionelt synspunkt, men på trods af dette er disse modeller brugt til at beskrive fysiske fænomener i en række felter så som faststof fysik, kerne fysik, osv. Denne afhandling diskuterer hvilke effekter der opstår når man påfører en ekstern begrænsning på almindelige spin systemer. Afhandlingen består af to dele; i den første del undersøges effekten af spin-bane koblingen på partikler fanget i en to-dimensional harmonisk oscillator. Det analyseres hvordan deformation af fælden, vekselvirkning mellem de enkelte partikler og eksterne magnetfelter påvirker systemet. Den statistiske analyse af enkelt-partikel energispektret og hvordan dette relaterer sig i forhold til kvantemekanisk kaos diskuteres. Den anden del af afhandlingen omhandler kvantetilstandes forandringer i en én-dimensional spinkæde. Egenskaberne som kræves for at opnå en betinget overgang af kvantetilstandene, dvs. "tilladte" eller "forbudte" overgange som afhænger af spinkædens parametre, diskuteres ligeledes.

Contents

Preface and Acknowledgments

This thesis concludes the three years of my PhD education at the Department of Physics and Astronomy at Aarhus University.

First of all, I want to thank people without whom this project would not be possible, my supervisors Dmitri Fedorov, Aksel Jensen, and Nikolaj Zinner. Their guidance and support helped me to keep going. They showed me the world of real physics and I am forever grateful for that.

Also I would like to mention all the people I was working with during these three years, who become not just colleagues but friends. They are Filipe Bellotti, Amin Dehkharghani, Hans Fynbo, Dennis Hove, Alan Howard, Oliver Kirsebom, Jakob Knorborg, Gunvor Koldste, Kasper Laursen, Morten Lund, Michael Munch, Jonas Refsgaard, Karsten Riisager, and Artem Volosniev. Among them I want specifically mention Morten and Amin. Morten was kind enough to help me with the translation of the Abstract and Amin read parts of the dissertation and gave valuable comments. Both of them were very supportive during my writing, especially in July :)

I would like to express my deepest gratitude to Filipe and Artem, who read most of the thesis and helped a lot in my struggle with English language.

Last but not least, I would like to thank my parents and all of my friends back home, in Ukraine. You are always in my thoughts.

List of Publications

This thesis is based on the following papers

- O. V. Marchukov, A. G. Volosniev, D. V. Fedorov, A. S. Jensen, and N. T. Zinner, *"Spectral Gaps of Spin-orbit Coupled Particles in Deformed Traps"* , J. Phys. B: At. Mol. Opt. Phys. **46**, 134012 (2013).
- O. V. Marchukov, A. G. Volosniev, D. V. Fedorov, A. S. Jensen, and N. T. Zinner, *"Spin-Orbit Coupling in Deformed Harmonic Traps"*, Few-Body Systems Volume 55, Issue 8-10, pp 1045-1047 (Proceedings of the 22nd European Conference on Few-Body Problems in Physics, Kraków 2013)
- O. V. Marchukov, A. G. Volosniev, D. V. Fedorov, A. S. Jensen, and N. T. Zinner, *"Statistical properties of spectra in harmonically trapped spin-orbit coupled systems"* , J. Phys. B: At. Mol. Opt. Phys. **47**, 195303 (2014).
- O. V. Marchukov, D. V. Fedorov, A. S. Jensen, A. G. Volosniev, and N. T. Zinner, "*Repulsively interacting fermions in a two-dimensional deformed trap with spin-orbit coupling*" , Eur. Phys. J. D **69** 3 73 (2015).
- O. V. Marchukov, E. M. Eriksen, J. M. Midtgaard, A. A. S. Kalaee, D. V. Fedorov, A. S. Jensen, and N. T. Zinner, "*Computation of local exchange coefficients in strongly interacting one-dimensional few-body systems - local density approximation and exact results*" , submitted for peer-review to European Physical Journal D, *e-print*: http://arxiv.org/abs/1508.07164

CHAPTER 1

Introduction and Thesis Outline

1.1 Introduction

Despite very rapid progress in physical sciences for the past hundred years or so we still know very little of the world we live in. But it only encourages us more and more to seek new answers. In our search we create better and more sophisticated tools: models, state-of-the-art experiments, computational methods, etc., in order to learn the truth about the Universe. And with every new secret unveiled we are astonished by how vast and complex the world is, but also how beautiful it is.

One of the most impressive tools in our toolbox is the systems of ultracold atomic and molecular gases [Bloch 2008]. The achievement of Bose-Einstein condensation (BEC) in dilute gases [Anderson 1995,Bradley 1995,Davis 1995] was the first great success and after that the exploration of such systems was increasing rapidly. Just few years after the achievement of BEC, atomic degenerate Fermi gases were achieved [DeMarco 1999,Schreck 2001,Truscott 2001].

This progress led to the understanding that Feynman's idea of quantum simulators can be realized in these systems [Bloch 2012, Lewenstein 2012]. Indeed, quite a few phenomena known from solid state or condensed matter physics were observed in the cold atomic and molecular gases: the crossover from weakly coupled Bardeen-Cooper-Schrieffer (BCS) pairs to BEC of tightly bounds pairs [Chin 2004, Zwierlein 2005], quantum phase transitions from a superfluid to a Mott insulator [Greiner 2002] and many others.

These systems provide unprecedented level of manipulation, control, purity and detection [Lewenstein 2012]. For instance, by varying the parameters of optical lattices an experimentalist can control the population, density and purity of the gas cloud [Bloch 2008]. Also, the powerful tool of Feshbach

resonances provides the control over the interparticle interaction between the atoms [**?**].

The cold atomic gases trapped in external potentials become an exceptional tool to mimic and explore the physics of low-dimensional systems [Bloch 2008, Lewenstein 2012]. The strong optical lattices are able to block the atoms' motional degrees of freedom in one or more directions, such that the motion of atoms is confined either to a plane or even to just one direction. Thus, it is possible to simulate quasi-one-dimensional and quasi-two-dimensional systems in the cold atomic set-ups. In the following we dismiss the prefix *quasi* and talk about one-dimensional (1D) and two-dimensional (2D) systems.

This dissertation can be divided into two parts: spin-orbit coupling in 2D traps and quantum state transfer in 1D spin chains. In chapters 2 and 6 we introduce both systems in more details, discuss their properties and provide the relevant references to available literature.

1.2 Thesis Outline

Chapter 2 we present the spin-orbit interaction, discuss some of the properties and briefly describe how the spin-orbit coupling is realized in cold-atom systems.

In Chapter 3 we consider a particle trapped in a two-dimensional harmonic potential with a spin-orbit coupling and an external Zeeman field. We solve the corresponding Schrödiner equation and analyze the behavior of the single-particle energy levels, which depends on the deformation of the trap and the strengths of the spin-orbit coupling and the Zeeman field. The results are presented in the paper [Marchukov 2013].

Chapter 4 considers the effects of the zero-range interparticle interaction for N particles in the same set-up as in Chapter 3. We implement the Hartree-Fock self-consistent method to include the effects of the interaction and investigate their influence on the single-particle energy levels. These results are presented

in the paper [Marchukov 2014b, Marchukov 2015b].

In Chapter 5 we show that the single-particle spectra obtained in the previous chapters may reveal the so-called quantum signatures of chaos after a statistical procedure named *unfolding of the spectrum*. This signifies that the discussed systems might be used in the investigation of the quantum irregular dynamics. The results are presented in the paper [Marchukov 2014a].

Chapter 6 serves as an introduction to the state transfer problem. We briefly describe the realization of a spin chain in the strongly-interacting atom set-ups.

In Chapter 7 we consider quantum state transfer in spin chains consisting of three, four and five particles. We show that if the edges of the spin chain are interacting weakly comparing to the middle of the chain then the fidelity of state transfer can be controlled and even “turned on” and “off” for specific values of the external magnetic field.

Chapter 8 concludes the thesis with the summary of the results presented in the previous chapters.

CHAPTER 2

Spin-orbit coupling. Introduction

As was said in Chapter 1 this thesis consists of two parts: the effects of spin-orbit coupling for particles trapped in two-dimensional (2D) potentials and state transfer in one-dimensional (1D) spin chains. In this Chapter we introduce the former part, discuss some of its properties and briefly describe the experimental realizations in cold atoms. For further details one should address the comprehensive reviews by J. Dalibard *et al.* [Dalibard 2011], H. Zhai [Zhai 2011], and V. Galitski and I. Spielman [Galitski 2013].

The name 'spin-orbit coupling' refers to many phenomena from different fields of physics: from the fine and hyperfine splitting in atomic and nuclear physics [Landau 1981, Weinberg 2013, Siemens 1993], to topological insulators and quantum spin Hall effect in condensed mater physics [Bernevig 2013, Hasan 2010] or Rashba [Rashba 1960, Bychkov 1984] and Dresselhaus [Dresselhaus 1955] spin-orbit interactions in semiconductors. The general feature of all these phenomena is the interplay between particle's internal degree of freedom and its motion in coordinate space.

Nowadays many experimental groups are aiming to create spin-orbit coupled systems with ultracold atomic set-ups. The first step in that direction was done by Spielman's group [Lin 2011]. They engineered a spin-orbit coupling in a neutral Bose-Einstein condensate by dressing two atomic hyperfine states with a pair of propagating lasers. After that, in 2012, spin-orbit coupled Fermi gases were produced
by two groups [Cheuk 2012, Wang 2012]. To the best of our knowledge only a very specific kind of the spin-orbit interactions (the equal Rashba and Dresselhaus spin-orbit coupling) are realized so far. It is mainly due to techni-

cal difficulties and there is little doubt that the other spin-orbit couplings will be realized in the nearest future. Note several promising proposals [Goldman 2014, Liu 2014, Huang 2015] coming from theoretical and experimental research groups.

2.1 Hamiltonian of a spin-orbit coupled particle

One usually first encounters the spin-orbit coupling terms in atomic physics, when the relativistic corrections linear in spin are included in the Hamiltonian [Landau 1981, Weinberg 2013, Winkler 2003] of electrons in an atom. The corresponding correction can be written as

$$\hat{H}_{SO} = -\frac{\hbar}{4m_e^2c^2}\hat{\boldsymbol{\sigma}} \cdot \boldsymbol{p} \times (\nabla V_0), \tag{2.1}$$

where m_e is the mass of an electron, $\boldsymbol{p}$ is the three-dimensional momentum operator, $\hat{\boldsymbol{\sigma}} = (\hat{\sigma}_x, \hat{\sigma}_y, \hat{\sigma}_z)$ is the vector of the Pauli matrices, and V_0 is the Coulomb potential of the atomic core. Here and in the following the *hat* over operators indicates that they act as 2×2 matrices on two-component spinors. We see that in Eq. (2.1) the spin degree of freedom is coupled to the momentum of the particle giving the name to the interaction. However, the terms of this kind are ubiquitous in different areas of physics and take different forms in accordance to the underlying physical processes. Since in this work we focus on 2D, we will consider the two most famous expressions for spin-orbit coupling: the Rashba and Dresselhaus spin-orbit interaction terms.

Both terms originate in the realm of semiconductor physics and both are due to the breaking of the inversion symmetry in crystals [Winkler 2003]. The Rashba spin-orbit interaction is due to the structure inversion asymmetry [Rashba 1960] and can be expressed as

$$\hat{V}_R = \alpha_R(\hat{\sigma}_x p_y - \hat{\sigma}_y p_x), \tag{2.2}$$

where α_R is the strength of Rashba spin-orbit coupling. The Dresselhaus term is due to the bulk inversion asymmetry [Dresselhaus 1955] in 2D semiconductor

crystals and reads

$$\hat{V}_D = \alpha_D(\hat{\sigma}_x p_y + \hat{\sigma}_y p_x), \tag{2.3}$$

where α_D is the strength of Dresselhaus spin-orbit coupling.

These two terms play an important role in the fast-developing field of quantum simulations in ultracold atoms. The combination of these terms with the same strength i.e., $\hat{V}_{SOC} = \alpha\hat{\sigma}_x p_y$, where $\alpha = 2\alpha_R = 2\alpha_D$, is the only form of spin-orbit interaction realized today in ultracold atoms. Later on we describe in a few words the scheme of this realization.

In this work we mostly focus on the Rashba spin-orbit coupling, although we consider some systems of both the Rashba and Dresselhaus terms in Chapter 3. We discuss some properties of the Rashba spin-orbit coupling in the next Section.

2.2 Properties of spin-orbit interaction

Let us consider a particle moving freely in two dimensions with the spin-orbit interaction in the Rashba form. The Hamiltonian of such a particle reads

$$\hat{H} = \frac{\boldsymbol{p}^2}{2m} + \alpha_R\left(\hat{\sigma}_x p_y - \hat{\sigma}_y p_x\right), \tag{2.4}$$

where $\boldsymbol{p} = (p_x, p_y)$ is the 2D momentum operator, m is the mass of the particle. The energy dispersion law for this Hamiltonian is

$$E_\pm = \frac{p^2}{2m} \pm \alpha_R p, \tag{2.5}$$

where $p = \sqrt{p_x^2 + p_y^2}$ is the length of $\boldsymbol{p}$, i.e., $|\boldsymbol{p}| = p$. The index $\pm$ corresponds to different helicity states, i.e. the spin-projection being either parallel (+) or antiparallel (−) to the direction of the momentum.

The energy dispersion can be seen in Fig. 2.1. This dispersion law was observed experimentally by Zwierlein's group [Cheuk 2012] in atomic Fermi gases for the equal in magnitude Rashba and Dresselhaus spin-orbit couplings.

Clearly, the presence of a trapping potential makes the problem more com-

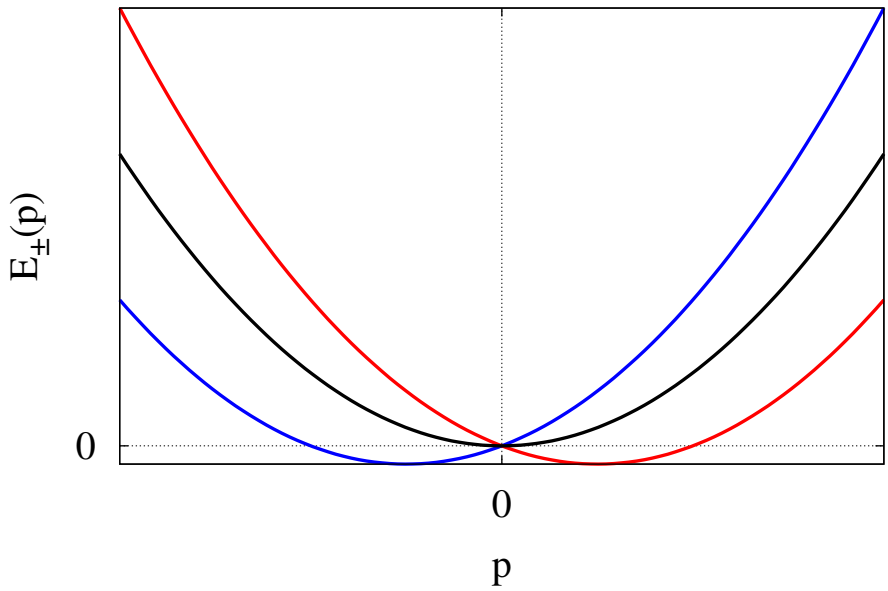

Figure 2.1: The energy dispersion of a free particle with the Rashba spin-orbit coupling. The *black* curve shows the dispersion of a free particle without the spin-orbit coupling, the *blue* curve corresponds to the E_+ state and the *red* curve corresponds to the E_-, see text for details.

plicated. In this thesis we focus on spin-orbit coupled systems trapped in a 2D harmonic potential. We consider non-equal transverse oscillator frequencies, i.e. we work with deformed, non-cylindrical harmonic potentials. The interplay between the deformation of the trap and the spin-orbit coupling causes a distinctive energy levels structure. We address this interplay in the next chapters but now let us take a look at the symmetry properties of the Rashba and Dresselhaus spin-orbit coupling terms.

2.2.1 Rotational symmetry and parity

Both the Rashba and Dresselhaus spin-orbit terms commute [Hu 2012b] with the operator $\hat{\Pi} \equiv \hat{\sigma}_z P$, where P is the parity operator and $\hat{\sigma}_z$ is the third Pauli matrix. Indeed, due to the anticommutation relations of the Pauli matrices,

$\{\hat{\sigma}_i, \hat{\sigma}_j\} = 2\delta_{ij}\hat{I}$, where I is the 2×2 identity matrix, the commutator reads

$$\alpha_{SOC}\left[\hat{\sigma}_z P, (\hat{\sigma}_x p_y \pm \hat{\sigma}_y p_x)\right] = -\alpha_{SOC}\left\{p_y(\hat{\sigma}_z\hat{\sigma}_x + \hat{\sigma}_x\hat{\sigma}_z) \mp p_x(\hat{\sigma}_z\hat{\sigma}_y + \hat{\sigma}_y\hat{\sigma}_z)\right\} = 0, \tag{2.6}$$

where α_{SOC} is generic spin-orbit coupling strength.

Both the Rashba and Dresselhaus spin-orbit terms do not commute with either $\hat{\sigma}_z$ or the orbital angular momentum, L_z. However, they do commute with the operators $L_z + \frac{1}{2}\hat{\sigma}_z$ and $-L_z + \frac{1}{2}\hat{\sigma}_z$, respectively. Indeed,

$$[\pm L_z + \frac{1}{2}\hat{\sigma}_z, \hat{\sigma}_x p_y] = i(\hat{\sigma}_y p_y \mp \hat{\sigma}_x p_x)\ , \tag{2.7}$$

$$[\pm L_z + \frac{1}{2}\hat{\sigma}_z, \hat{\sigma}_y p_x] = i(\pm\hat{\sigma}_y p_y - \hat{\sigma}_x p_x)\ , \tag{2.8}$$

and

$$[L_z + \frac{1}{2}\hat{\sigma}_z, \alpha_R(\hat{\sigma}_x p_y - \hat{\sigma}_y p_x)] = 0\ , \tag{2.9}$$

$$[-L_z + \frac{1}{2}\hat{\sigma}_z, \alpha_D(\hat{\sigma}_x p_y + \hat{\sigma}_y p_x)] = 0\ . \tag{2.10}$$

The "mixed" case with finite α_R and α_D does not have this symmetry.

2.2.2 Time-reversal symmetry. Kramers degeneracy

The spin-orbit coupling terms also commute with the time-reversal operator which for a spin-$\frac{1}{2}$ particle can be written [Sakurai 1994] as $T = i\hat{\sigma}_y K$, where K is the complex conjugation operator. Indeed,

$$\alpha\left[i\hat{\sigma}_y K, (\hat{\sigma}_x p_y \pm \hat{\sigma}_y p_x)\right] = \alpha\left\{-ip_y(\hat{\sigma}_y\hat{\sigma}_x + \hat{\sigma}_x\hat{\sigma}_y) \pm i \mp i\right\} = 0. \tag{2.11}$$

The consequence of this commutation relation is the two-fold degeneracy of the energy levels, due to the Kramers theorem [Landau 1981], which states that the energy levels of a system with half-integer total spin must be two-fold degenerate. Notice, that an external magnetic field lifts this degeneracy.

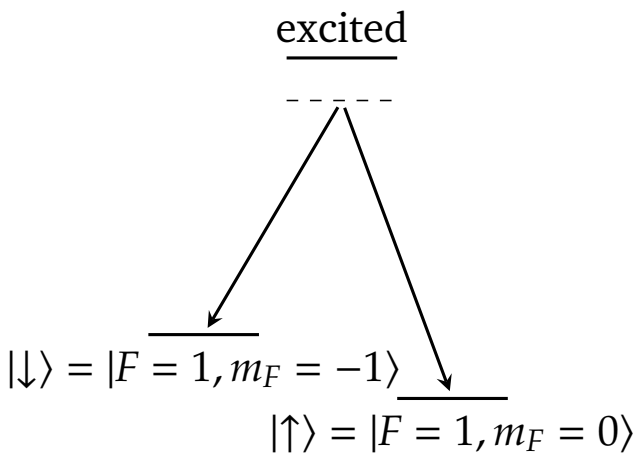

Figure 2.2: A level diagram of spin-orbit coupling experimental realization. The pseudo-spin states $|\uparrow\rangle$ and $|\downarrow\rangle$ are coupled via a pair of counterpropagating Raman lasers through an off-resonant state.

2.3 Realization of spin-orbit coupling in cold atoms

In this Section we briefly discuss how the spin-orbit coupling is realized with cold atoms. For the first time in cold atoms the spin-orbit coupling was demonstrated by Spielman's group [Lin 2011] in a ^{87}Rb Bose-Einstein condensate using Raman lasers which coupled some internal atomic states and momentum. The internal states, dubbed pseudo-spin (or just spin for brevity) states, are selected from the manifold of electron levels of the same total atomic angular momentum, F. Due to the hyperfine splitting the degeneracy of the levels is lifted and states with a different magnetic quantum number, $m_F = 0, \pm 1$ have different energies. In the experiment with ^{87}Rb the states spin-up and spin-down were selected, as $|\uparrow\rangle = |F = 1, m_F = 0\rangle$ and $|\downarrow\rangle = |F = 1, m_F = -1\rangle$. The counterpropagating Raman lasers couple these states with motion of the atom along the direction of the propagation. In Fig. 2.2 we show a schematic level diagram of the process.

The similar scheme was since realized by many groups in both Bose [Aidelsburger 2011, Zhang 2012] and Fermi [Wang 2012, Cheuk 2012, Huang 2015] gases. As was mentioned before this scheme allows one to realize a "one-dimensional" spin-orbit coupling, i.e. the equal in magnitude Rashba and

Dresselhaus terms. However, creating different types of a spin-orbit coupling should be possible by adding more lasers [Galitski 2013,Dalibard 2011,Lin 2011].

The aim of this Section is to give the general idea of the experimental realizations and provide the necessary references for a deeper understanding of the topic. In the next chapters we do not refer to the details of these realizations, keeping in mind, however, that contemporary state-of-the-art experiments are able in principle to provide the data related to our theoretical findings.

CHAPTER 3

A spin-orbit coupled particle in a two-dimensional trap

In this chapter we solve the Schrödinger equation for a particle trapped in a two-dimensional(2D) harmonic trap and subjected to a spin-orbit coupling and the Zeeman field. We discuss the behavior of particle's energy spectrum depending on values of external parameters, such as transverse frequencies of the trapping potential, value of the Zeeman magnetic field, and the spin-orbit coupling strengths. We show that the resulting spectrum has a non-trivial structure with multiple avoided crossings.
The Hamiltonian for the system reads

$$\hat{H} = \left(\frac{{p_x}^2}{2m} + \frac{1}{2}m\omega_x^2 x^2 + \frac{{p_y}^2}{2m} + \frac{1}{2}m\omega_y^2 y^2\right) \otimes \hat{I} + \\ + (\alpha_R + \alpha_D)\hat{\sigma}_x p_y - (\alpha_R - \alpha_D)\hat{\sigma}_y p_x - h\hat{\sigma}_z, \tag{3.1}$$

where $\mathbf{p} = \{p_x, p_y\}$ is a 2D momentum operator, $\mathbf{r} = \{x, y\}$ is a 2D coordinate operator, m is mass of the particle, ω_x and ω_y are the harmonic trap frequencies, which generally are not equal; $\hat{I}$ is the 2×2 identity matrix and $\hat{\sigma}_x$, $\hat{\sigma}_y$, and $\hat{\sigma}_z$ are the 2×2 Pauli matrices; h is the strength of the Zeeman magnetic field which acts in the z-directions. It is common practice to consider spin-orbit coupling in the cold atomic gases as a combination of two terms: Rashba spin-orbit coupling [Rashba 1960] $V_R = \alpha_R(\hat{\sigma}_x p_y - \hat{\sigma}_y p_x)$ and Dresselhaus spin-orbit coupling [Dresselhaus 1955] $V_D = \alpha_D(\hat{\sigma}_x p_y + \hat{\sigma}_y p_x)$, where parameters α_R and α_D are the Rashba and Dresselhaus spin-orbit interaction strengths, correspondingly. One notes that the parameters α_R and α_D possess the units of velocity. Both of the spin-orbit coupling terms originate in the field of semiconductor

physics. As mentioned in chapter 2 the spin-orbit coupling terms conserve the time-reversal symmetry. However, the Zeeman term in Hamiltonian (3.1) does not, hence, due to the Kramers theorem the eigenlevels of the Hamiltonian are doubly degenerate in the absence of the external Zeeman field, $h = 0$.

To describe the wavefunctions of the particle we use the spinor notation, $\Psi = \binom{\psi_\uparrow}{\psi_\downarrow}$, since the particle has both spatial and spin degrees of freedom. We write the Schrödinger equation in the matrix form

$$\begin{pmatrix} H_{0x} + H_{0y} - h & \alpha_R(p_y + ip_x) + \alpha_D(p_y - ip_x) \\ \alpha_R(p_y - ip_x) + \alpha_D(p_y + ip_x) & H_{0x} + H_{0y} + h \end{pmatrix} \begin{pmatrix} \psi_\uparrow \\ \psi_\downarrow \end{pmatrix} = E \begin{pmatrix} \psi_\uparrow \\ \psi_\downarrow \end{pmatrix}, \tag{3.2}$$

where we introduce the shorthand $H_{0x} = \frac{{p_x}^2}{2m} + \frac{1}{2}m\omega_x^2 x^2$ and $H_{0y} = \frac{{p_y}^2}{2m} + \frac{1}{2}m\omega_y^2 y^2$.

To solve the equation numerically we expand the spatial components of the wavefunction in the basis of the 2D harmonic oscillator:

$$\begin{aligned} \psi_\uparrow &= \sum_{n_x,n_y} a_{n_x,n_y} \left|n_x, n_y\right\rangle, \\ \psi_\downarrow &= \sum_{n_x,n_y} b_{n_x,n_y} \left|n_x, n_y\right\rangle, \end{aligned} \tag{3.3}$$

where $\left|n_x, n_y\right\rangle = |n_x\rangle \left|n_y\right\rangle$ are vectors in the Hilbert space of the 2D harmonic oscillator solutions. In coordinate representation these solutions read

$$|n_x\rangle = N_x e^{-\frac{m\omega_x x^2}{2\hbar}} H_{n_x}\left(\sqrt{\frac{m\omega_x}{\hbar}} x\right), \tag{3.4}$$

with $N_x = \frac{1}{\sqrt{2^{n_x} n_x!}} \left(\frac{m\omega_x}{\pi\hbar}\right)^{\frac{1}{4}}$ and

$$\left|n_y\right\rangle = N_y e^{-\frac{m\omega_y y^2}{2\hbar}} H_{n_y}\left(\sqrt{\frac{m\omega_y}{\hbar}} y\right), \tag{3.5}$$

with $N_y = \frac{1}{\sqrt{2^{n_y} n_y!}} \left(\frac{m\omega_y}{\pi\hbar}\right)^{\frac{1}{4}}$. Here $H_{n_x(n_y)}$ are the "physicists'" Hermite polynomials of degree $n_x(n_y)$. We introduce the standard ladder operators $a_{x(y)}$ and $a^\dagger_{x(y)}$. The coordinate and momentum operators can be expressed in terms of these

operators as

$$x = \sqrt{\frac{\hbar}{2m\omega_x}}(a_x^\dagger + a_x), \qquad p_x = i\sqrt{\frac{m\hbar\omega_x}{2}}(a_x^\dagger - a_x),$$
$$y = \sqrt{\frac{\hbar}{2m\omega_y}}(a_y^\dagger + a_y), \qquad p_y = i\sqrt{\frac{m\hbar\omega_y}{2}}(a_y^\dagger - a_y), \tag{3.6}$$

we define the dimensionless entities in the Schrödinger equation in order to simplify both the equation and our numerical procedures. From now on we use $\hbar\omega_y$ as the energy unit and we set $\hbar = 1$ and $m = 1$. Also, we introduce the frequencies ratio, $\gamma = \omega_x/\omega_y$ and dimensionless Rashba and Dresselhaus spin-orbit coupling strengths $\alpha'_R \equiv \alpha_R\sqrt{\frac{m}{2\hbar\omega_y}}$ and $\alpha'_D \equiv \alpha_D\sqrt{\frac{m}{2\hbar\omega_y}}$. Then Schrödinger equation (3.2) reads

$$\begin{pmatrix} \gamma(a_x^\dagger a_x + \frac{1}{2}) + (a_y^\dagger a_y + \frac{1}{2}) - h & (\alpha'_R + \alpha'_D)p_y + i\sqrt{\gamma}(\alpha'_R - \alpha'_D)p_x \\ (\alpha'_R + \alpha'_D)p_y - i\sqrt{\gamma}(\alpha'_R - \alpha'_D)p_x & \gamma(a_x^\dagger a_x + \frac{1}{2}) + (a_y^\dagger a_y + \frac{1}{2}) + h \end{pmatrix}\begin{pmatrix}\psi_\uparrow \\ \psi_\downarrow\end{pmatrix}$$
$$= E\begin{pmatrix}\psi_\uparrow \\ \psi_\downarrow\end{pmatrix}. \tag{3.7}$$

Now we use the 2D harmonic oscillator expansion from Eq. (3.3) to obtain the system of linear equations for the coefficients $a_{n,m}$ and $b_{n,m}$, where n and m are positive integers.

$$\begin{aligned}
&\left(E_{osc}(n_x, n_y) - h - E\right)a_{n_x,n_y} + (\alpha'_R + \alpha'_D)\left[i\sqrt{n_y}b_{n_x,n_y-1} - i\sqrt{n_y+1}b_{n_x,n_y+1}\right] - \\
&- (\alpha'_R - \alpha'_D)\left[\sqrt{\gamma n_x}b_{n_x-1,n_y} + \sqrt{\gamma(n_x+1)}b_{n_x+1,n_y}\right] = 0, \\
&\left(E_{osc}(n_x, n_y) + h - E\right)b_{n_x,n_y} + (\alpha'_R + \alpha'_D)\left[i\sqrt{n_y}a_{n_x,n_y-1} - i\sqrt{n_y+1}a_{n_x,n_y+1}\right] + \\
&+ (\alpha'_R - \alpha'_D)\left[\sqrt{\gamma n_x}a_{n_x-1,n_y} - \sqrt{\gamma(n_x+1)}a_{n_x+1,n_y}\right] = 0,
\end{aligned} \tag{3.8}$$

where $E_{osc}(n_x, n_y) = \gamma(n_x + \frac{1}{2}) + (n_y + \frac{1}{2})$. This set of equations cannot be solved analytically and one has to resort to numerical methods. In the symmetric case where $\gamma = 1$, one could also have used a basis based on the solutions of the harmonic oscillator potential in cylindrical coordinates [Sinha 2011,Hu 2012a, Hu 2012b]. However, we do not use these solutions since the cylindrical sym-

metry is broken in the plane for $\gamma \neq 1$ and the problem is therefore better handled using the Cartesian basis expansion from Eqs. (3.3).

Let us take a closer look at the spin-orbit coupling terms. If we write them down in the matrix form, the Rashba term $V_R = \alpha_R \begin{pmatrix} 0 & (p_y+ip_x) \\ (p_y-ip_x) & 0 \end{pmatrix}$ and the Dresselhaus term $V_D = \alpha_D \begin{pmatrix} 0 & (p_y-ip_x) \\ (p_y+ip_x) & 0 \end{pmatrix}$ and choose the strengths of the coupling to be equal, $\alpha_R = \alpha_D$, we see that the matrix representations are mutually transposed, $V_D^T = V_R$. It means, that the Hamiltonian in the cases of pure Rashba, $\alpha_R \neq 0, \alpha_D = 0$, and pure Dresselhaus, $\alpha_R = 0, \alpha_D \neq 0$, spin-orbit couplings has the same eigenvalues. Hence, it is sufficient to investigate only one of the two cases. Below we consider only the pure Rashba coupling case. The equations (3.8) read

$$\begin{aligned}
&\Big(E_{osc}(n_x,n_y) - h - E\Big)a_{n_x,n_y} + \alpha'_R\Big[i\sqrt{n_y}b_{n_x,n_y-1} - i\sqrt{n_y+1}b_{n_x,n_y+1} - \\
&- \sqrt{\gamma n_x}b_{n_x-1,n_y} + \sqrt{\gamma(n_x+1)}b_{n_x+1,n_y}\Big] = 0, \\
&\Big(E_{osc}(n_x,n_y) + h - E\Big)b_{n_x,n_y} + \alpha'_R\Big[i\sqrt{n_y}a_{n_x,n_y-1} - i\sqrt{n_y+1}a_{n_x,n_y+1} + \\
&+ \sqrt{\gamma n_x}a_{n_x-1,n_y} - \sqrt{\gamma(n_x+1)}a_{n_x+1,n_y}\Big] = 0.
\end{aligned} \tag{3.9}$$

3.1 Single-particle spectra

In this section we consider several specific values of $\gamma = \omega_x/\omega_y$ and solve Eqs. (3.9). Then we analyze the behavior of the energy levels and their dependence on γ, α'_R and B. To numerically diagonalize the corresponding matrix we use subroutines from the GNU Scientific Library [Galassi 2009], which is distributed under the GNU General Public License. The results were obtained in the regime $0 \leq \alpha'_R \leq 1.5$ and using a basis with no less than 700 single-particle states. As a basis cutoff we choose a value of the harmonic oscillator energy, $\gamma(n_x + \frac{1}{2}) + (n_y + \frac{1}{2}) \leq E_{cutoff}$, for all n_x and n_y in the basis. This lets us include the states properly for the deformed cases, since for $\gamma > 1$ more states should be included in y-direction than in x-direction.

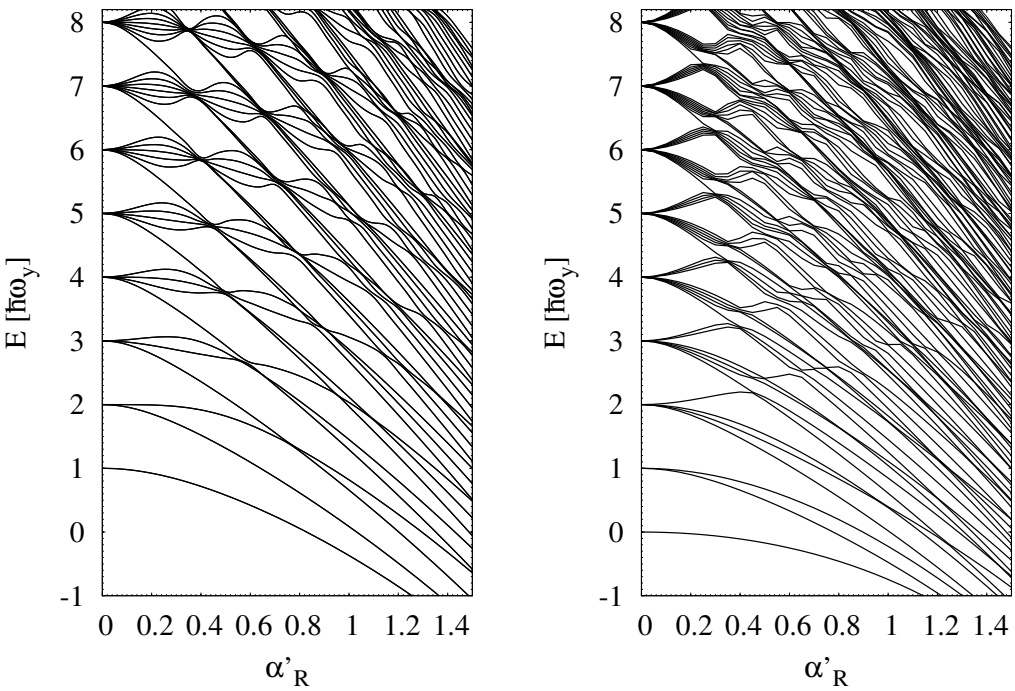

Figure 3.1: Energy spectrum of (3.9) as function of the dimensionless spin-orbit coupling parameter α'_R for the case of equal frequencies $\omega_x = \omega_y$ with no Zeeman shift (left panel) and including a Zeeman shift of magnitude $h = \hbar\omega_y$ (right panel).

3.1.1 Symmetric trapping potential, $\omega_x = \omega_y$

We start with the cylindrically symmetric trapping potential, i.e. the case $\gamma = 1$. We solve Eqs. (3.8) and plot the eigenenergies (the lowest 140 of them) as functions of the dimensionless spin-orbit coupling strength $\alpha'_R \equiv \alpha_R \sqrt{\frac{m}{2\hbar\omega_y}}$ in Fig. 3.1. In the left panel of Fig. 3.1 the Zeeman magnetic field is absent ($h = 0$). It is clear that for $\alpha'_R = 0$ the eigenlevels are degenerate as energy levels of 2D harmonic oscillator. However, the degeneracies are lifted as α'_R increases and the oscillator shells become more and more mixed. Also, since magnetic field is absent each level is doubly degenerate due to the time reversal symmetry mentioned above. The energies of the lowest levels decreases and for sufficiently large strengths approaches a parabolic dependence on α'_R which

can be reproduced by a semi-classical treatment [Ghosh 2011].

The quadratic behavior of the lowest states in the limit of the large coupling strength can be easily understood from a simple dimensional analysis (for this discussion we of course step back from the dimensionless quantities). Indeed, in the limit of large α_R we can disregard the harmonic oscillator part of the Hamiltonian which means that the energy of the particle should be proportional to $\frac{m\alpha_R^2}{2}$, since $|\alpha_R|$ is the only velocity available in this limit [Vyasanakere 2012]. Interestingly enough the similar behavior can be obtained in the one-dimensional limit for $\frac{\omega_x}{\omega_y} \gg 1$ via perturbation theory in the limit $\alpha_R \to 0$. We discuss these limits in subsections 3.1.3 and 3.1.4, respectively.

The majority of levels for not too strong values of the spin-orbit coupling ($\alpha'_R < 1.1$) form a particular band structure.This can be clearly understood. Indeed, the energy levels in a 2D harmonic oscillator appear as a 'shell' structure with energy levels degeneracy of $2N$, where $N = 1, 2, 3, \ldots$ is the number of the shell and the coefficient 2 is due to the Kramers degeneracy. The energy levels distance between the shells always equals $\hbar\omega_y$. However, the spin-orbit couping lifts the oscillator degeneracies and so the gap between the shells tends to be smaller than $\hbar\omega_y$, but still larger than the energy levels distance between the levels inside the shell. The lowest level in every shell resembles approximately parabolic behavior until it avoids crossing with levels below.

We note many avoided crossings that can be seen in the spectrum, which is due to the fact that the Hamiltonian with the spin-orbit coupling term does not preserve the cylindrical symmetry of the 2D oscillator, which means that one cannot decouple sectors of given angular momentum or parity. Only the time-reversal symmetry remains (in the absence of a Zeeman term). Other studies have used cylindrical expansions [Hu 2012a, Hu 2012b] but at the expense of coupling different angular momenta. We use the Cartesian basis since we find this more convenient. In Chapter 5 we discuss how the symmetry of the Hamiltonian and the avoided crossings of the single-particle eigenlevels are related to the so-called signatures of quantum chaotic behavior.

We see that the spin-orbit coupling has an immense effect on the spacing between the eigenlevels of the particle. For instance, the spacing of the

trap levels at $\alpha'_R = 0$ of one $\hbar\omega_y$ is strongly reduced at $\alpha'_R \sim 0.2$ for energies above $\sim 5\hbar\omega_y$. These sorts of changes should be reflected on the properties of a many-body system in a symmetric trap as discussed for the case of condensates in Refs. [Sinha 2011], [Hu 2012a] and [Hu 2012b]. The similar spectra can be obtained in various physical problems, for instance from the mapping of the similar set-up to a quantum Rabi model [Hu 2013] or from the electronic shell structure of quasi-two-dimensional semiconductor quantum dots [Reimann 2002].

On the right panel in Fig. 3.1 we show how the inclusion of the Zeeman field changes the spectrum in the non-deformed trap. The magnitude of the field is $h = \hbar\omega_y$, which is equal to the energy level difference in a harmonic oscillator. For $\alpha_R = 0$ the Zeeman field shifts the oscillator levels depending on the spin component but does not influence the structure. Note that the absolute ground state of the spectrum now starts at zero energy and then decreases almost parabolically. Note that, since the Zeeman field breaks the time-reversal symmetry, in general two-fold degeneracy of the enegy levels is lifted. However, in the case shown in Fig. 3.1 all the levels, with the exception of the ground state, are still two-fold degenerate at $\alpha'_R = 0$. It is due to the fact that the magnitude of the field is equal to the harmonic oscillator energy levels spacing, that is to say this degeneracy is accidental and occurs only for the values $h = k\hbar\omega_y$, where k is an integer. The conclusion is that both the Rashba and Zeeman terms can be used as an experimental handle to change the density of states in the single-particle spectrum.

3.1.2 Deformed trapping potential

Now we consider a harmonic oscillator trap with the unequal frequencies in x and y directions, $\omega_x \neq \omega_y$. In this case the rotational symmetry of the trap is broken and the degeneracies of the isotropic 2D harmonic oscillator are lifted. However, for the integer frequency ratio, γ, the energy levels of the anisotropic 2D harmonic oscillator are still degenerate. In Fig. 3.2 we show the spectrum for frequency ratios $\gamma = 2$ (left panel) and $\gamma = 3$ (right panel) as a function of the Rashba coupling strength, α'_R, with no Zeeman field. We see that for these ratios the overall structure of the energy spectrum remains the same as for a

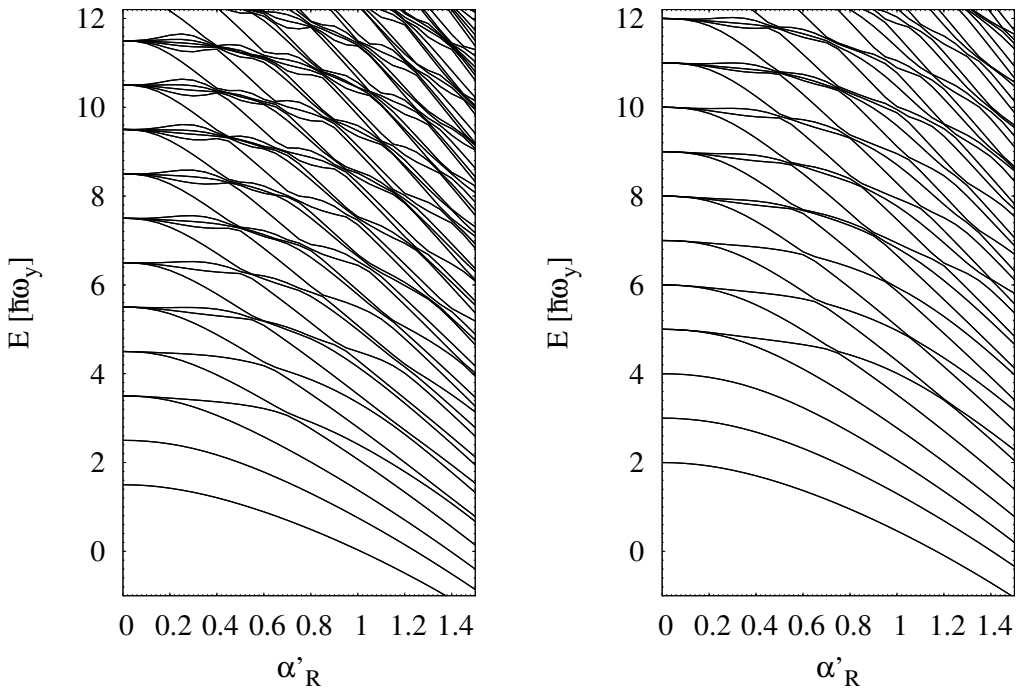

Figure 3.2: The energy levels of a spin-orbit coupled particle in a deformed harmonic trap as function of dimensionless spin-orbit coupling parameter α'_R for the case where the oscillator potential is deformed. The left panel has $\gamma = \frac{\omega_x}{\omega_y} = 2$ and the right panel has $\gamma = 3$.

non-deformed trap. The shell-like structure is preserved, but we see that for integer γ there are several shells with the same degeneracies of the levels.

A different scenario is displayed for incommensurable γ, i.e. when γ is not an integer number. In Fig. 3.3 we show the single-particle spectrum for $\gamma = 1.57$ (left panel) and $\gamma = 2.71$ (right panel). For these ratios the states are more evenly distributed and the spacing between levels tends to decrease, especially for higher energies. For $\gamma = 1.57$ we see that the spectral density is almost constant for energies of $5\hbar\omega_y$ and above, while for $\gamma = 2.71$ this is not seen until about $10\hbar\omega_y$ and above. Comparing the panels in Fig. 3.3, we see an overall tendency for larger γ to have a smaller overall density of levels since this is closer to the one-dimensional limit that we will return to

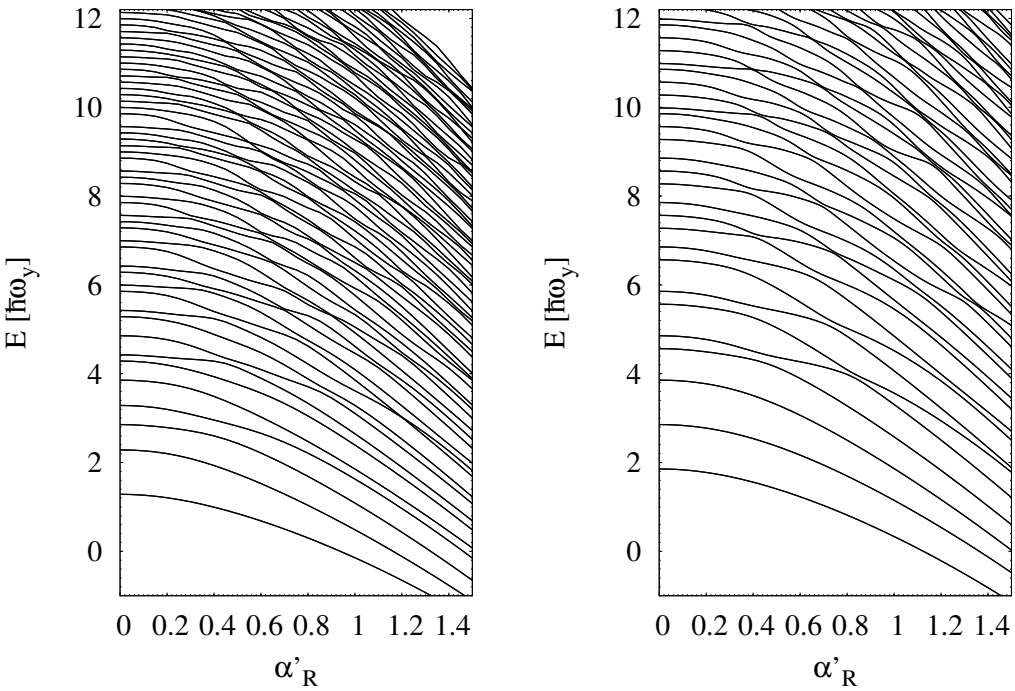

Figure 3.3: The energy levels of a spin-orbit coupled particle in a deformed harmonic trap as function of dimensionless spin-orbit coupling parameter α'_R for the case where the oscillator potential is deformed. The deformation ratios are $\gamma = 1.57$ (left panel) and $\gamma = 2.71$ (right panel).

momentarily. The overall quadratic decrease with α'_R is still seen as in Figs. 3.1 and 3.2. Comparing the results presented in Fig. 3.2 for the ratios $\gamma = 2$ and $\gamma = 3$ to those of Fig. 3.3 with $\gamma = 1.57$ and $\gamma = 2.71$ we thus conclude that the deformation of the trap is another experimental way to change the spectral structure and density. However, for the latter ratios the influence of the Rashba coupling is diminished somewhat as the density changes in a much more smooth manner as compared to Figs. 3.1 and 3.2. This implies that the choice of deformation is very important when studying the effects of spin-orbit coupling on trapped systems. As we will show in Chapter 5, the lack of the rotational symmetry in the anisotropic harmonic trap proves to be helpful in order to find signatures of irregular dynamics of a spin-orbit coupled system.

3.1.3 One-dimensional limit

Increasing the frequency ratio γ towards infinity separates the Hamiltonian into two weakly coupled one-dimensional (1D) parts: the high-energy part in the x-direction and the low-energy one in the y-direction. These decoupled one-dimensional equations with the corresponding Rashba couplings can be solved analytically. The Schrödinger equation for the motion in y-direction reads

$$\left[\left(\frac{p_y^2}{2m} + \frac{1}{2}m\omega_y^2 y^2\right) \otimes \hat{I} + \alpha_R p_y \hat{\sigma}_x - E\right]\Psi(y) = 0. \tag{3.10}$$

The wavefunction $\Psi(y)$ can be factorized into the spin part $\frac{1}{\sqrt{2}}\begin{pmatrix}1\\ \pm 1\end{pmatrix}$, which is the eigenvector of the Pauli matrix $\hat{\sigma}_x$, and the spatial part, $f_\pm(y)$. The one-dimensional Schrödinger equation then becomes

$$\left(\frac{p_y^2}{2m} + \frac{1}{2}m\omega_y^2 y^2 \pm \alpha_R p_y - E\right)\begin{pmatrix}1\\ \pm 1\end{pmatrix} f_\pm(y) = 0, \tag{3.11}$$

We rewrite these equations as

$$\left[\frac{1}{2m}(p_y \pm m\alpha_R)^2 + \frac{1}{2}m\omega_y^2 y^2 - \frac{m\alpha_R^2}{2} - E\right]\begin{pmatrix}1\\ \pm 1\end{pmatrix} f_\pm(y) = 0, \tag{3.12}$$

from which the harmonic oscillator eigenenergies can be directly inferred to be

$$E_{n_y} = -\frac{1}{2}m\alpha_R^2 + \hbar\omega_y(n_y + \frac{1}{2}), \tag{3.13}$$

where n_y is number of energy level of the harmonic oscillator in y-direction. The first term is simply the quadratic decrease of the energy with α_R that we already noted above. It can be interpreted as a Galilean boost by the Rashba velocity, α_R.

In figure 3.4 we show the spectral structure as one approaches the one-dimensional limit. In the left panel of Fig. 3.4 we have $\gamma = 5$ and in the right panel $\gamma = 10$. The low-energy eigenvalues reduce to the equidistant harmonic oscillator spectrum with the same frequency but shifted quadratically

with the spin-orbit coupling strength. The remarkably simple emerging feature is that the lowest part of the spectrum for an even modest deformation already resembles the equidistant one-dimensional limit. This can be clearly seen by making a comparison of Fig. 3.4 to Figs. 3.2 and 3.3. As the deformation increases an increasing part of the low-energy spectrum approaches the one-dimensional limit. This feature can be understood from the weak coupling of two oscillators with very different frequencies. The perturbation on the lowest energy states in the spectrum from the lowest of the large frequency (ω_x) states is proportional to the square of the coupling strength divided by the energy difference by second order perturbation theory. This tells us that the one-dimensional limit is approached in the bottom of the spectrum with increasing deformation. This low-energy spectrum is much simpler and much less dense than that of the 2D cylindrical oscillator. Note that the spectrum is still two-fold degenerate due to the time-reversal symmetry, but now it is practically back to the standard equidistant scheme typical to the harmonic confinement.

3.1.4 Perturbation theory for weak spin-orbit coupling

The weak coupling limit, $\alpha'_R \to 0$, can be investigated in detail using perturbation theory. In the absence of deformation and external magnetic field, the system is highly degenerate (Kramers and oscillator degeneracies) and requires degenerate perturbation theory to second order (first order vanishes, since the momentum operator is not diagonal in the energy representation). The easiest way to avoid the complicated expressions of the degenerate formalism is to consider a deformed oscillator trap with an external magnetic field which lifts all degeneracies. Taking the limit at the end of calculation we get the non-deformed and zero external field expressions. The Hamiltonian is $\hat{H} = \hat{H}_0 + \hat{V}_R$, where

$$\hat{H}_0 = \left(\frac{p_x^2}{2m} + \frac{1}{2} m\omega_x^2 x^2 + \frac{p_y^2}{2m} + \frac{1}{2} m\omega_y^2 y^2 \right) \otimes \hat{I} - h\hat{\sigma}_z \tag{3.14}$$

is the unperturbed part of the Hamiltonian and the perturbation is

$$\hat{V}_R = \alpha_R(\hat{\sigma}_x p_y - \hat{\sigma}_y p_x). \tag{3.15}$$

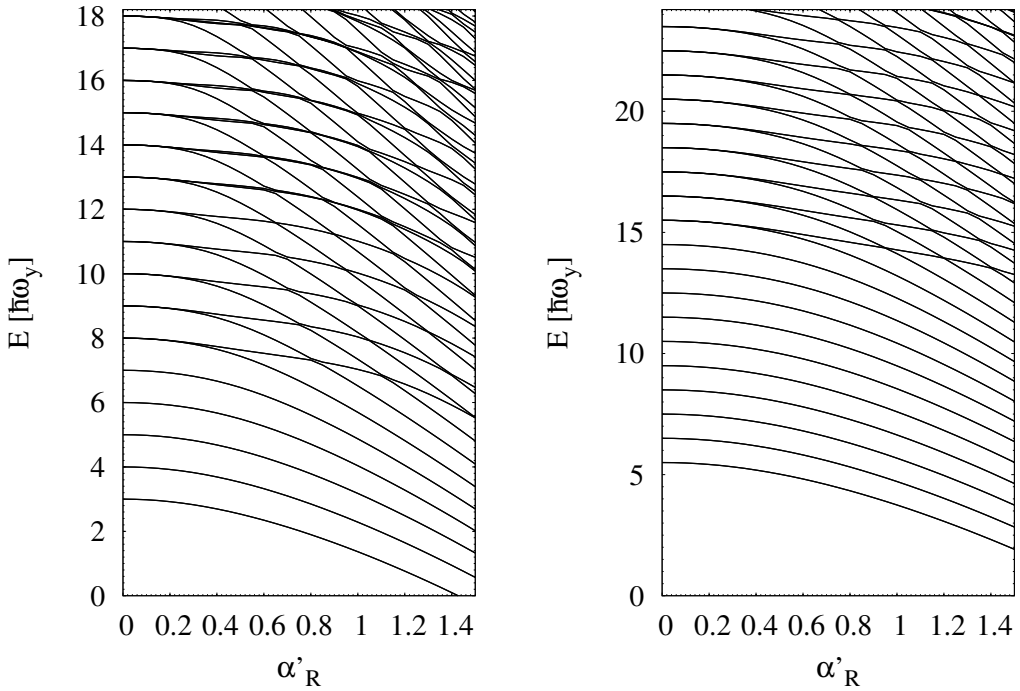

Figure 3.4: The energy levels of a spin-orbit coupled particle in a deformed harmonic trap as function of dimensionless spin-orbit coupling parameter α'_R for the case where the oscillator potential is deformed. The deformation ratios are $\gamma = 5$ (left panel) and $\gamma = 10$ (right panel). These results approach the limit of an effectively one-dimensional system.

Then the Schrödinger equation for the unperturbed Hamiltonian is

$$\hat{H}_0\psi^{(0)}(x, y, \sigma) = E^{(0)}\psi^{(0)}(x, y, \sigma), \tag{3.16}$$

with the following solutions $\psi^{(0)}(x, y, \uparrow) = \phi_{n_x,n_y}(x, y)\left(\begin{smallmatrix}1\\0\end{smallmatrix}\right)$ and $\psi^{(0)}(x, y, \downarrow) = \phi_{n_x,n_y}(x, y)\left(\begin{smallmatrix}0\\1\end{smallmatrix}\right)$. The eigenenergies are $E^{(0)}_{n_x,n_y,\sigma} = \hbar\omega_x(n_x + \frac{1}{2}) + \hbar\omega_y(n_y + \frac{1}{2}) - \sigma h$, where $\sigma = \pm 1$ for spin up and down, respectively. The spatial parts $\phi_{n_x,n_y}(x, y)$ are the 2D harmonic oscillator solutions.

Now we can directly find corrections to the energy. As we mentioned, the diagonal matrix element for V_R is zero, thus the first-order correction will be

zero as well. The second-order correction reads [Landau 1981]

$$E^{(2)}_{n_x,n_y,\sigma} = \sum_{m_x,m_y,\sigma'}{}' \frac{|\langle n_x, n_y, \sigma|V_R|m_x, m_y, \sigma'\rangle|^2}{E^{(0)}_{n_x,n_y,\sigma} - E^{(0)}_{m_x,m_y,\sigma'}}, \tag{3.17}$$

where the *prime* near the sum sign indicates that the summation does not include the term $E_{m_x,m_y,\sigma'} = E_{n_x,n_y,\sigma}$. It is important to note that we can explicitly write down the matrix elements. Due to the structure of the Pauli matrices $\hat{\sigma}_x$ and $\hat{\sigma}_y$ only the matrix elements with different spin projections will contribute to the summations.

$$\langle n_x, n_y, \uparrow |\hat{V}_R|m_x, m_y, \downarrow\rangle = -\alpha_R \sqrt{\frac{m\hbar}{2}}\Big[\sqrt{\omega_x}\Big(\sqrt{m_x+1}\delta_{n_x,m_x+1} - \\ - \sqrt{m_x}\delta_{n_x,m_x-1}\Big)\delta_{n_y,m_y} - i\sqrt{\omega_y}\Big(\sqrt{m_y+1}\delta_{n_y,m_y+1} - \sqrt{m_y}\delta_{n_y,m_y-1}\Big)\delta_{n_x,m_x}\Big] \tag{3.18}$$

and

$$\langle n_x, n_y, \downarrow |\hat{V}_R|m_x, m_y, \uparrow\rangle = \alpha_R \sqrt{\frac{m\hbar}{2}}\Big[\sqrt{\omega_x}\Big(\sqrt{m_x+1}\delta_{n_x,m_x+1} - \\ - \sqrt{m_x}\delta_{n_x,m_x-1}\Big)\delta_{n_y,m_y} + i\sqrt{\omega_y}\Big(\sqrt{m_y+1}\delta_{n_y,m_y+1} - \sqrt{m_y}\delta_{n_y,m_y-1}\Big)\delta_{n_x,m_x}\Big]. \tag{3.19}$$

We also see that only the elements between the nearest states are non-zero. It is straightforward now to write down the second-order corrections for the ground state energy

$$E^{(2)}_{0,0,\uparrow} = -\frac{m\alpha_R^2}{2}\left[\frac{\hbar\omega_x}{\hbar\omega_x + 2h} + \frac{\hbar\omega_y}{\hbar\omega_y + 2h}\right]. \tag{3.20}$$

For the case of $h \ll \hbar\omega_y$ we get a simple term, which appears natural considering that the dimension of α_R is the velocity

$$E^{(2)}_{0,0,\uparrow} = -m\alpha_R^2. \tag{3.21}$$

This equation is valid for coupling parameter values smaller than the oscillator velocity, $\alpha_R \ll \sqrt{\frac{\hbar\omega}{m}}$. For a regime of larger α_R the contribution of all states

becomes crucial, therefore one has to consider the higher-order perturbation corrections to the energy. However, for the case of $\alpha_R \gtrsim \sqrt{\frac{\hbar\omega}{m}}$ the behavior of the ground state energy is still quadratic in α_R [Hu 2012b].

3.1.5 Rashba and Dresselhaus spin-orbit coupling, $\alpha_R \neq 0$, $\alpha_D \neq 0$

In this subsection we discuss several cases of the "inhomogeneous" spin-orbit coupling. By this we mean that both Rashba and Dresselhaus spin-orbit coupling strengths are not zero, i.e. $\alpha_R \neq 0$ and $\alpha_D \neq 0$. For convenience, we introduce notation $\alpha_1 = \alpha_R + \alpha_D$ and $\alpha_2 = \alpha_R - \alpha_D$. Then the Hamiltonian in Eq. (3.1) reads

$$H = \left(\frac{{p_x}^2}{2m} + \frac{1}{2}m\omega_x^2 x^2 + \frac{{p_y}^2}{2m} + \frac{1}{2}m\omega_y^2 y^2\right) \otimes \hat{I} + \\ + \alpha_1 \hat{\sigma}_x p_y - \alpha_2 \hat{\sigma}_y p_x - \hat{\boldsymbol{\mu}} \cdot \mathbf{B}. \tag{3.22}$$

The case $\alpha_1 = \alpha_2$ corresponds to $\alpha_R \neq 0$, $\alpha_D = 0$, which was considered in the previous subsections. Below we consider several cases of different α_1 and α_2. We plot the dependence of the energy levels of the particle as a function of α_1 for fixed α_2. We consider only the isotropic harmonic trap since the deformation of the trap was thoroughly discussed.

Let us consider the special case of $\alpha_2 = 0$, which corresponds to the equal Rashba and Dresselhaus spin-orbit interaction strengths case, $\alpha_R = \alpha_D$. This example is especially important since it is the only reported case of the spin-orbit coupling in cold atom systems [Ketterle 2008, Lin 2011]. We see that this case is in many ways similar to the one-dimensional limit we discussed in 3.1.3. Indeed, in the case of $\alpha_R = \alpha_D \equiv \alpha$ Hamiltonian (3.1) looks like

$$H = \left(\frac{{p_x}^2}{2m} + \frac{1}{2}m\omega_x^2 x^2 + \frac{{p_y}^2}{2m} + \frac{1}{2}m\omega_y^2 y^2\right) \otimes I + \alpha \hat{\sigma}_x p_y, \tag{3.23}$$

where we do not include the external magnetic field. Similar to the 1D case the solution of the corresponding Schrödinger equation can be factorized into spin and spatial parts. Evidently, the spin wavefunction,$\Phi_\pm$, is a eigenfunction

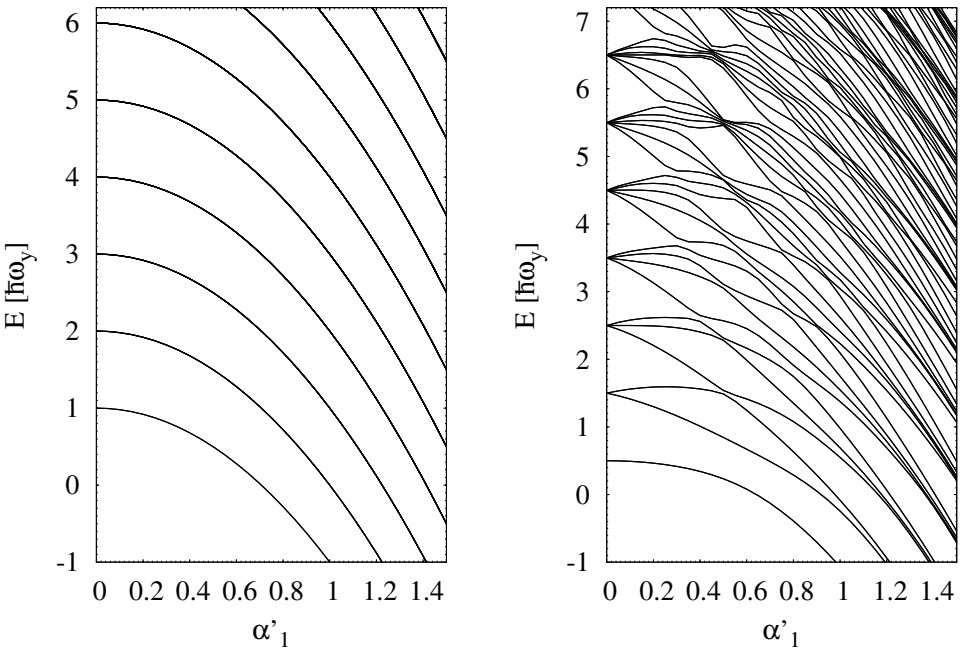

Figure 3.5: Energy as a function of the dimensionless spin-orbit coupling strength, α_1', for the fixed α_2' spin-orbit coupling strengths. The trap frequencies are equal, $\gamma = 1$. The *left* panel shows the $\alpha_2' = 0$ case and the *right* panel shows the $\alpha_2' = 0.5$.

of the Pauli matrix σ_x,

$$\Phi_\pm = \begin{pmatrix} 1 \\ \pm 1 \end{pmatrix}. \tag{3.24}$$

Moreover, the x- and y-directions decouple

$$\left(\frac{{p_x}^2}{2m} + \frac{1}{2} m\omega_x^2 x^2 + \frac{{p_y}^2}{2m} + \frac{1}{2} m\omega_y^2 y^2 \pm \alpha p_y - E \right) \Phi_\pm f(x) g_\pm(y) = 0, \tag{3.25}$$

where $f(x)$ is a 1D harmonic oscillator solution and $g_\pm(y)$ is the y-dependent wavefunction. We rewrite these equations as

$$\left[\frac{1}{2m}(p_y \pm m\alpha)^2 + \frac{1}{2} m\omega_y^2 y^2 - \frac{m\alpha^2}{2} - \left(E - \hbar\omega_x \left(n_x + \frac{1}{2} \right) \right) \right] \Phi_\pm f_{n_x}(x) g_\pm(y) = 0, \tag{3.26}$$

with eigenenergies

$$E_{n_x,n_y} = \hbar\omega_x\left(n_x + \frac{1}{2}\right) + \hbar\omega_y\left(n_y + \frac{1}{2}\right) - \frac{m\alpha^2}{2}. \tag{3.27}$$

The energy spectrum is similar to the one-dimensional case with the only difference is the contribution from the harmonic oscillator energies in the x-direction. This spectrum can be seen in Fig. 3.5 in the *left* panel. We see that the spectral gap structure of pure Rashba (or Dresselhaus) spin-orbit coupling does not appear here.

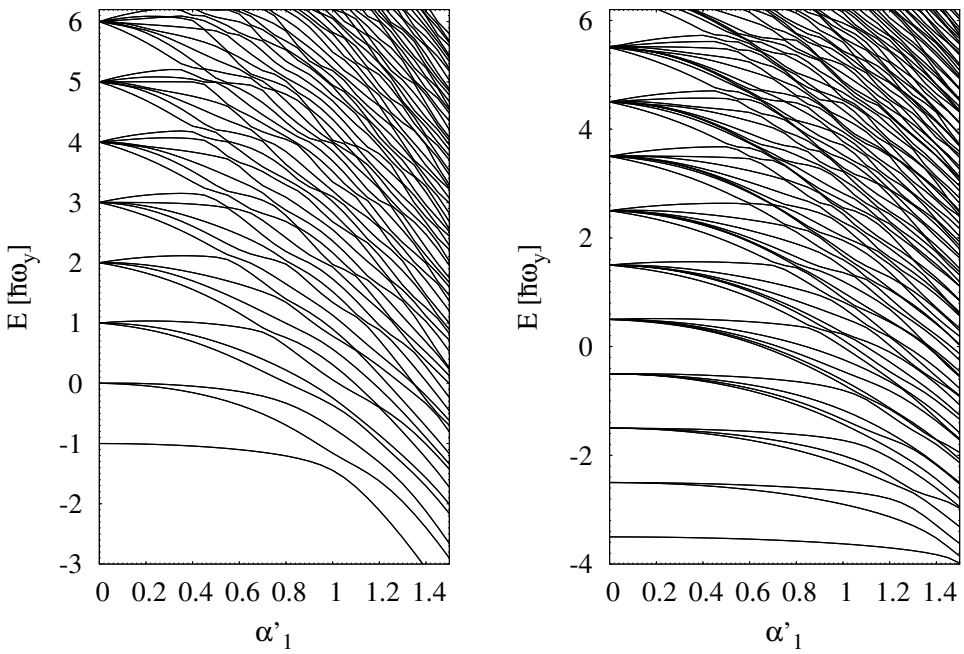

Figure 3.6: Energy as a function of the dimensionless spin-orbit coupling strength, α_1', for the fixed α_2' spin-orbit coupling strengths. The trap frequencies are equal, $\gamma = 1$. The *left* panel shows the $\alpha_2' = 1.0$ case and the *right* panel shows the $\alpha_2' = 1.5$.

We also show several cases of both α_1 and α_2 being non-zero. In Figs. 3.5 (*right* panel) and 3.6 we show the energy levels as function of α_1 for several fixed values of α_2. For the figure we employ the dimensionless spin-orbit coupling strengths, $\alpha_1' = \alpha_1\sqrt{\frac{m}{2\hbar\omega_y}}$ and $\alpha_2' = \alpha_2\sqrt{\frac{m}{2\hbar\omega_y}}$. The structure of the energy

levels in these cases reminds the structure of the spectra for a particle in the deformed harmonic trap, especially for incommensurable values of the frequency ratio γ, as shown in Fig. 3.3. For the small values of α_1', when α_2' dominates the spin-orbit part of the Hamiltonian, the spectrum resembles the behavior of the one-dimensional limit, which is consistent with the $\alpha_2 = 0$ case discussed previously. For $\alpha_1' > \alpha_2'$ the spectrum also tends to approach the 1D limit.

CHAPTER 4

Interacting fermions in a 2D harmonic trap with Rashba spin-orbit coupling

In this Chapter we discuss a system of N fermions confined in a 2D harmonic trap and subjected to Rashba spin-orbit coupling. The main difference with the previous Chapter case is the inclusion of a two-body interaction between particles. We choose the interaction to be of short-range, and, since the particles are fermions, the Pauli principle only allows the interacting particle to be in a singlet spin state, i.e. to have different spin projections and zero total spin. The Hamiltonian reads

$$\hat{H} = \sum_{i=1}^{N}\Big[\frac{\mathbf{p_i}^2}{2m} + \frac{1}{2}m(\omega_x^2 x_i^2 + \omega_y^2 y_i^2)\Big] \otimes \hat{I} + \alpha_R \sum_{i=1}^{N}(\hat{\sigma}_{xi}p_{yi} - \hat{\sigma}_{yi}p_{xi}) + h\sum_{i=1}^{N}\hat{\sigma}_{zi} + \frac{1}{2}g\sum_{i\neq j}\hat{V}(\mathbf{r}_i - \mathbf{r}_j), \tag{4.1}$$

where $\mathbf{p}_i = (p_{xi}, p_{yi})$ and $\mathbf{r}_i = (x_i, y_i)$ are the 2D momentum and position vectors, respectively. The values ω_x and ω_y are the frequencies of the 2D harmonic trap in transverse directions and they are not necessarily equal, m is the mass of a particle, $\hat{I}$ is the identity matrix, α_R is the strength of Rashba spin-orbit coupling; $\hat{\boldsymbol{\sigma}}_{\boldsymbol{i}} = (\hat{\sigma}_{xi}, \hat{\sigma}_{yi}, \hat{\sigma}_{zi})$ is the Pauli matrices vector and h is the strength of the external Zeeman field. The two-body interaction term, $gV(\mathbf{r}_i - \mathbf{r}_j)$, is modeled by the Dirac delta function, $gV(\mathbf{r}_i - \mathbf{r}_j) = g\delta(\mathbf{r}_i - \mathbf{r}_j)\hat{P}_{S=0}$, where $\hat{P}_{S=0} = (\hat{I} - \hat{\boldsymbol{\sigma}}_{\boldsymbol{i}} \cdot \hat{\boldsymbol{\sigma}}_{\boldsymbol{j}})/4$ is the operator, which projects to singlet spin states. Here the strength g has

the units $\hbar^2/m$, such that $\hat{V}$ maintains dimension of energy. Below we dismiss the units $\hbar^2/m$ for simplicity. Applying such a (pseudo)-potential must be done with considerable care to avoid inconsistencies [Olshanii 2001, Valiente 2012], and we make sure that we do not work in the strongly-interacting regime of large g. We choose the interaction strength, g, to be positive, $g > 0$, so that we only consider repulsive interaction between particles.

In order to estimate the interaction effects in such system we apply a well-known Hartree-Fock method and solve the obtained equations self-consistently with proper numerical procedures. This Chapter is divided into several sections. First, we remind and discuss the Hartree-Fock approximation. Next we take a look at the details of our numerical calculations. Finally, we present and discuss the results.

4.1 Hartree-Fock equations

In this section we describe the Hartree-Fock method of approximation to calculate the wavefunction and the energy of the many-body system in a stationary state. It is a powerful tool, which is well-known in computational physics and quantum chemistry. The description of the method can be found in most textbooks on quantum mechanics, however, we follow the spirit and notation of Ref. [Landau 1981, Siemens 1993, Weinberg 2013]. The Hartree-Fock method is a variational approach, based on the theorem that the ground state energy is less or equal to the expectation value of the Hamiltonian in any state [Weinberg 2013]. To utilize this observation we construct the functional

$$E[\Psi] = \frac{\langle\Psi|\hat{H}|\Psi\rangle}{\langle\Psi|\Psi\rangle}, \tag{4.2}$$

where $\hat{H}$ is the Hamiltonian of the system and Ψ is the trial wave function. The variational principle states that minimizing this functional on the whole Hilbert space provides one with the ground state energy. However, for numerical computations it might not be (and usually is not) accessible, so one is required to choose the "good enough" approximation to the wavefunction. "Good enough" usually means that the minimization is possible for a given set

of functions and the approximation to the ground state energy converges in a reasonable time. The choice of such wavefunctions is a cornerstone of the variational methods implementation.

In particular, the Hartree-Fock method is based on the following recipe to choose the trial wave function: the many-body wavefunction is picked as the product of the single-particle wave functions. At this point it becomes important whether the particles are fermions or bosons. As was said before, we will discuss only the fermionic case, so that the wavefunction of the system must be antisymmetric upon the exchange of any two particles. Provided that, the Hartree-Fock wave functions are constructed as the antisymmetrized product of the single-particle states, the Slater determinant

$$|\Psi_{HF}\rangle = \frac{1}{\sqrt{N!}} \begin{vmatrix} \psi_1(\mathbf{r}_1) & \psi_2(\mathbf{r}_1) & \cdots & \psi_N(\mathbf{r}_1) \\ \psi_1(\mathbf{r}_2) & \psi_2(\mathbf{r}_2) & \cdots & \psi_N(\mathbf{r}_2) \\ \vdots & \vdots & \ddots & \vdots \\ \psi_1(\mathbf{r}_N) & \psi_2(\mathbf{r}_N) & \cdots & \psi_N(\mathbf{r}_N) \end{vmatrix}, \tag{4.3}$$

where N is the number of particles and $\psi_i(\mathbf{r}_\alpha)$, for $i, \alpha = 1, \ldots, N$, are the single-particle wavefunctions, which we consider to be normalized and orthogonal to one another. The single-particle wavefunctions can be written as a spinor $\psi_i(\boldsymbol{r}) = \begin{pmatrix} \psi_{i\uparrow}(\boldsymbol{r}) \\ \psi_{i\downarrow}(\boldsymbol{r}) \end{pmatrix}$, since the particles in a trap are fermions with spin-1/2. We consider the wavefunction $|\Psi_{HF}\rangle$ to be normalized, i.e. $\langle\Psi_{HF}|\Psi_{HF}\rangle = 1$.

We will now formulate the Hartree-Fock equations. The expectation value of Hamiltonian (4.1) in the state (4.3) is

$$\langle\Psi_{HF}|\hat{H}|\Psi_{HF}\rangle = \frac{1}{N!}\int \ldots \int \mathrm{d}\mathbf{r}_1 \ldots \mathrm{d}\mathbf{r}_N \Psi^*_{HF}\hat{H}\Psi_{HF}. \tag{4.4}$$

This expression can be simplified if we use the fact that the one-particle eigenstates are orthonormalized, i.e. $\int \mathrm{d}\mathbf{r}\psi_i^*(\mathbf{r})\psi_j(\mathbf{r}) = \delta_{ij}$. One notices that for the two-particle interaction only two integrals are left in the expectation value ex-

pression, namely

$$\frac{1}{2}g\,\langle\Psi_{HF}|\sum_{i\neq j}\hat{V}(\mathbf{r_i}-\mathbf{r_j})\,|\Psi_{HF}\rangle = \tag{4.5}$$
$$= \frac{1}{2}g\sum_{i\neq j}\int\int \mathrm{d}\mathbf{r}_1\mathrm{d}\mathbf{r}_2\psi_i^*(\mathbf{r}_1)\psi_j^*(\mathbf{r}_2)\hat{V}(\mathbf{r}_1-\mathbf{r}_2)\left[\psi_i(\mathbf{r}_1)\psi_j(\mathbf{r}_2)-\psi_j(\mathbf{r}_1)\psi_i(\mathbf{r}_2)\right].$$

Note that the factor $\frac{1}{N!}$ is gone, because it is precisely the number of identical terms in the expectation value. Similarly, in the first two terms of Hamiltonian (4.1) only one integral is left

$$\langle\Psi_{HF}|\,\hat{H}_{0i}+\hat{V}_{Ri}+h\hat{\sigma}_{zi}\,|\Psi_{HF}\rangle = \sum_{i=1}^{N}\int \mathrm{d}\mathbf{r}_1\psi_i^*(\mathbf{r}_1)\left(\hat{H}_{0i}+\hat{V}_{Ri}+h\hat{\sigma}_{zi}\right)\psi_i(\mathbf{r}_1), \tag{4.6}$$

where $\hat{H}_{0i} = \left[\frac{\mathbf{p_i}^2}{2m}+\frac{1}{2}m(\omega_x^2x_i^2+\omega_y^2y_i^2)\right]\otimes\hat{I}$ is the oscillator part of the system Hamiltonian and the $\hat{V}_{Ri} = \alpha_R(\hat{\sigma}_{xi}p_{yi}-\hat{\sigma}_{yi}p_{xi})$ is the spin-orbit one. They both act only on the i-th particle state. Finally, the expectation value of the Hamiltonian in Eq. (4.1) is

$$\langle\Psi_{HF}|\,\hat{H}\,|\Psi_{HF}\rangle = \Big\{\sum_{i=1}^{N}\int \mathrm{d}\mathbf{r}_1\psi_i^*(\mathbf{r}_1)\left(\hat{H}_{0i}+\hat{V}_{Ri}+h\hat{\sigma}_{zi}\right)\psi_i(\mathbf{r}_1)+ \tag{4.7}$$
$$+\frac{1}{2}g\sum_{i\neq j}\int\int \mathrm{d}\mathbf{r}_1\mathrm{d}\mathbf{r}_2\psi_i^*(\mathbf{r}_1)\psi_j^*(\mathbf{r}_2)\hat{V}(\mathbf{r}_1-\mathbf{r}_2)\left[\psi_i(\mathbf{r}_1)\psi_j(\mathbf{r}_2)-\psi_j(\mathbf{r}_1)\psi_i(\mathbf{r}_2)\right]\Big\}.$$

Next we minimize the expectation value (4.7) with respect to the single-particle wave functions ψ_i and their complex conjugates ψ_i^*. Thus, the variational equation is written as

$$\delta\left(\langle\Psi_{HF}|\,\hat{H}\,|\Psi_{HF}\rangle-\sum_{j=1}^{N}\varepsilon_j\int \mathrm{d}\mathbf{r_1}\psi_j^*\psi_j\right) = 0, \tag{4.8}$$

where ε_j are the Lagrangian multipliers, introduced due to the normalization

constraints $\int \mathrm{d}\boldsymbol{r}\psi_i^*\psi_j = \delta_{ij}$. Performing the variation we obtain

$$\sum_i \int \mathrm{d}\mathbf{r_1}\delta\psi_i^*(\mathbf{r}_1)\varepsilon_i\psi_i(\mathbf{r}_1) - \sum_i \int \mathrm{d}\mathbf{r_1}\delta\psi_i^*(\mathbf{r}_1)\left(\hat{H}_{0i} + \hat{V}_{Ri}\right)\psi_i(\mathbf{r}_1) + \\ + g\sum_{i,j}\int\int \mathrm{d}\mathbf{r_1}\mathrm{d}\mathbf{r_2}\delta\psi_i^*(\mathbf{r}_1)\psi_j^*(\mathbf{r}_2)\hat{V}(\mathbf{r}_1 - \mathbf{r}_2)\left[\psi_i(\mathbf{r}_1)\psi_j(\mathbf{r}_2) - \psi_j(\mathbf{r}_1)\psi_i(\mathbf{r}_2)\right] = 0. \tag{4.9}$$

This equality should be true for any $\delta\psi_i^*$ and since the integral over $\mathbf{r_1}$ is zero we obtain

$$\varepsilon_i\psi_i(\mathbf{r}_1) - \left(\hat{H}_{0i} + \hat{V}_{Ri} + h\hat{\sigma}_{zi}\right)\psi_i(\mathbf{r}_1) + \\ + g\sum_j \int \mathrm{d}\mathbf{r_2}\psi_j^*(\mathbf{r}_2)\hat{V}(\mathbf{r}_1 - \mathbf{r}_2)\left[\psi_i(\mathbf{r}_1)\psi_j(\mathbf{r}_2) - \psi_j(\mathbf{r}_1)\psi_i(\mathbf{r}_2)\right] = 0, \tag{4.10}$$

which are the renowned Hartree-Fock equations. Until now we have not used the explicit form of the interaction term. As was said earlier, we approximate it with the two-body contact potential, with the restriction that the particles interact only in the spin singlet channel. Then Eq. (4.10) reads

$$\varepsilon_i\psi_i(\mathbf{r}_1) - \left(\hat{H}_{0i} + \hat{V}_{Ri} + h\hat{\sigma}_{zi}\right)\psi_i(\mathbf{r}_1) + \\ + g\sum_j \int \mathrm{d}\mathbf{r_2}\psi_j^*(\mathbf{r}_2)\delta(\mathbf{r}_1 - \mathbf{r}_2)\hat{P}_{S=0}\left[\psi_i(\mathbf{r}_1)\psi_j(\mathbf{r}_2) - \psi_j(\mathbf{r}_1)\psi_i(\mathbf{r}_2)\right] = 0. \tag{4.11}$$

The projection operator acts on the spinors $\psi_i\psi_j$ in the following way

$$\hat{P}_{S=0}\psi_i(\mathbf{r})\psi_j(\mathbf{r}') = \frac{1}{2}\left(\psi_{i\uparrow}(\mathbf{r})\psi_{j\downarrow}(\mathbf{r}') - \psi_{i\downarrow}(\mathbf{r})\psi_{j\uparrow}(\mathbf{r}')\right)\left(|\uparrow\rangle_i|\downarrow\rangle_j - |\downarrow\rangle_i|\uparrow\rangle_j\right), \tag{4.12}$$

where $|\uparrow\rangle = \begin{pmatrix}1\\0\end{pmatrix}$ and $|\downarrow\rangle = \begin{pmatrix}0\\1\end{pmatrix}$. The integration in Eq. (4.11) is trivial and the

resulting equations are

$$(\hat{H}_{0i} + \hat{V}_{Ri} + h\hat{\sigma}_{zi})\begin{pmatrix}\psi_{i\uparrow}\\ \psi_{i\downarrow}\end{pmatrix} + \frac{g}{2}\Big[(n_\downarrow\psi_{i\uparrow} - n_{\downarrow\uparrow}\psi_{i\downarrow})\begin{pmatrix}1\\0\end{pmatrix} + \\ + (n_\uparrow\psi_{i\downarrow} - n_{\uparrow\downarrow}\psi_{i\uparrow})\begin{pmatrix}0\\1\end{pmatrix}\Big] = \varepsilon_i\begin{pmatrix}\psi_{i\uparrow}\\ \psi_{i\downarrow}\end{pmatrix}, \tag{4.13}$$

where we have introduced the densities

$$n_\uparrow = \sum_{j=1}^{N}|\psi_{j\uparrow}|^2\ ,\ n_\downarrow = \sum_{j=1}^{N}|\psi_{j\downarrow}|^2\ , \tag{4.14}$$

$$n_{\uparrow\downarrow} = \sum_{j=1}^{N}\psi^*_{j\uparrow}\psi_{j\downarrow}\ ,\ n_{\downarrow\uparrow} = \sum_{j=1}^{N}\psi^*_{j\downarrow}\psi_{j\uparrow}\ . \tag{4.15}$$

Note that $n_{\downarrow\uparrow}$ is actually the complex conjugate of $n_{\uparrow\downarrow}$. The Hartree-Fock equations can be written in a matrix form

$$\begin{pmatrix}\hat{H}_{0i} + h + \frac{g}{2}n_\downarrow & \alpha_R(\hat{p}_{iy} + i\hat{p}_{ix}) - \frac{g}{2}n_{\downarrow\uparrow}\\ \alpha_R(\hat{p}_{iy} - i\hat{p}_{ix}) - \frac{g}{2}n_{\uparrow\downarrow} & \hat{H}_{0i} - h + \frac{g}{2}n_\uparrow\end{pmatrix}\begin{pmatrix}\psi_{i\uparrow}\\ \psi_{i\downarrow}\end{pmatrix} = \varepsilon_i\begin{pmatrix}\psi_{i\uparrow}\\ \psi_{i\downarrow}\end{pmatrix}, \tag{4.16}$$

i.e. the Hartree-Fock Hamiltonian can be written as

$$\hat{H}_{HF} = \begin{pmatrix}\hat{H}_{0i} + h + \frac{g}{2}n_\downarrow & \alpha_R(\hat{p}_{iy} + i\hat{p}_{ix}) - \frac{g}{2}n_{\downarrow\uparrow}\\ \alpha_R(\hat{p}_{iy} - i\hat{p}_{ix}) - \frac{g}{2}n_{\uparrow\downarrow} & \hat{H}_{0i} - h + \frac{g}{2}n_\uparrow\end{pmatrix}. \tag{4.17}$$

The Hartree-Fock equations are Schrödinger-like equations of a particle in a trap with the additional potential due to interaction of the particle with the averaged densities of the others. The values ε_i can be interpreted as the single-particle energy levels of such system. Evidently, in the absence of the inter-particle interactions ($g = 0$) the energies ε_i correspond to the single-particle eigenlevels we discussed in the Chapter 3. For the small values of $g = 0$ the energy spectrum is still dominated by the effects of the external potentials, i.e. the harmonic oscillator trap and Rashba spin-orbit coupling. However, even the small interaction strengths affects the spectrum, although maintaining the general structure. We obtain the numerical solutions of the Hartree-Fock equa-

tions and discuss them in more details in the Section 4.3.

The single-particle eigenenergies can be readily used to obtain the total energy of the interacting system in the ground state. It can be written in one of two forms

$$E[\Psi_{HF}] = \sum_{i=1}^{N} \langle \psi_i | \hat{H}_{0i} + \hat{V}_{Ri} + h\hat{\sigma}_{zi} | \psi_i \rangle + \frac{g}{2} \int \mathrm{d}\mathbf{r}(n_\downarrow n_\uparrow - |n_{\downarrow\uparrow}|^2) =$$
$$= \sum_{i=1}^{N} \varepsilon_i - \frac{g}{2} \int \mathrm{d}\mathbf{r}(n_\downarrow n_\uparrow - |n_{\downarrow\uparrow}|^2). \tag{4.18}$$

In the non-interacting case the total energy of the system is simply the sum of the N single-particle eigenenergies of the particle in a trap. The difference between the total energy of the interacting and non-interacting systems is also shown in the Section 4.3.

4.2 Numerical calculations

In this section we discuss the details of the numerical calculations aimed to solve the Hartree-Fock equations for different parameters of the system, such as the deformation of the trap, the strength of Rashba spin-orbit coupling, the strength of Zeeman magnetic field, and the interaction strength. First we will discuss the time-reversal symmetry of the system since, as we will see further, the presence of the symmetry affects the calculations. Next we indicate the rather straightforward method employed in the iteration procedure. After that we offer a perturbative treatment for small values of the interaction strength g. In the next section the resulting Hartree-Fock spectra are compared with the results of both non-interacting systems and a perturbative treatment of the interparticle interaction. We also discuss the change in total energy of the system due to repulsion.

4.2.1 Time-reversal symmetry

As was mentioned in the Chapter 2 the spin-orbit coupled particle in a harmonic oscillator trap is symmetric under time reversal, which for spin-1/2 par-

ticles leads to the two-fold degeneracy of the single-particle eigenenergies due to the Kramers theorem. It means that the Hamiltonian of the system commutes with the time-reversal operator

$$\hat{T} = i\hat{\sigma}_y \hat{K}, \tag{4.19}$$

where $\hat{K}$ is the complex conjugation operator [Sakurai 1994]. For the non-interacting system the symmetry is broken by applying external magnetic field.

The Hartree-Fock Hamiltonian does not necessarily possesses this kind of symmetry, i.e. the symmetry can be spontaneously broken if it is energetically favorable. The commutation relation for the Hartree-Fock Hamiltonian in Eq. (4.17) and the time-reversal operator in Eq. (4.19) is

$$\begin{aligned} &\left[\hat{H}_{0i} + \hat{V}_{Ri}, \hat{T}\right] + \left[\begin{pmatrix} \frac{g}{2}n_\downarrow + h & -\frac{g}{2}n_{\downarrow\uparrow} \\ -\frac{g}{2}n_{\uparrow\downarrow} & \frac{g}{2}n_\uparrow - h \end{pmatrix}, \begin{pmatrix} 0 & 1 \\ -1 & 0 \end{pmatrix}\hat{K}\right] \\ &= \begin{pmatrix} gn_{\downarrow\uparrow} & \frac{g}{2}(n_\uparrow - n_\downarrow) + 2h \\ \frac{g}{2}(n_\uparrow - n_\downarrow) + 2h & -gn^*_{\downarrow\uparrow} \end{pmatrix}. \end{aligned} \tag{4.20}$$

The commutator $\left[\hat{H}_{0i} + \hat{V}_{Ri}, \hat{T}\right]$ is zero since we know that the single-particle Hamiltonian preserves the time-reversal symmetry (the magnetic field is included in the second term). For $h = 0$ and $g = 0$ the commutator vanishes as expected. However, $h = 0$ and $g > 0$ in general can preserve the time-reversal symmetry for $n_\uparrow = n_\downarrow$ and $n_{\downarrow\uparrow} = 0$. If these conditions are not satisfied then the time-reversal symmetry is broken and the Kramers degeneracy is lifted. Evidently, even for $h > 0$ the off-diagonal elements could be equal to zero and with $n_{\downarrow\uparrow} = 0$ the commutator in Eq. (4.20) could also be equal to zero when magnetic field is $h = \frac{g}{4}(n_\uparrow - n_\downarrow)$. However, this condition requires quite peculiar choice of the system's parameters and we do not discuss it in this work.

Since the densities $n_\uparrow, n_\downarrow, n_{\uparrow\downarrow}$ and $n_{\downarrow\uparrow}$ are constructed from the eigenstates of the non-interacting system, the interparticle interaction is not allowed to break the time-reversal symmetry. This fact allows us to force the conditions $n_\uparrow = n_\downarrow$ and $n_{\downarrow\uparrow} = 0$ in our numerical calculations.

Thus, the Schrödinger-like equation for the system maintaining time-reversal

symmetry reads

$$\begin{pmatrix} \hat{H}_{0i} + \frac{g}{2}n_\uparrow & \alpha_R(\hat{p}_{iy} + i\hat{p}_{ix}) \\ \alpha_R(\hat{p}_{iy} - i\hat{p}_{ix}) & \hat{H}_{0i} + \frac{g}{2}n_\uparrow \end{pmatrix} \begin{pmatrix} \psi_{i\uparrow} \\ \psi_{i\downarrow} \end{pmatrix} = \varepsilon_i \begin{pmatrix} \psi_{i\uparrow} \\ \psi_{i\downarrow} \end{pmatrix}. \tag{4.21}$$

We see that the two-body interaction amounts to an additive term proportional to the density $n_\uparrow$, which is the only independent density functional for the time-reversal symmetric system. This term is linear in the interaction strength g and, since we do not discuss the large, comparing to the harmonic oscillator energy scale, strengths of the interaction, it may be considered with the help of the perturbation theory. We show the comparison of the single-particle energy levels of the non-interacting and interacting systems for different values of g in the Section 4.3.

4.2.2 Iteration procedure

In this subsection we discuss the details of our numerical calculations. We start with the iteration procedure employed to solve the Hartree-Fock equations and discuss the perturbative treatment of the problem. In the Section 4.3 we will see that the results of the self-consistent calculation and the perturbation theory agree very well, which in the hindsight is not surprising.

The Hartree-Fock equations are a set of Schrödinger-like equations with wavefunction density dependent potentials. The density, $n_\uparrow$, depends on the solution and the equations must be solved self-consistently. Thus, a given density produces a potential which in turn has single-particle solutions adding up to the initial density used to produce the potential. For N identical fermions the solution consists of N orthogonal single-particle states with corresponding energies. Therefore it is advantageous to use a method where the lowest N eigenstates are simultaneously obtained.

Since the external potentials in the Hamiltonian are of the same form as for the single-particle Hamiltonian in Chapter 3, we adopt the same method employed there for obtaining of the eigenstates of the interacting Hamiltonian. We expand $\psi_{i\uparrow}$ and $\psi_{i\downarrow}$ on 2D harmonic oscillator eigenfunctions diagonalize Hamiltonian in Eq. (4.17). The basis states are terminated by maxi-

mum quantum numbers, n_{xmax} and n_{ymax} in the x- and y-directions such that $\hbar\omega_x n_{xmax} = \hbar\omega_y n_{ymax}$, where the oscillator frequencies vary with deformation. Since the iteration procedure is more numerically challenging than the regular diagonalization for the single-particle problem, the total number of basis states in our calculations is less than we used in Chapter 3. However, we consider only relatively small number of occupied single-particle levels and use the basis size larger than 250, which is more than sufficient. The absolute error is always not larger than $10^{-4}\hbar\omega_y$ for all the single-particle energies we employed in the calculations.

To construct the matrix representation of the Hamiltonian in the 2D harmonic oscillator basis we need to find the matrix elements of the interacting terms. For the time-reversal symmetric system it is sufficient to calculate the following

$$\left\langle m_x m_y \right| n_\uparrow \left| m'_x m'_y \right\rangle = \int_{-\infty}^{+\infty} \int_{-\infty}^{+\infty} \mathrm{d}x\mathrm{d}y \phi_{m_x}(x)\phi_{m_y}(y) \sum_{i=1}^{N} |\psi_i|^2 \phi_{m'_x}(x)\phi_{m'_y}(y), \tag{4.22}$$

where ϕ_m are the 2D harmonic oscillator eigenfunctions. The wavefunction ψ_i can be expanded in the same basis, $\psi_i(x,y) = \sum_{j,k} a_{jk}^{(i)} \phi_j(x)\phi_k(y)$, where $a_{jk}^{(i)}$ are the expansion coefficients for the ith wavefunction ψ_i. We see that the variables in the expression for the matrix element can be separated

$$\begin{aligned}\left\langle m_x m_y \right| n_\uparrow \left| m'_x m'_y \right\rangle = \sum_{i=1}^{N} \sum_{j,k,j',k'} a_{jk}^{(i)*} a_{j'k'}^{(i)} \int_{-\infty}^{+\infty} \mathrm{d}x \phi_{m_x}(x)\phi_j(x)\phi_k(x)\phi_{m'_x}(x) \\ \int_{-\infty}^{+\infty} \mathrm{d}y \phi_{m_y}(y)\phi_{j'}(y)\phi_{k'}(y)\phi_{m'_y}(y).\end{aligned} \tag{4.23}$$

We calculate the integrals of four 2D harmonic oscillator eigenfunctions numerically with the help of the Gauss-Hermite quadratures approximation [Abramowitz 1965] which states

$$\int_{-\infty}^{+\infty} e^{-x^2} f(x)\mathrm{d}x \approx \sum_{i=1}^{n} w_i f(x_i), \tag{4.24}$$

where x_i are sample points, w_i are the associated weights and n is the number

of sample points. We store the results of the integration for use in the subsequent calculations, which accelerates the computations. The interaction matrix elements are now obtained by summing over these basic matrix elements weighted by the expansion coefficients of the single-particle wave functions.

All matrix elements are combined to give the full Hartree-Fock matrix, which by diagonalization produces eigenenergies and eigenfunctions. These eigenfunctions yield to a new set of densities which are used to construct a new Hartree-Fock Hamiltonian where the solutions are either unchanged or inserted in yet another step of the iterative procedure. Convergence to self-consistency is usually achieved after relatively few iterations, obviously depending on the set of initial wave functions. Since we vary at least one continuous parameter, like the spin-orbit coupling strength, we choose the converged solution as initial guess for a slightly different strength. This choice substantially reduces the number of iterations, and thus speeds up the computations. The results of the calculations are presented in the next Section.

4.2.3 Perturbation theory approximation

Now we discuss the perturbation treatment of the small values of the interaction strength g. We follow the standard textbook procedure to obtain the first order energy corrections. First, we compute the unperturbed ($g = 0$) solution, $\psi_i^{(0)}$, from

$$\left(\hat{H}_{0i} + \hat{V}_{Ri}\right)\psi_i^{(0)} = \varepsilon_i^{(0)}\psi_i^{(0)}. \tag{4.25}$$

Now we find the solutions of the Schrödinger equation

$$\hat{H}_{HF}\psi_i = \varepsilon_i\psi_i \tag{4.26}$$

with the perturbed Hamiltonian, i.e. we include the interparticle interaction and treat it as a perturbation. For brevity we denote the interacting part of the Hamiltonian as $\hat{U}$, with

$$\hat{U} = \frac{g}{2}\begin{pmatrix} n_\downarrow & -n_{\downarrow\uparrow} \\ -n_{\uparrow\downarrow} & n_\uparrow. \end{pmatrix} \tag{4.27}$$

We expand the wavefunction ψ_i into the basis of the unperturbed solutions $\psi_i = \sum_n c_n^{(i)} \psi_n^{(0)}$. Then the Schrödinger equation reads

$$\sum_n c_n^{(i)} \left[\varepsilon_n^{(0)} + \hat{U}\right] \psi_n^{(0)} = \sum_n c_n^{(i)} \varepsilon_i \psi_n^{(0)}. \tag{4.28}$$

If now we multiply both sides of the equation by $\psi_m^{(0)*}$ and integrate over spatial dependence we obtain

$$\left(\varepsilon - \varepsilon_m^{(0)}\right) c_m^{(i)} = \sum_n c_n^{(i)} \int \mathrm{d}\boldsymbol{r} \psi_m^{(0)*} \hat{U} \psi_n^{(0)}. \tag{4.29}$$

To find the first order corrections we write the wavefunction as $\psi_i = \psi_i^{(0)} + \delta\psi_i$, where $\delta\psi_i$ is assumed to be small compared to $\psi_i^{(0)}$ and the energy ε_i as $\varepsilon_i = \varepsilon_i^{(0)} + \delta\varepsilon_i$, where $\delta\varepsilon_i$ is a small correction to the single-particle energy.

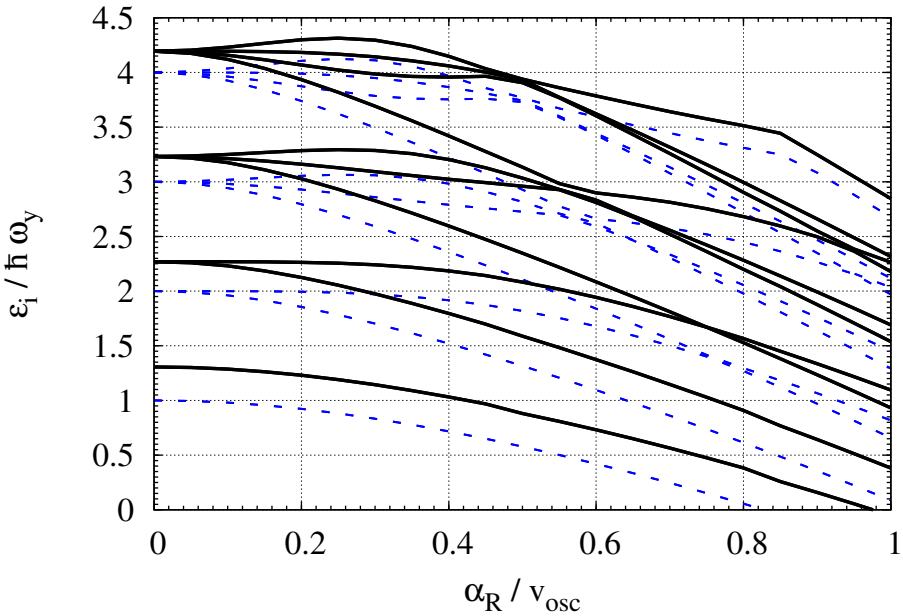

Figure 4.1: The self-consistent single-particle energy levels, ε_i, divided by $\hbar\omega_y$ are compared for interacting $g = 0.5$ (black solid) and non-interacting $g = 0.0$ (blue dashed) particles. The parameters are $N = 20$, $\omega_x = \omega_y$, $h = 0$.

The linear perturbation correction to single-particle energy of the ith particle is given by

$$\delta\varepsilon_i = \frac{g}{2}(\psi_{i\uparrow}^{(0)*}, \psi_{i\downarrow}^{(0)*}) \begin{pmatrix} n_\downarrow & -n_{\downarrow\uparrow} \\ -n_{\uparrow\downarrow} & n_\uparrow \end{pmatrix} \begin{pmatrix} \psi_{i\uparrow}^{(0)} \\ \psi_{i\downarrow}^{(0)} \end{pmatrix}. \tag{4.30}$$

For $h = 0$ the identities $n_\uparrow = n_\downarrow$ and $n_{\uparrow\downarrow} = 0$ hold and are the densities independent of the interaction strength, g. The energy correction is therefore simply given by

$$\delta\varepsilon_i = \frac{g}{2}\int (|\psi_{i\uparrow}^{(0)}|^2 + |\psi_{i\downarrow}^{(0)}|^2) n_\uparrow \mathrm{d}\mathbf{r}. \tag{4.31}$$

We calculate the correction and compare it to the results obtained via the iteration procedure. We see that the perturbation theory reproduces the exact results very well which is probably not too surprising considering the type of the interaction and rather small values of the interaction strength.

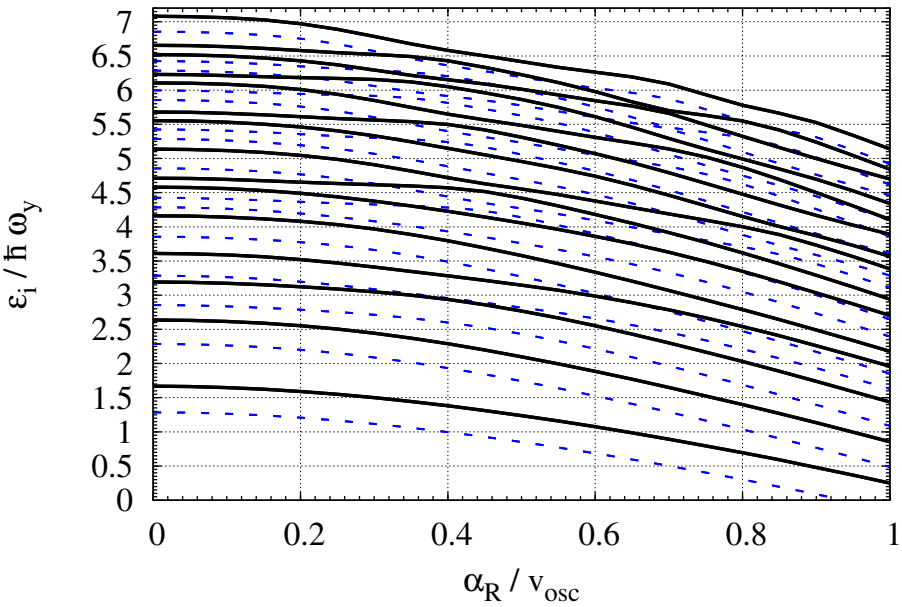

Figure 4.2: The self-consistent single-particle energy levels, ε_i, divided by $\hbar\omega_y$ are compared for interacting $g = 0.5$ (black solid) and non-interacting $g = 0.0$ (blue dashed) particles. The parameters are $N = 30$, $\omega_x = 1.57\omega_y$, $h = 0$.

4.3 Hartree-Fock single-particle spectra

In this Section we discuss the solutions obtained after solving the Hartree-Fock equations. The most direct quantities to study are the single-particle states, so we begin our discussion with them. They depend on both the external parameters, such as the deformation of the trapping potential, Rashba spin-orbit coupling strength or Zeeman magnetic field, and the internal ones, such as the number of particles and the interaction strength between the particles. To maintain the logical consistency with Chapter 3 we use the dimensionless spin-orbit coupling strength as the continuous parameter, with the single-particle energies depending on it. Since the the spin-orbit coupling strength has the dimension of velocity, we define suitable "oscillator velocity", $v_{osc} = \sqrt{\frac{2\hbar\omega_y}{m}}$. Then the dimensionless spin-orbit coupling strength is $\alpha'_R = \frac{\alpha_R}{v_{osc}}$, as in Chapter 3. In Figs. 4.1-4.3 we compare sets of ε_i for interacting and non-interacting particles. The single-particle eigenvalues of non-interacting particles are equivalent to the eigenlevels of a single particle in a harmonic trap influenced by Rashba spin-orbit coupling and Zeeman magnetic field, which were discussed in Chapter 3. This comparison lets us emphasize the effects of two-body interaction on energy spectrum of the N-particle system.

In Fig. 4.1 we start with a cylindrical harmonic trap ($\omega_x = \omega_y$) without Zeeman field. We choose the number of particles $N = 20$ since it completely fills the first four degenerate shells of 2D harmonic oscillator (recall that the levels are two-fold degenerate due to time-reversal symmetry). We see that the overall behavior of the single-particle eigenlevels of the interacting system is very similar to the non-interacting ones but for a shift in energy which is roughly independent of spin-orbit coupling. The other features of the spectrum such as the breaking of cylindrical symmetry and the avoided crossings in the spectrum are present, since they are due to the effects of spin-orbit coupling.

In Fig. 4.2 we show the eigenlevels for the deformed harmonic trap, with a "almost irrational" frequency ratio $\omega_x/\omega_y = 1.57$ which we also used in Chapter 3. The particle number is increased to $N = 30$ to see more occupied levels. The deformation lifts the cylindrical degeneracy of the non-deformed 2D harmonic oscillator and breaks the shell structure of the spectrum. The levels

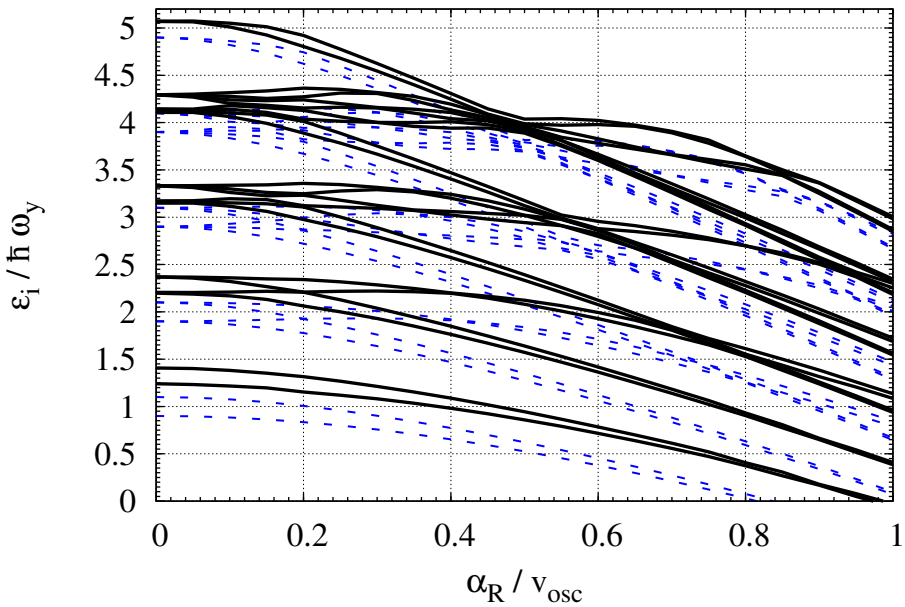

Figure 4.3: The self-consistent single-particle energy levels, ε_i, divided by $\hbar\omega_y$ are compared for interacting $g = 0.5$ (black solid) and non-interacting $g = 0.0$ (blue dashed) particles. The parameters are $N = 22$, $\omega_x = \omega_y$, $h = 0.1$.

structure appears more regular since there are less avoided crossings in the spectrum. We see that the interaction still provides an energy shift to the single-particle energy levels compared to the non-interacting case. Note that the shift is getting smaller for higher energy levels.

In Fig. 4.3 we include Zeeman magnetic field $h = 0.1\hbar\omega_y$ and break the time-reversal symmetry but maintain the cylindrical symmetry. As a result the two-fold degeneracy due to Kramers theorem is lifted but for $\alpha_R = 0$ some of the levels with higher angular momentum are still degenerate due to the degeneracies of the 2D harmonic oscillator. The total angular momentum J_z is still a good quantum number and the energy levels from different total angular momentum multiplets are allowed to cross for finite values of α_R. The particle number of $N = 22$ only partially fill the last oscillator shell for $\alpha_R = 0$. The effect of the interaction does not change from the inclusion of magnetic field and still can be seen as a shift of the single-particle energy levels ε_i.

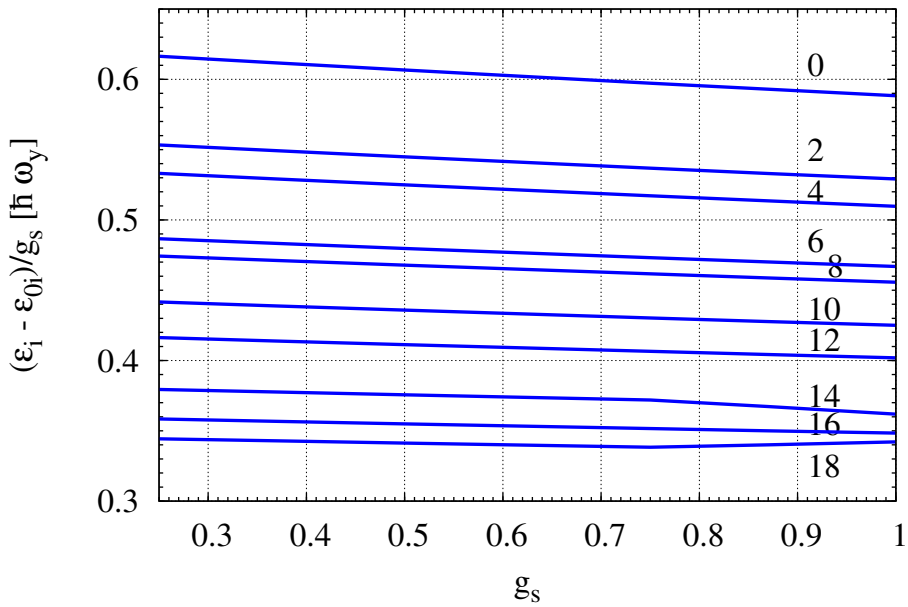

Figure 4.4: The difference between the single-particle energy levels divided by g of interacting and non-interacting systems as function of the dimensionless interaction strength g. The number of particles is $N = 20$, the harmonic trap is cylindrical ($\omega_x = \omega_y$), the Zeeman strength is $h = 0$, the Rashba spin-orbit coupling strength is $\alpha_R = 0.5v_{osc}$. The curves are numbered correspondingly to the numbers of the eigenlevels.

To assess more directly the effect of the two-body repulsion we show in Fig. 4.4 the difference between non-interacting and self-consistent Hartree-Fock single-particle energies as functions of the dimensionless interaction strength g. We plot the differences divided by the strength g to underline the nearly linear behavior. In Fig. 4.4 we plot the differences for the Rashba spin-orbit strength $\alpha_R = 0.5v_{osc}$ but the dependence is similar for the different spin-orbit strengths. The curves are numbered correspondingly to the numbers of the eigenlevels. Since magnetic field is turned off the levels are doubly degenerate and we plot only even-numbered ones. The curves are denser in the lowest parts of the figure where the largest single-particle energies appear, and thereby demonstrating that the effect decreases with increasing energy. In any case, we find that all these curves in Fig. 4.4 are almost precisely horizontal,

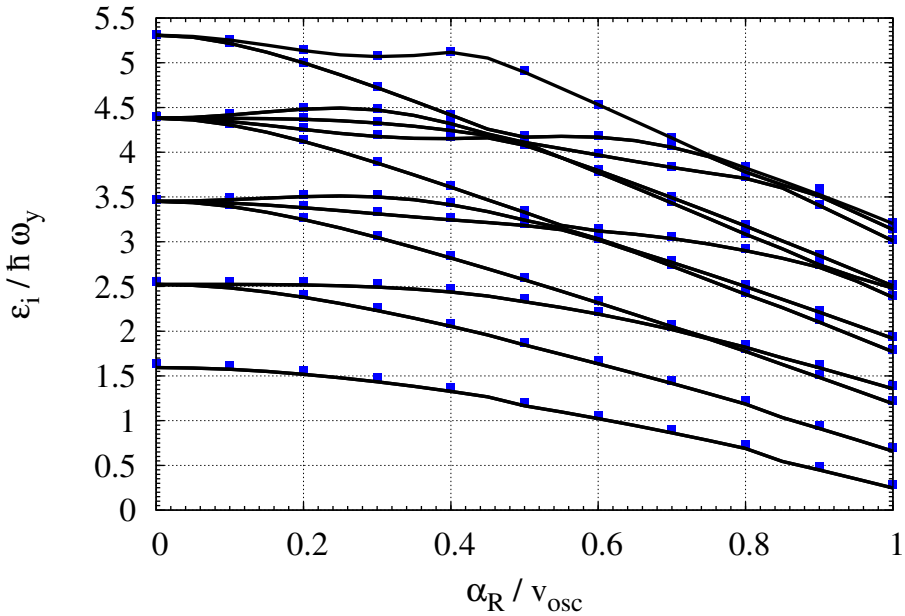

Figure 4.5: The single-particle energy levels (divided by $\hbar\omega_y$) of interacting systems as function of the dimensionless spin-orbit coupling strength α_R/v_{osc}. The number of particles is $N = 20$, the harmonic trap is cylindrical ($\omega_x = \omega_y$), the Zeeman strength is $h = 0$. The interaction strength is $g = 1.0$. The blue squares are the first order perturbation results, and the black curves are from the Hartree-Fock solutions.

which means that the dependence on the strength of the interaction is almost linear. This strongly suggests that perturbation theory would also be accurate in the same parameter range.

We turn to compare the Hartree-Fock single-particle energy spectra with the lowest order perturbation results (4.31). In Fig. 4.5 we show the comparison for cylindrical trap with the interaction strength, $g = 1$, which is the largest we use in our calculations throughout the Chapter. We see that the agreement is remarkably good, with the deviations being hardly noticeable on the figure. Evidently, for smaller interaction strengths the perturbation theory agrees with the Hartree-Fock calculation even better. Thus, the full parameter range can be concluded to be in the weakly repulsive regime. The perturbation theory also provides a good approximation for deformed traps. This can be seen in

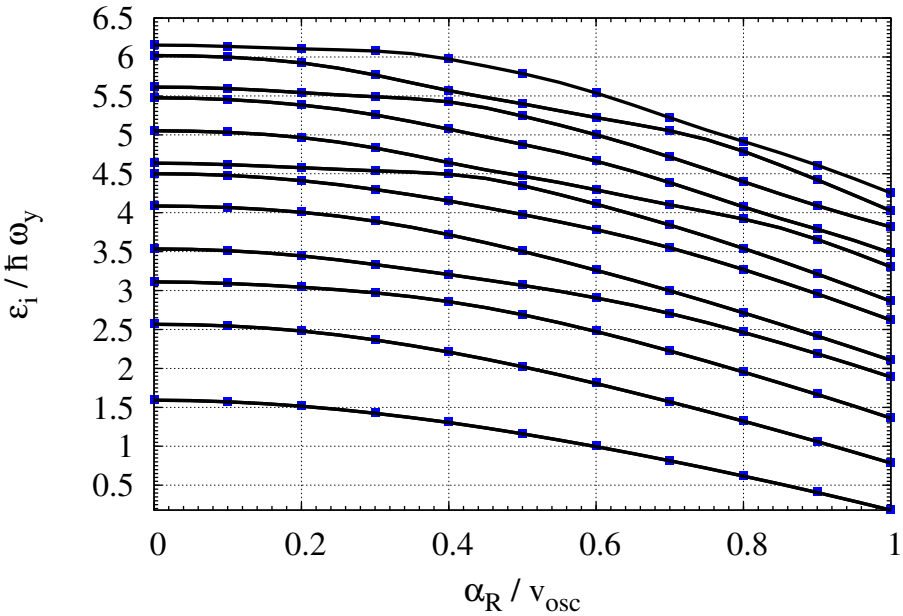

Figure 4.6: The single-particle energy levels (divided by $\hbar\omega_y$) of interacting systems as function of the dimensionless spin-orbit coupling strength α_R/v_{osc} in a deformed trap. The number of particles is $N = 20$, the interaction strength is $g = 0.5$ and the Zeeman strength is $h = 0$. The frequency ratio is $\omega_x/\omega_y = 1.57$. The *black* solid lines are Hartree-Fock solutions, and the *blue* squares are the first order perturbation theory approximation.

Figs. 4.6-4.7 for two non-integer frequency ratios, and still for time-reversal symmetric systems. The interaction strength is moderate, $g = 0.5$, but the agreement is very similar to the more degenerate cases in Fig. 4.5.

Finally, we investigate the influence of the remaining one-body parameter, that is the Zeeman field, h, which lifts the time-reversal symmetry and the corresponding degeneracy. The interplay between deformation, spin-orbit terms and Zeeman effect is seen in the self-consistent solution shown in Figs. 4.8-4.9. Comparing to Fig. 4.5, we first notice that the main features are maintained, except of course the lifting of the degeneracy. The comparison between interacting and non-interacting cases shows an overall upwards shift of all levels in the spectra by inclusion of the repulsion as in previous cases. There is also a

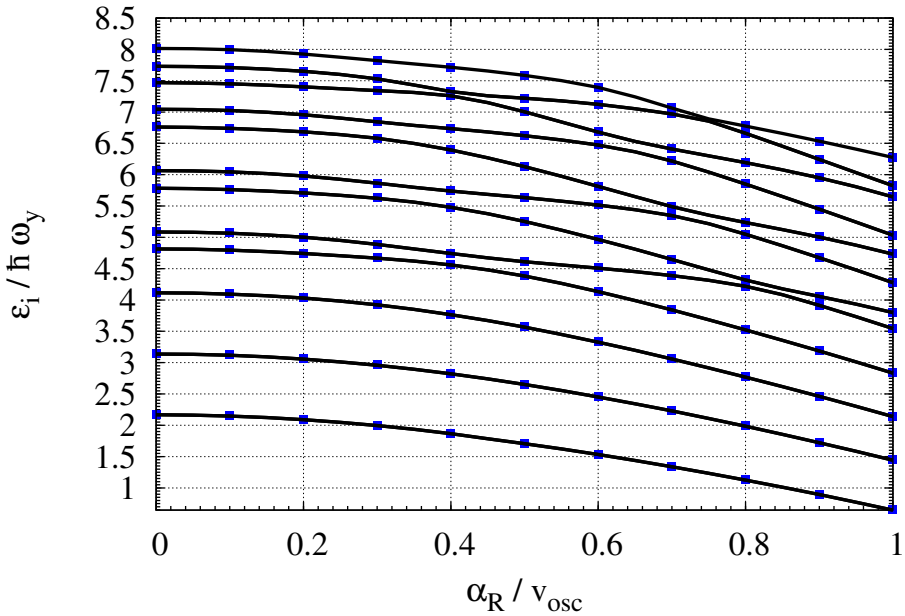

Figure 4.7: The single-particle energy levels (divided by $\hbar\omega_y$) of interacting systems as function of the dimensionless spin-orbit coupling strength α_R/v_{osc} in a deformed trap. The number of particles is $N = 20$, the interaction strength is $g = 0.5$ and the Zeeman strength is $h = 0$. The frequency ratio is $\omega_x/\omega_y = 2.71$. The *black* solid lines are Hartree-Fock solutions, and the *blue* squares are the first order perturbation theory approximation.

similar tendency of a decreasing shift with increasing ε_i.

The value of magnetic field is $h = 0.6\hbar\omega_y$ and we see in Figs. 4.8-4.9, that the levels are substantially split compared to doubly degenerate levels in Figs. 4.6-4.7. This is most clearly seen for the lowest level which is substantially below its previous time-reversed partner for small α_R. We also note that this split decreases systematically for all levels with increasing α_R. Finally, it is remarkable that the more complicated perturbation treatment of the two-body interaction still is fairly accurate even for relatively large h and moderate to substantial g-values.

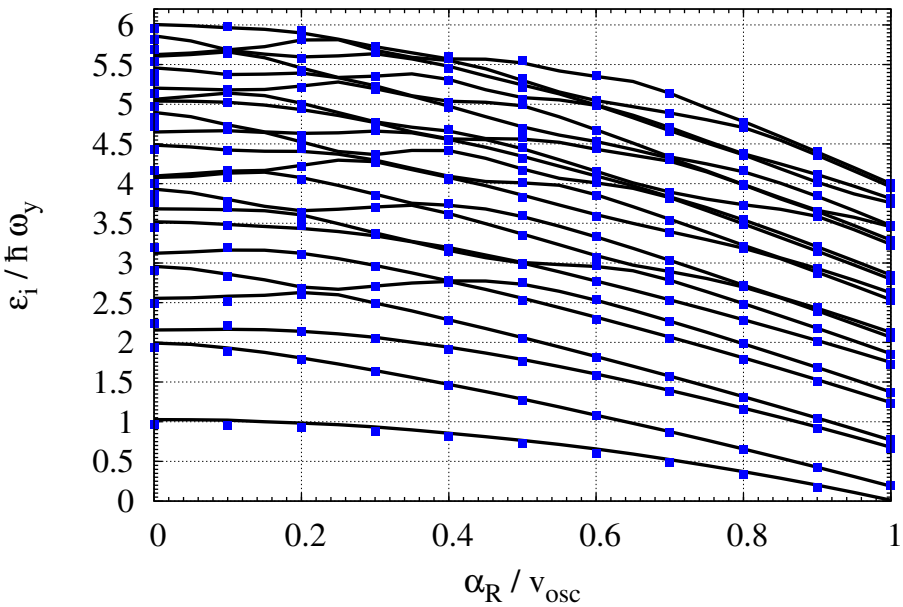

Figure 4.8: The single-particle energy levels (divided by $\hbar\omega_y$) of interacting systems as function of the dimensionless spin-orbit coupling strength α_R/v_{osc}. The number of particles is $N = 20$, the interaction strength is $g = 0.5$ and the Zeeman strength is $h = 0.6$. The frequency ratio is $\omega_x/\omega_y = 1.57$. The *black* solid lines are Hartree-Fock solutions, and the *blue* squares are the first order perturbation theory approximation.

4.4 Total energy of the interacting N-particle system

In this Section we show the difference of total energies between interacting and non-interacting systems per particle number to underline the effects of the two-body repulsion

$$\Delta E_N = \frac{1}{N}(E_N - \sum_{j=1}^{N} \varepsilon_j^0), \tag{4.32}$$

where ε_j^0 are the single-particle eigenenergies of the non-interacting Hamiltonian and E_N is the total energy of the interacting N-body system (4.18).

In Fig. 4.10 we present the results for a cylindrical ($\omega_x = \omega_y$) system with moderate repulsion strength and varying the Zeeman field. We notice that the total energy difference depends weakly on the strength of the spin-orbit

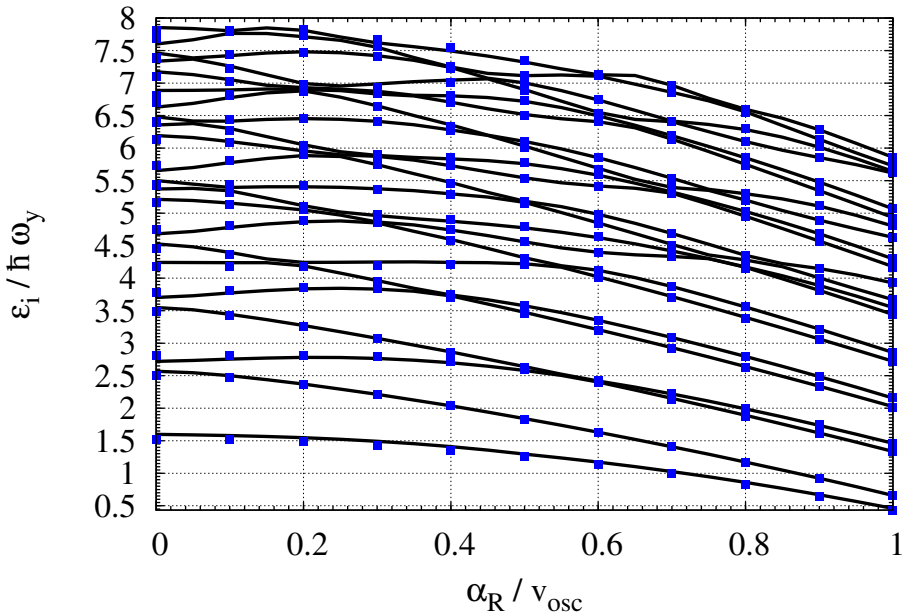

Figure 4.9: The single-particle energy levels (divided by $\hbar\omega_y$) of interacting systems as function of the dimensionless spin-orbit coupling strength α_R/v_{osc}. The number of particles is $N = 20$, the interaction strength is $g = 0.5$ and the Zeeman strength is $h = 0.6$. The frequency ratio is $\omega_x/\omega_y = 2.71$. The *black* solid lines are Hartree-Fock solutions, and the *blue* squares are the first order perturbation theory approximation.

coupling and increases with particle number. The rapid decrease of the energy differences correspond to the points of spectra where many levels come close to each other. The small Zeeman strength $h = 0.1\hbar\omega_y$ does not affect the total energy difference much, except for the points where the Fermi energy is in the vicinity of the avoided crossings. The level repulsion in a system with broken time-reversal symmetry is weaker and the additional smaller fluctuations of the total energy differences can be seen, especially for stronger Zeeman field, e.g. $h = 0.6\hbar\omega_y$.

The energy difference is obviously increasing with the strength of the repulsion as seen by the larger numerical values on the vertical axis in Fig. 4.11. The deformation dependence is in contrast very weak for all investigated particle numbers. In both Figs. 4.10 and 4.11 we see a few abrupt changes of the

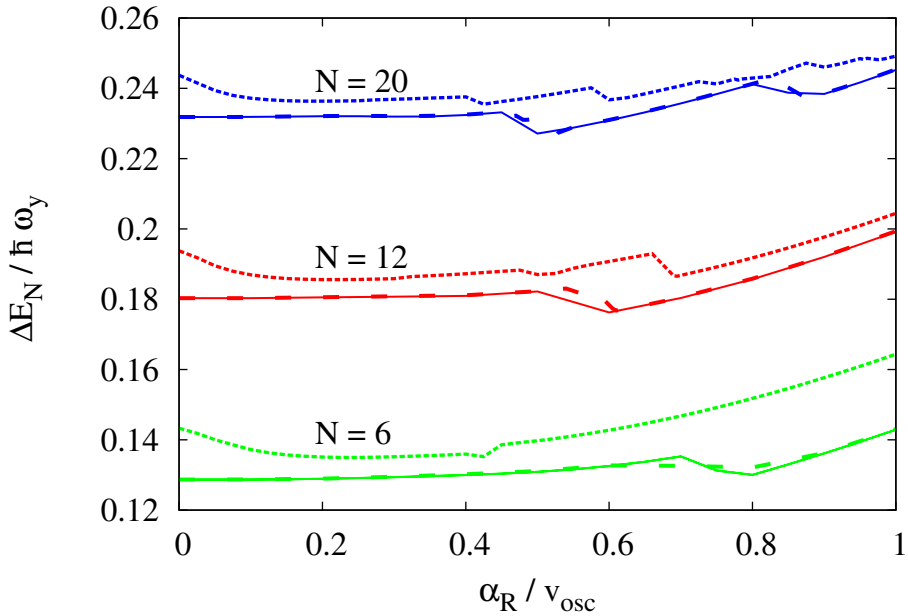

Figure 4.10: The total energy difference (divided by $\hbar\omega_y$) per particle as function of the dimensionless spin-orbit coupling strength α_R/v_{osc} from non-interacting to self-consistent Hartree-Fock solution. The system is cylindrical ($\omega_x = \omega_y$) and the repulsive strength is $g = 0.5$. The number of particles are $N = 6$ (green, lower manifold), $N = 12$ (red, middle manifold), and $N = 20$ (blue, upper manifold). The Zeeman strength is $h = 0$ (full), $h = 0.1\hbar\omega_y$ (dashed), and $h = 0.6\hbar\omega_y$ (dotted).

energy at different spin-orbit couplings depending on N. They arise when two single-particle levels avoid crossing each other at the Fermi energy. The last occupied single-particle wave function changes structure over a small range of coupling strengths precisely in these regions. For a relatively weak interaction this happens very quickly over a very small change of spin-orbit parameter. Therefore the abrupt change would disappear only with a very much finer grid, and this continuity would only be invisible on a much smaller scale than exhibited on these figures. Other avoided crossings below the Fermi energy do not change the total antisymmetrized product wave function in this abrupt manner because the system populates those levels both before and after the crossings. The same conclusion of no abrupt changes is even more obvious for crossings

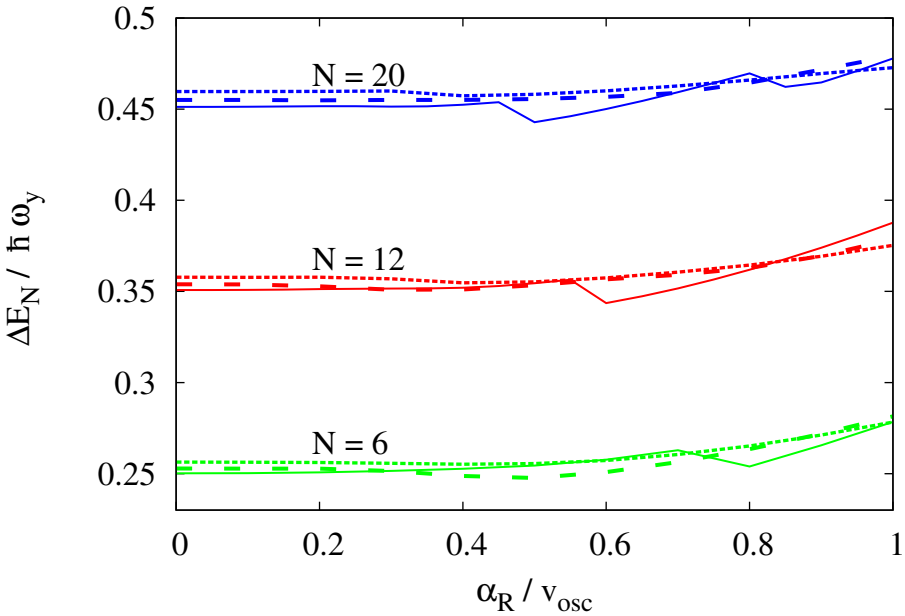

Figure 4.11: The total energy difference (divided by $\hbar\omega_y$) per particle as function of the dimensionless spin-orbit coupling strength α_R/v_{osc} from non-interacting to self-consistent Hartree-Fock solution. The Zeeman strength is $h = 0$ and the interaction strength is $g = 1$. The deformations are cylindrical ($\omega_x = \omega_y$) (full), $\omega_x = 1.57\omega_y$ (dashed), and $\omega_x = 2.71\omega_y$ (dotted).

above the Fermi level since none of them can influence the total wave function.

CHAPTER 5

Statistical treatment

In this Chapter we discuss connections between the systems discussed in chapters 3-4 to the complicated world of quantum chaos. Note that, classical chaos is a well-defined problem which was investigated for more than a century now. The definition of classical chaotic systems can be formulated in terms of Lyapunov exponent: if we follow a bunch of trajectories originated very close to each other in the phase space, then the distance between the trajectories for the regular (non-chaotic) motion may increase but will not increase too fast, in contrast to the irregular (chaotic) motion, for which the distance between the trajectories grows exponentially. The rate of such increase is called the Lyapunov exponent. With the development of quantum mechanics the question of quantum chaotic systems arose.

However, in quantum systems such definition is meaningless, since the phase-space trajectories are not well-defined in a proper quantum mechanics formalism. On the other hand, one may argue that quantum systems may also show the irregular behavior. Indeed, applying the limit $\hbar \to 0$ to a quantum system it reduces to a classical system, which must be either regular or chaotic. Moreover, even though the separation of phase-space trajectories is not a valid method to determine the irregularity of quantum systems, there are so-called signatures of quantum chaos [Fritz 2010] that provide evidence of the irregular behavior. It is also important to bear in mind that the quantum chaotic behavior shows up only if the "underlying" classical system is irregular. In other words, if the system is classically integrable, i.e., the number of degrees of freedom equals to the number of integrals of motion, then its behavior is not chaotic neither in classical nor quantum meaning.

One of signatures of quantum chaos is the spacing between neighboring single-particle energy levels of a system, which is practically immediately avail-

able for our spin-orbit coupled system from chapters 3-4. It was discovered [Berry 1977], that the statistical behavior of the single-particle nearest neighbor eigenlevels spacing distribution, $P(S)$, can be used to characterize whether the system is regular or chaotic. The variable, $S > 0$, is the energy difference between nearest neighbor levels in the energy spectrum. For classically integrable systems the nearest neighbor spacing should not correlate and $P(S)$ should have a Poisson-like form, $P(S) = e^{-S}$. On the other hand, for irregular (chaotic) motion the eigenlevels repel each other, and correlations appear between level separations. The single-particle eigenlevels spectrum shows multiple avoided crossings. In this case the celebrated Bohigas-Giannoni-Schmit conjecture [Bohigas 1984] states that the statistical behavior of the levels can be described by random matrix theory.

In this Chapter we present the statistical treatment of the single-particle energy levels of the systems discussed in Chapters 3 and 4. We do not set the full-scale analysis of the possibility of the chaotic dynamics in these systems as our goal we rather aim to show that spin-orbit coupled systems may show evidence (or signatures) of such a behavior. We describe the statistical treatment and obtained results below.

First, we consider the system discussed in Chapter 3, i.e. a particle in a deformed harmonic trap with coupled spin and motional degrees of freedom. Recall, that the Hamiltonian for such a system reads

$$\begin{aligned} H = &\left(\frac{{p_x}^2}{2m} + \frac{1}{2}m\omega_x^2 x^2 + \frac{{p_y}^2}{2m} + \frac{1}{2}m\omega_y^2 y^2\right) \otimes \hat{I} + \\ &+ \alpha_R(\hat{\sigma}_x p_y - \hat{\sigma}_y p_x) - h\hat{\sigma}_z, \end{aligned} \tag{5.1}$$

where $\mathbf{p} = \{p_x, p_y\}$ is a 2D momentum operator, $\hat{\mathbf{r}} = \{x, y\}$ is a 2D coordinate operator, ω_x and ω_y are the harmonic trap frequencies, which generally are not equal; $\hat{I}$ is a 2×2 identity matrix and $\hat{\sigma}_x$ and $\hat{\sigma}_y$ are 2×2 Pauli matrices, h is Zeeman magnetic field and α_R is the strength of Rashba spin-orbit coupling (here we stick to only Rashba term, and do not include Dresselhaus spin-orbit coupling).

The set of eigenvalues of the Hamiltonian in Eq. (5.1), $\{\varepsilon_i\}$, is the object of our statistical analysis. In particular we focus on distributions of the nearest

neighbor energy levels spacings for different values of parameters in Hamiltonian (5.1). These distributions are compared to the standard distributions obtained from random matrix spectra with specified symmetries. It was Wigner who first realized that the nearest neighbor single-particle eigenlevels spacing in nuclei follow the specific statistical distribution, depending on the symmetries of the system. These standard distributions are named after Wigner and Dyson. We shall compare the distributions obtained from the set $\{\varepsilon_i\}$ with the well known distributions named Poisson, P_P, and Wigner-Dyson distributions where the latter appears in three variations, P_{WD1}, P_{WD2} and P_{WD4}. For numerical comparison we specify these normalized distributions, i.e.,

$$P_P(S) = \exp(-S), \tag{5.2}$$

$$P_{WD1}(S) = \frac{\pi S}{2}\exp\left(-\frac{\pi S^2}{4}\right), \tag{5.3}$$

$$P_{WD2}(S) = \frac{32S^2}{\pi^2}\exp\left(-\frac{4S^2}{\pi}\right), \tag{5.4}$$

$$P_{WD4}(S) = \frac{2^{18}S^4}{3^6\pi^3}\exp\left(-\frac{64S^2}{9\pi}\right). \tag{5.5}$$

The Poisson distribution is obtained for the nearest neighbor spacing for a random matrix spectrum when the system would exhibit classically regular motion or equivalently is integrable [Fritz 2010]. In quantum mechanics this corresponds to sufficiently many quantum numbers. The energy levels are said to be uncorrelated in the sense that one eigenvalue energy is unaffected by the presence of its neighbors.

On the other hand, the three other distributions obtained from a random matrix spectrum corresponds to irregular motion where the levels avoid crossings. The main difference is the power, $\beta = 1, 2, 4$ of S in the distribution. The value of β defines a degree of energy levels repulsion [Fritz 2010]. Clearly an increasing β increases the size of the small S region as seen in Fig. 5.1. The value of β depends on the symmetries of the system. By the symmetries we mean the time-reversal symmetry and spatial rotational and/or reflection symmetries. For different "combinations" of these symmetries the parameter β gets different values. For instance, $\beta = 1$ corresponds to systems invariant un-

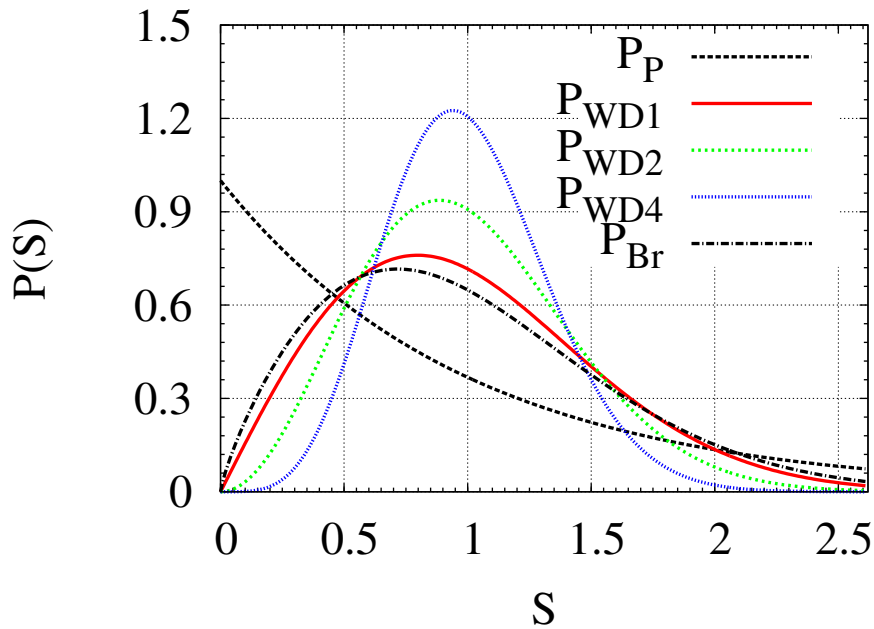

Figure 5.1: The five standard distributions in Eqs. (5.2)-(5.6). Here P_P is peaked at small S, and the peaks for the three Wigner-Dyson distributions move to larger S-values as the power of S increases. The Brody distribution is plotted for a value of the Brody parameter of $\kappa = 0.4$

der the time-reversal and with spatial rotational and/or reflection symmetries. Systems with the broken time-reversal symmetry correspond to $\beta = 2$, and systems with the time-reversal symmetry and the Kramers degeneracy (i.e. spin-$\frac{1}{2}$ particles) but without spatial symmetries correspond to $\beta = 4$ distribution.

It is worth to have in mind an "intermediate" Brody distribution [Brody 1981, Santos 2010], which describes a transition between the linear Wigner-Dyson (5.3) and Poisson distributions. The expression for the Brody distribution reads

$$P_{Br}(S) = (\kappa + 1)bS^{\kappa}\exp\left(-bS^{\kappa+1}\right), \tag{5.6}$$

where κ $(0 \leq \kappa \leq 1)$ is the Brody parameter and $b = \left[\Gamma\left(\frac{\kappa+2}{\kappa+1}\right)\right]^{\kappa+1}$. It is shown in Fig. 5.1 for $\kappa = 0.4$, and it is straightforward to see the two limits of Poisson (5.2) and Wigner (5.3) distributions obtained for $\kappa = 0$ and $\kappa = 1$, re-

spectively. The physical meaning of κ can be determined only in particular cases [Sakhr 2005].

5.0.1 Unfolding of the spectrum

In order to make the comparison between the nearest neighbor energy levels spacing distribution and the standard distributions in Eqs. (5.2)-(5.5) one has to "prepare" the set of the eigenlevels beforehand. First, we note that for the analysis of nearest neighbor distributions systematic degeneracies can be removed, since they only add points to zero spacing, $S = 0$. As we know for zero magnetic field the system obeys the time-reversal symmetry, and the energy levels are two-fold degenerate due to the Kramers theorem. Second, the analysis in terms of dimensionless distributions requires removal of the scale carrying the unit of energy. In addition, it is also necessary to even out the average scales of the spacings between the nearest energy levels arising from the different density of the energy spectrum.

We introduce the staircase function:

$$\sigma(\varepsilon) = \frac{1}{N}\int_{-\infty}^{\varepsilon}\sum_{i=1}^{N}\delta(\varepsilon' - \varepsilon_i)\mathrm{d}\varepsilon', \tag{5.7}$$

where ε is an energy value, N is the number of levels included in the analysis, and δ is the Dirac delta function. This function calculates the number of available levels below a given energy.

To smooth out $\sigma(\varepsilon)$ we substitute each delta function with a continuous normalized distribution centered at the same energy. For calculational simplicity we choose normalized Gaussians, hence obtaining

$$\begin{aligned}\bar{\sigma}_{\Delta}(\varepsilon) = &\frac{1}{\Delta\sqrt{\pi}}\frac{1}{N}\int_{-\infty}^{\varepsilon}\mathrm{d}\varepsilon'\sum_{i=1}^{N}e^{-\left(\frac{\varepsilon'-\varepsilon_i}{\Delta}\right)^2}\\ &\times\left(\frac{15}{8} - \frac{5}{2}\left(\frac{\varepsilon'-\varepsilon_i}{\Delta}\right)^2 + \frac{1}{2}\left(\frac{\varepsilon'-\varepsilon_i}{\Delta}\right)^4\right),\end{aligned} \tag{5.8}$$

where the smearing parameter, Δ, appears as the width of the Gaussians. The fourth order polynomial guarantees that any initial smooth behavior repro-

ducible by such a polynomial correctly reappears after the smoothing [BRACK 1972]. Different polynomial orders can be chosen but fourth order is sufficient to provide a reasonable stability range in Δ, where $\bar{\sigma}_\Delta(\varepsilon)$ in practice is essentially independent of Δ.

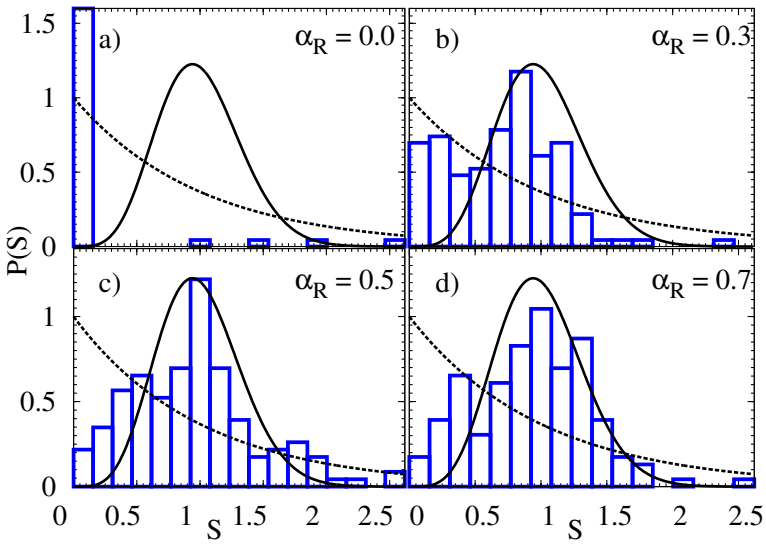

Figure 5.2: The nearest neighbor level spacing distribution for different values of the spin-orbit coupling parameter, α_R: a) $\alpha_R = 0$, b) $\alpha_R = 0.3$, c) $\alpha_R = 0.5$, d) $\alpha_R = 0.7$. We use $h = 0$ and the harmonic trap frequencies ratio is $\frac{\omega_x}{\omega_y} = 2$. The distributions are compared to the Poisson (dashed line) and Wigner (5.5) (solid line) distributions. We use 150 non-degenerate levels in our analysis. Note that α_R is in units of $\sqrt{\frac{2\hbar\omega_y}{m}}$.

Finally, to obtain a spectrum with an average level spacing normalized to one, we map the spectrum $\{\varepsilon_i\}$ onto a new spectrum, $\{e_i\}$, defined by

$$e_i = N\bar{\sigma}_\Delta(\varepsilon_i), \tag{5.9}$$

for $i = 1, \ldots, N$. This procedure is usually called *unfolding of the spectrum* [Fritz 2010, Reichl 2004]. The statistical analysis is now applied on the new scale-independent and dimensionless spectrum, $\{e_i\}$.

It is not surprising that for a reasonable statistical analysis the number of levels N should be "big enough". The size of it is of course always specific to a problem at hand. The rule of thumb is to make sure that the levels are more or

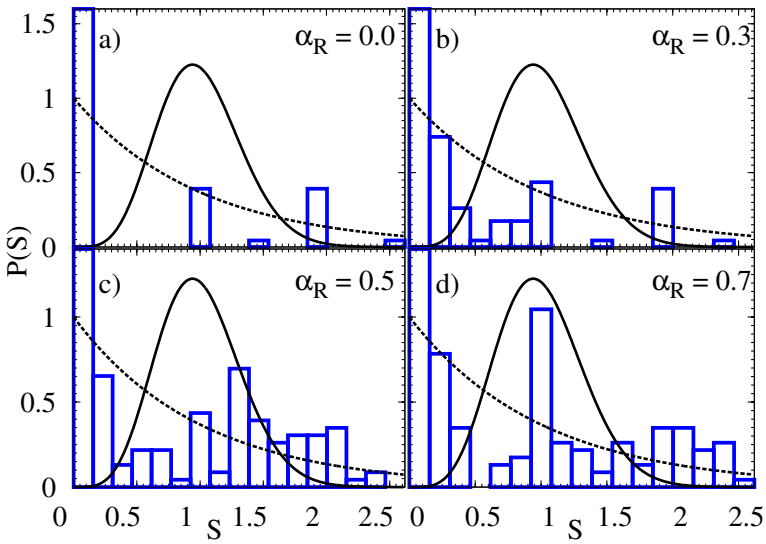

Figure 5.3: The nearest neighbor level spacing distribution for different values of the spin-orbit coupling parameter, α_R: a) $\alpha_R = 0$, b) $\alpha_R = 0.3$, c) $\alpha_R = 0.5$, d) $\alpha_R = 0.7$. We use $h = 0$ and the harmonic trap frequencies ratio $\frac{\omega_x}{\omega_y} = 10$. The distributions are compared to the the Poisson (dashed line) and Wigner (5.5) (solid line) distributions. We use 150 non-degenerate levels in our analysis. Note that α_R is in units of $\sqrt{\frac{2\hbar\omega_y}{m}}$.

less evenly distributed even before the unfolding of the spectrum. In that case the unfolding works the best and the statistical properties of spectra are the most evident. For the systems without the Zeeman term we used 300 (doubly degenerate) energy levels and in the presence of the Zeeman field we used 150 eigenlevels. We make sure that the increase of the number of levels does not change the qualitative character of levels statistics.

5.0.2 Nearest neighbor distributions (non-interacting case)

Now we apply the statistical analysis described above to the single-particle energy levels of Hamiltonian (5.1). We consider different values of frequency ratios of the 2D harmonic trap and strengths of the Rashba spin-orbit coupling. Finally, we introduce the Zeeman magnetic field to see how it affects the distributions. We compare the histograms, obtained after unfolding of the spectra, to the Poisson and Wigner-Dyson distributions from Eqs. (5.2) and (5.5). It is

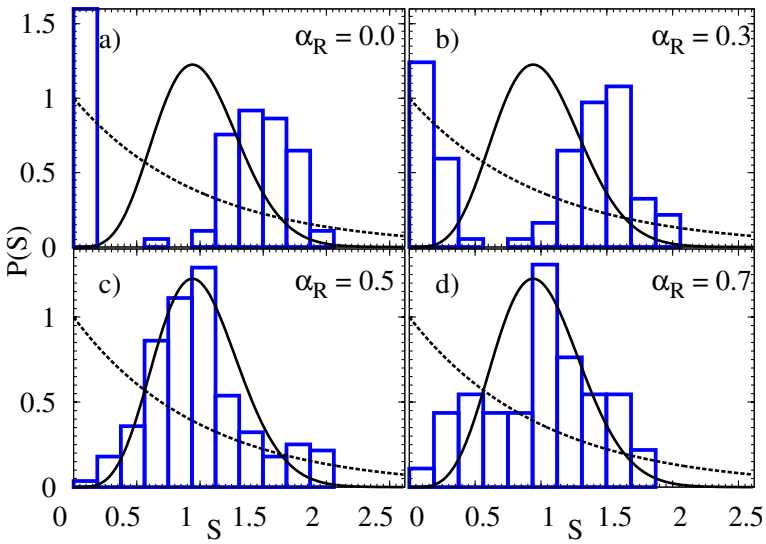

Figure 5.4: The nearest neighbor level spacing distribution for different values of the spin-orbit coupling parameter, α_R: a) $\alpha_R = 0$, b) $\alpha_R = 0.3$, c) $\alpha_R = 0.5$, d) $\alpha_R = 0.7$. The harmonic trap frequencies ratio $\frac{\omega_x}{\omega_y} = 1.57$. The distribution is compared to the Poisson (dashed line) and Wigner (5.5) distributions. We use 150 non-degenerate levels in our analysis. Note that α_R is in units of $\sqrt{\frac{2\hbar\omega_y}{m}}$.

important to notice that the magnetic field is absent and the trapping potential is deformed we use the Wigner distribution from Eq. (5.5).

We avoid the most symmetric case of the cylindrically symmetric oscillator ($\omega_x = \omega_y$) where the regular structure and large degeneracy initially prohibits a meaningful statistical analysis. That is why we first consider the $\omega_x/\omega_y = 2$ case since the deformation breaks the spatial symmetry and lifts corresponding degeneracies. Still, for $\alpha_R = 0$ case there are many degenerate energy levels since the frequency ratio is an integer number. However, with $\alpha_R > 0$ these degeneracies are also lifted and in Fig. 5.2 we see that the nearest neighbor spacings distributed more evenly, although they do not resemble the Wigner distribution in Eq. (5.5).

In Fig. 5.3 we show the distributions for larger deformation $\omega_x/\omega_y = 10$. As we saw in Chapter 3 the Hamiltonian in Eq. (5.1) has the energy spectrum reminiscent to the one of a spin-orbit coupled particle in 1D harmonic trap. The energy levels are not only degenerate but also equidistant (at least for

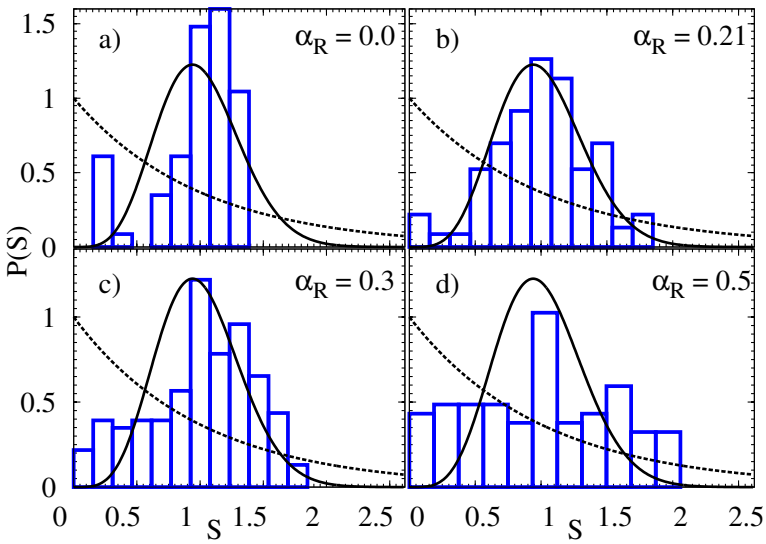

Figure 5.5: The nearest neighbor level spacing distribution for different values of the spin-orbit coupling parameter, α_R: a) $\alpha_R = 0$, b) $\alpha_R = 0.21$, c) $\alpha_R = 0.3$, d) $\alpha_R = 0.5$. Note that the choice of spin-orbit strengths differs from the previous figures, due to the faster transition to the Wigner-regime. The harmonic trap frequencies ratio $\frac{\omega_x}{\omega_y} = 2.71$. The distribution is compared to the Poisson (dashed line) and Wigner (5.5) distributions. We use 150 non-degenerate levels in our analysis. Note that α_R is in units of $\sqrt{\frac{2\hbar\omega_y}{m}}$.

the lowest part of the spectrum) which leads to not so well distributed nearest neighbor spacings with a large peak at $S \to 0$, due to the degeneracies in the spectrum. For stronger Rashba spin-orbit coupling strengths the spacings distributed more evenly but the peak remains and the histogram does not resemble the Wigner distribution at all.

Thus, we see that for integer frequency ratios the spectrum of the particle is still too regular and does not lead to the Wigner-Dyson distribution. However, the case changes for non-integer frequency ratios. We consider two cases: $\omega_x/\omega_y = 1.57$ and $\omega_x/\omega_y = 2.71$, to maintain consistency with the previous chapters.

The interplay between the deformed harmonic oscillator and spin-orbit coupling contributions leads to the spectrum with multiple avoided crossings, since the spatial symmetries are broken and the actual crossings are prohibited.

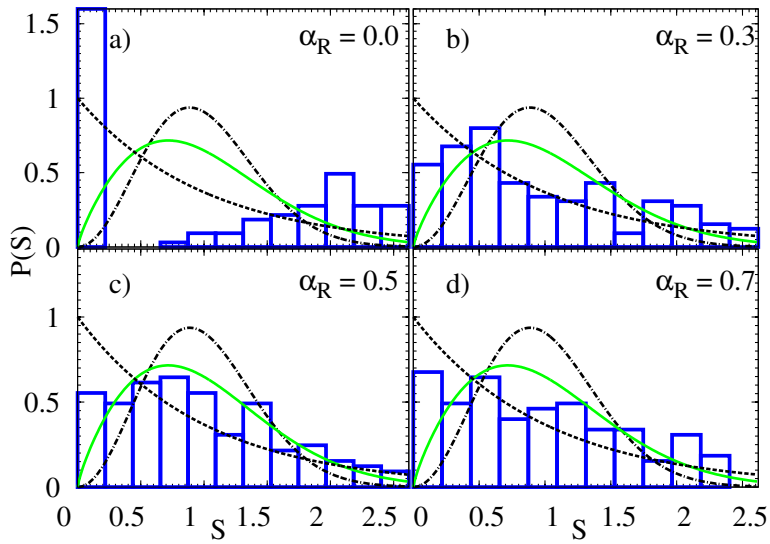

Figure 5.6: The nearest neighbor level spacing distribution for different values of spin-orbit coupling parameter, α_R: a) $\alpha_R = 0$, b) $\alpha_R = 0.3$, c) $\alpha_R = 0.5$, d) $\alpha_R = 0.7$. The harmonic trap frequencies ratio $\frac{\omega_x}{\omega_y} = 1.57$. The distributions are compared to the Poisson (dashed line), Brody (solid blue line) (5.6), quadratic Wigner (solid green line) (5.4) distributions, and quartic Wigner (solid black line) (5.5) distributions. The energy of Zeeman magnetic field is $\hbar\omega_y/2$. The Brody parameter value is $\kappa = 0.4$. We use 150 non-degenerate levels in our analysis. Note that α_R is in units of $\sqrt{\frac{2\hbar\omega_y}{m}}$.

In this case the spacing distribution is expected to follow quartic Wigner-Dyson distribution in Eq. (5.5), since the two-fold Kramers degeneracy is present.

The lack of symmetries for non-integer frequency ratios leads to the distributions shown in Figs. 5.4 and 5.5. We can see that in both cases the histograms resemble the Wigner-Dyson distribution, P_{WD4}, very well for some values of the spin-orbit coupling strength, i.e., $\alpha_R = 0.5\sqrt{\frac{2\hbar\omega_y}{m}}$ for $\omega_x/\omega_y = 1.57$, Fig. 5.4c, and $\alpha_R = 0.21\sqrt{\frac{2\hbar\omega_y}{m}}$ for $\omega_x/\omega_y = 2.71$, Fig. 5.5b. As we discussed earlier, such a distribution of nearest neighbor spacings of the energy levels signifies that the dynamics of the system is quantum chaotic.

The inclusion of the Zeeman magnetic field, h, breaks the time-reversal symmetry and changes the distributions. In Figs. 5.6 and 5.7 we show them for the same values of trap deformations, $\omega_x/\omega_y = 1.57$ and $\omega_x/\omega_y = 2.71$, respectively, and several Rashba spin-orbit couplings. In Fig. 5.6 the value of

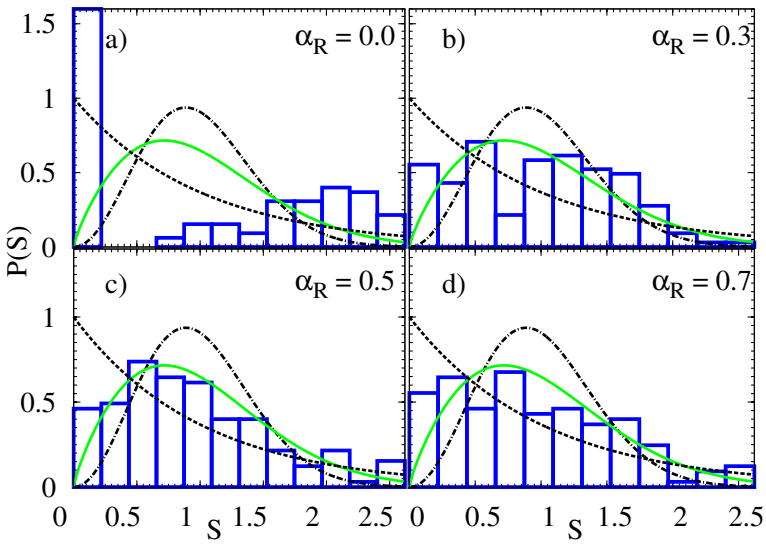

Figure 5.7: The nearest neighbor level spacing distribution for different values of spin-orbit coupling parameter, α_R: a) $\alpha_R = 0$, b) $\alpha_R = 0.3$, c) $\alpha_R = 0.5$, d) $\alpha_R = 0.7$. The harmonic trap frequencies ratio $\frac{\omega_x}{\omega_y} = 1.57$. The distributions are compared to the Poisson (dashed black line), Brody (dashed and dotted green line) (5.6), and quadratic Wigner (solid black line) (5.4) distributions. The energy of Zeeman magnetic field is $\hbar\omega_y$. The Brody parameter value is $\kappa = 0.4$. We use 150 non-degenerate levels in our analysis. Note that α_R is in units of $\sqrt{\frac{2\hbar\omega_y}{m}}$.

magnetic field is $h = 0.5\hbar\omega_y$ and in Fig. 5.7 the value is $h = \hbar\omega_y$. We compare the obtained histograms with the Poisson (5.2), quadratic Wigner-Dyson (5.4) and Brody (5.6) with $\kappa = 0.4$ distributions. We use the quadratic Wigner-Dyson distribution instead of the quartic one since the magnetic field breaks the time-reversal symmetry. Thus, it is expected that systems with irregular dynamics have the nearest neighbor spacing distribution which resembles the distribution from Eq. (5.4).

However, in Figs. 5.6-5.7 we see that in fact the histograms better resemble the Brody distribution (5.6), especially for the strength of Rashba spin-orbit coupling $\alpha_R \gtrsim 0.5$ in the units of $\sqrt{2\frac{\hbar\omega_y}{m}}$. Moreover, we notice the tendency for the histograms to shift towards Poisson distribution (5.2) with increasing α_R.

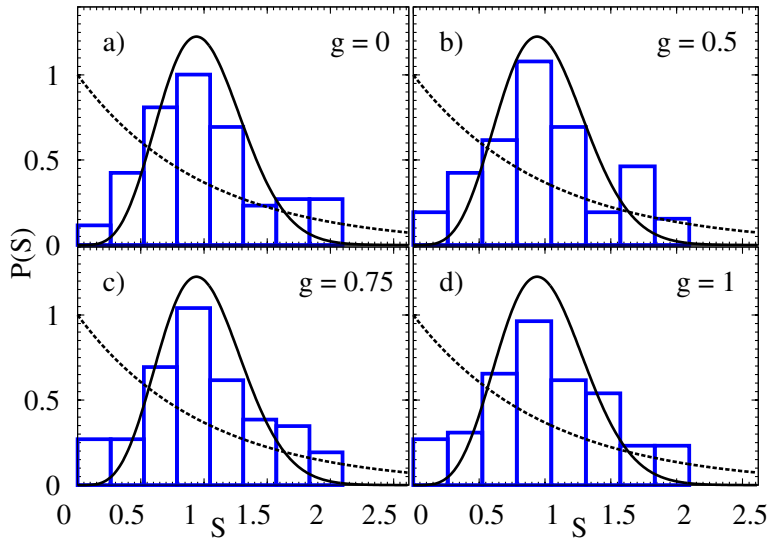

Figure 5.8: The nearest neighbor level spacing distribution of the Hartree-Fock single-particle energy levels for frequency ratio $\omega_x/\omega_y = 1.57$ and spin-orbit coupling $\alpha_R = 0.5$. Every panel corresponds to different interaction strength g. The distributions are compared to the Poisson (dashed line) and quartic Wigner (solid black line) (5.5) distributions. We use 100 non-degenerate levels in our analysis. Note that α_R is in units of $\sqrt{\frac{2\hbar\omega_y}{m}}$.

5.0.3 Nearest neighbor distributions (interacting case)

Let us now perform the statistical analysis of the single-particle Hartree-Fock energy levels obtained in Chapter 4. We follow the same procedure: we start with the unfolding of the energy spectrum and then compare the histograms depicting the distribution of the nearest neighbor levels spacing to the Poisson and Wigner-Dyson distributions. The comparison is made for the cases that show Wigner-like distributions in a single-particle case, i.e. for deformed harmonic traps with non-integer frequency ratios and values of Rashba spin-orbit coupling strength used in the non-interacting case. The number of interacting particles is $N = 100$ and in the analysis we use 100 non-degenerate single-particle levels, which means that the lower half of the levels used in the analysis is occupied. In Figs. 5.8-5.9 we present our findings for different interaction strengths. We see that the interparticle interactions can affect the distributions in different ways: In Fig. 5.8 we see that the Wigner-like distribu-

tion in the non-interacting case is not affected too strongly by the interaction and conserves the main features of the distribution even for stronger interaction strengths. However, in Fig. 5.9 we see that the non-interacting distribution is not too close to the quartic Wigner-Dyson distributions but the interaction improves it a lot.

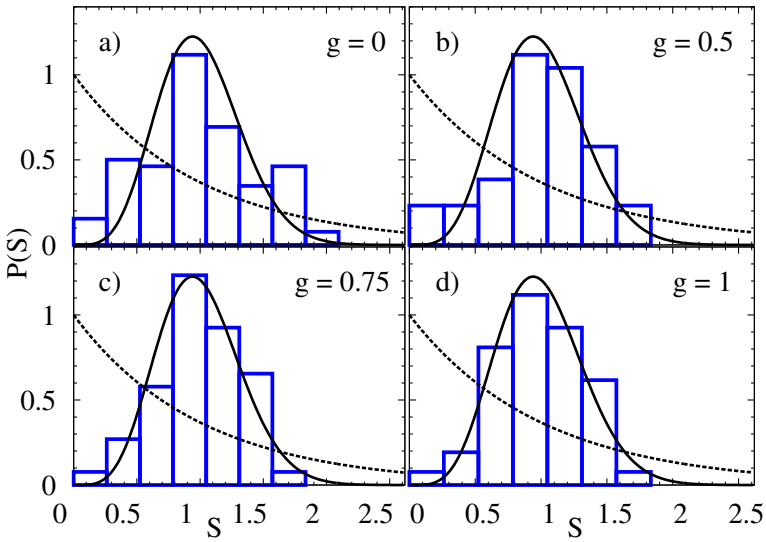

Figure 5.9: The nearest neighbor level spacing distribution of the Hartree-Fock single-particle energy levels for frequency ratio $\omega_x/\omega_y = 2.71$ and spin-orbit coupling $\alpha_R = 0.5$. Every panel corresponds to different interaction strength g. The distributions are compared to the Poisson (dashed line) and quartic Wigner (solid black line) (5.5) distributions. We use 100 non-degenerate levels in our analysis. Note that α_R is in units of $\sqrt{\frac{2\hbar\omega_y}{m}}$.

In conclusion, it is important to say that the goal of this Chapter was to show that systems of particles in a deformed harmonic trap show the so-called signatures of quantum chaos. A more thorough investigation of such systems in the context of irregular dynamics may be an interesting and informative task. Unfortunately, such an investigation is beyond the scope of this work and here we only tried to show the potentially interesting properties of the system. We saw that several sets of parameters lead to the required signatures even in the non-interacting system of particles. Moreover, the interaction between particles affects the spectrum of the system and may lead to better correspondence

between the nearest neighbor energy level spacing distribution and Wigner-Dyson distributions, i.e. the control over the strength of interaction proves to be a valuable tool to change the dynamics of the system from regular to irregular.

CHAPTER 6

State transfer in strongly interacting systems. Introduction

In this Chapter we continue to the second part of this work. From systems with spin-orbit coupling we switch to quantum state transfer in spin chains. First of all, we introduce the system and set our goals.

The developments in quantum simulations, especially in cold atoms set-ups, give us an opportunity to access the physics of lower dimensions with an unprecedented level of control. We already discussed the two-dimensional systems in the previous chapters and in the following we will focus on one-dimensional set-ups. But first let us discuss our motivation in a few words.

It is a not a secret that despite the Moore's law [Moore 1998] the physical limit for the computation capacity of "conventional" computers is approaching, which leads to the continuous search for alternatives. One of such new approaches is the so-called quantum computations which aims to use the specific properties of quantum system to create new computational protocols. One of the main inspirers of this idea (and also of the concept of quantum simulations) was Richard Feynman [Feynman 1982].

The crucial part of any computation is data transfer and the whole field of quantum communication is determined to find both media and protocols for information transfer in quantum computing systems. The quantum analogy of a *bit*, as a unit of information, is a *qubit*, which is a two-state quantum-mechanical system. In contrast to a classical bit which takes only one of the two states (conventionally denoted as "0" and "1"), the qubit exists in a superposition of the both states simultaneously and due to this property it is necessary to

pick adequate physical systems to represent a qubit [Lambropoulos 2007]. In the original proposal [Cirac 1997] a strong coupling between photons and optical cavities was presented as a transmission protocol [Blinov 2004], however, later the attention was shifted towards using the polarization degree of freedom of a single photon to encode a qubit [Duan 2001, Duan 2010, Stute 2013]. Today there is a lot of research ongoing to use spin-$\frac{1}{2}$ chains as a transfer device on short distances with the spin-$\frac{1}{2}$ particle playing role of a qubit [Bose 2008, Christandl 2004, KAY 2010].

In order to realize state transfer in spin chains one requires a physical system that can be described by a spin model and a potential candidate is a system of strongly interacting atoms trapped in a 1D potential. Such systems are realizable [Moritz 2003, Stöferle 2004, Kinoshita 2004, Paredes 2004, Kinoshita 2006] and allow one to study various phenomena, such as fermionization for strong interaction [Zürn 2013a], pairing [Zürn 2013b], a two-site Hubbard model [Murmann 2015a], Heisenberg spin models [Murmann 2015b] and others.

Let us briefly discuss the Hamiltonian of strongly-interacting atoms in a 1D trapping potential and the mapping into Heisenberg XXZ spin model. Here we follow the results obtained in Refs. [Volosniev 2015a, Volosniev 2015b, Volosniev 2015c, Zinner 2014] in which a new method to solve exactly the systems of strongly-interacting atoms trapped in an arbitrary 1D potential. The results of the next Chapter are based on these solutions which are not a part of this dissertation, so we try to give a short description of the method and invite the reader to follow the original publications. The mapping of the Hamiltonian of strongly-interacting atoms in 1D trap into Heisenberg XXZ spin model is also discussed here but can be found in more details in Refs. [Volosniev 2015b, Levinsen 2015, Deuretzbacher 2014].

We consider a two-component Bose system of strongly-interacting atoms in one spatial dimension confined by a trapping potential. We denote the different components of atoms as spin-up and spin-down, such that the number of particles is $N = N_\uparrow + N_\downarrow$. The interaction between the atoms is modeled by a

Dirac delta function and the Hamiltonian can be written as (we set $\hbar = 1$)

$$H = \sum_{\sigma=\uparrow,\downarrow} \sum_{i=1}^{N_\sigma} \left[H_0(x_{\sigma,i}) + \frac{g_{\sigma\sigma}}{mL} \sum_{i'>i}^{N_\sigma} \delta(x_{\sigma,i} - x_{\sigma,i'}) \right] + \\ + \frac{g_{\uparrow\downarrow}}{mL} \sum_{i=1}^{N_\uparrow} \sum_{i'=1}^{N_\downarrow} \delta(x_{\uparrow,i} - x_{\downarrow,i'}) + \sum_{j=1}^{N} h_j \sigma_z^j, \tag{6.1}$$

where $\sigma = \{\uparrow,\downarrow\}$ denotes the component of atoms, $H_0(x) = -\frac{1}{2m}\frac{\partial^2}{\partial x^2} + \frac{1}{mL}V(x/L)$ is a single-particle Hamiltonian of a particle in a one-dimensional trapping potential $V(x/L)$, $x_{\sigma,i}$ is the coordinate of the ith particle of the component σ, m is the mass of a particle which is equal for all particles, L is characteristic length of the confining potential, h_j is a spatially inhomogeneous magnetic field, which is non-zero only in the middle, i.e. $h_1 = h_N = 0$ and $h_i = h$ for $i = 2, 3, \ldots, N-1$, and $\boldsymbol{\sigma}^j = (\sigma_x^j, \sigma_y^j, \sigma_z^j)$ are the Pauli matrices acting on a spin at site j. The interaction strengths are related as $g_{\uparrow\downarrow} = g_{\downarrow\uparrow} \equiv g > 0$ and $g_{\uparrow\uparrow} \equiv \kappa g$, with $\kappa > 0$. The parameter κ defines the interspecies interaction for bosonic atoms and in the limit of $\kappa \to \infty$, the Hamiltonian (6.1) can be used to describe fermions. The most general N-particle eigenstate of the system can be written as [Volosniev 2015c]

$$\Psi = \sum_k a_k \theta(x_{P_k(1)}, \ldots, x_{P_k(N)}) \Psi_0(x_1, \ldots, x_N), \tag{6.2}$$

where the summation goes over the $N!$ permutations, P_k, of the coordinates, a_k are the expansion coefficients that depend on the ordering of the particle, $\theta(x_1, \ldots, x_i, \ldots, x_j, \ldots, x_N) = 1$, if $x_1 < x_2 < \cdots < x_i < \cdots < x_j < \cdots < x_N$ and zero otherwise. The wavefunction Ψ_0 is a fully antisymmetrized N-particle wavefunction, a Slater determinant constructed from the single-particle solutions of the Schrödinger equation of a particle in the potential $V(x)$. It describes the non-interacting N-particle system with energy E_0. Note that the energy E_0 is $M(N_\uparrow, N_\downarrow) = N!/(N_\uparrow! N_\downarrow!)$ times degenerate since the energy of the non-interacting system does not depend on the particles ordering. It was shown [Zinner 2014, Volosniev 2015b, Volosniev 2015c] that in the limit $1/g \to 0$ the N-particle energy of the interacting system can be written in the

linear order in $1/g$ as

$$E = E_0 - \frac{1}{g}\frac{\sum_{j=1}^{N-1}(A_j + \frac{2}{\kappa}C_j + \frac{2}{\kappa}D_j)\alpha_j}{\sum_{k=1}^{M(N_\uparrow,N_\downarrow)} a_k^2}, \tag{6.3}$$

where $A_j = \sum_{k=1}^{M(N_\downarrow-1,N_\uparrow-1)}(a_{j|k}-b_{j|k})^2$, $C_j = \sum_{k=1}^{M(N_\downarrow,N_\uparrow-2)} c_{j|k}^2$ and $D_j = \sum_{k=1}^{M(N_\downarrow-2,N_\uparrow)} d_{j|k}^2$. Here the notation $a_{j|k}$ denotes those coefficients a_k in the expansion (6.2) with $x_\uparrow$ at position j followed by $x_\downarrow$ at position $j+1$. Similarly, the coefficients $b_{j|k}$ are the coefficients with $x_\downarrow$ at position j followed by $x_\uparrow$ at position $j+1$, the coefficients $c_{j|k}$ are are the coefficients with $x_\uparrow$ at position j followed by $x_\uparrow$ at position $j+1$, and the coefficients $d_{j|k}$ are the coefficients with $x_\downarrow$ at position j followed by $x_\downarrow$ at position $j+1$. For fermions the coefficients C_j and D_j are set to zero, due to the Pauli principle.

The coefficients α_j are geometric factors which depend both on the total number of particles and on the single-particle solutions of the Schrödinger equation of a particle in the potential $V(x)$. The explicit expression for α_j is given by

$$\alpha_j = \frac{1}{m^2}\frac{\int \prod_{i=1}^{N} \mathrm{d}x_i \theta(x_1,\ldots,x_N)\delta(x_1-x_j)(\partial\Psi_0)^2}{\langle\Psi \mid \Psi\rangle}, \tag{6.4}$$

where $\partial\Psi_0 = \left(\frac{\partial\Psi_0}{\partial x_1}\right)_{x_1=x_N}$, i.e. one first takes a partial derivative of the non-interacting N-particle wave function Ψ_0 with the respect to x_1 and then set $x_1 = x_N$.

Calculating the coefficients α_j is a complicated numerical task, since it involves multidimensional integration, and so it is natural to use approximations to obtain their values. A local density approximation (LDA) is often used to calculate the values α_j and proved to agree with the exact results very well for harmonic potential [Deuretzbacher 2014, Levinsen 2015]. However, for more complicated shapes of potential the LDA agreement with the exact results is much worse, which affects both static and dynamic properties of the system [Marchukov 2015a]. There are other approximate methods available that can be used to provide very accurate results for systems with up to $N = 30$ particles [Loft 2015].

As we mentioned before, for strong interactions ($g \to \infty$) the Hamilto-

nian in Eq. (6.1) can be mapped onto the Heisenberg XXZ spin model [Volosniev 2015a, Volosniev 2015b, Deuretzbacher 2014, Levinsen 2015]. The Hamiltonian of the spin model reads

$$H_s = -\frac{1}{2}\sum_{j=1}^{N-1}\left[J_j\hat{\sigma}^j\hat{\sigma}^{j+1} - \frac{2J_j}{\kappa}\hat{\sigma}_z^j\hat{\sigma}_z^{j+1}\right] + \sum_{j=1}^{N} h_j\hat{\sigma}_z^j, \tag{6.5}$$

Here the exchange interaction coefficients J_j are related to the geometric factors α_j as

$$J_j \equiv -\frac{\alpha_j}{g}. \tag{6.6}$$

This mapping confirms that the system of strongly-interacting atoms in 1D can be used to simulate spin chains and explore quantum state transfer in such systems. By manipulating the shape of the potential we can control the values of the exchange constants J_j. In the next Chapter we describe the idea of conditional state transfer in spin chains with $N = 3, 4$ and 5 particles. An important component of the idea is that the exchange coefficients follow the ratio $J_1/J_2 \ll 1$. In the next Chapter we also present a specific shape of the potential which allows one to obtain such a ratio.

CHAPTER 7

Quantum state transfer in spin chains

In this Chapter we discuss quantum state transfer in spin chains, which are realized in systems of strongly-interacting atoms trapped in a 1D potential. We define the Hamiltonian of the problem and discuss spin chains consisting from three, four and five atoms. We present the idea of conditional state transfer, which describes the conditions under which an initial state can and cannot be transfered with high fidelities (close to or equal unity). In the last Section we show an example of the trapping potential which could be use for such purposes.

7.1 Effective spin chain Hamiltonian

We consider a two-component Bose system of strongly-interacting atoms in one spatial dimension (1D) confined by a trapping potential. We denote the different components of atoms as spin-up and spin-down, such that the number of particles is $N = N_\uparrow + N_\downarrow$. The interaction between the atoms is modeled by a Dirac delta function and the Hamiltonian can be written as (we put $\hbar = 1$)

$$H = \sum_{\sigma=\uparrow,\downarrow} \sum_{i=1}^{N_\sigma} \left[H_0(x_{\sigma,i}) + \frac{g_{\sigma\sigma}}{mL} \sum_{i'>i}^{N_\sigma} \delta(x_{\sigma,i} - x_{\sigma,i'}) \right] + \frac{g_{\uparrow\downarrow}}{mL} \sum_{i=1}^{N_\uparrow} \sum_{i'=1}^{N_\downarrow} \delta(x_{\uparrow,i} - x_{\downarrow,i'}) + \sum_{j=1}^{N} h_j \sigma_z^j, \tag{7.1}$$

where $\sigma = \{\uparrow, \downarrow\}$ denotes the component of atoms, $H_0(x) = -\frac{1}{2m}\frac{\partial^2}{\partial x^2} + \frac{1}{mL}V(x/L)$ is a single-particle Hamiltonian of a particle in a one-dimensional trapping potential $V(x/L)$, $x_{\sigma,i}$ is a coordinate of the ith particle of the component σ, m is the mass of a particle and is assumed equal for all particles, and L is

characteristic length of the confining potential, h_j is a spatially inhomogeneous magnetic field, which is non-zero only in the middle, i.e. $h_1 = h_N = 0$ and $h_i = h$ for $i = 2, 3, \ldots, N-1$, and $\sigma^{\mathbf{j}} = (\sigma_x^j, \sigma_y^j, \sigma_z^j)$ are the Pauli matrices acting on a spin at site j. The interaction strengths are related as $g_{\uparrow\downarrow} = g_{\downarrow\uparrow} \equiv g > 0$ and $g_{\uparrow\uparrow} \equiv \kappa g$, with $\kappa > 0$. The parameter κ defines the interspecies interaction for bosonic atoms and in the limit of $\kappa \to \infty$, the Hamiltonian (7.1) can be used to describe fermions.

For strong interactions, $g \to \infty$, the Hamiltonian in Eq. (7.1) can be mapped onto the Heisenberg XXZ spin model [Volosniev 2015a,Volosniev 2015b,Deuretzbacher 2014, Levinsen 2015].

$$H_s = -\frac{1}{2}\sum_{j=1}^{N-1}\left[J_j\sigma^{\mathbf{j}}\sigma^{\mathbf{j+1}} - \frac{2J_j}{\kappa}\sigma_z^j\sigma_z^{j+1}\right] + \sum_{j=1}^{N} h_j\sigma_z^j, \tag{7.2}$$

where J_j are position-dependent interaction coefficients. Below we present the static and dynamic properties of spin chains of different length. We consider the spin chains with $N = 3, 4$ and 5 particles and cover all possible combinations of the spin-up and spin-down internal states.

The Hamiltonian in Eq. (7.2) can be rewritten as

$$H_s = -\frac{1}{2}\sum_{j=1}^{N-1}\left[J_j(\sigma_x^j\sigma_x^{j+1} + \sigma_y^j\sigma_y^{j+1}) + J_j\left(1 - \frac{2}{\kappa}\right)\sigma_z^j\sigma_z^{j+1}\right] + h\sum_{j=1}^{N}\sigma_z^j. \tag{7.3}$$

We see that κ works as a control parameter for the $\sigma_z^j\sigma_z^{j+1}$ interaction. There are several special cases for κ: If $\kappa = 2$ only the $\sigma_x^j\sigma_x^{j+1}$ and $\sigma_y^j\sigma_y^{j+1}$ terms are left and the Hamiltonian describes the Heisenberg XX spin model. The $\kappa = 1$ and $\kappa \to \infty$ cases are equivalent up to the sign in front of $\sigma_z^j\sigma_z^{j+1}$ term and describe the XXX Hamiltonian. In the cold atoms realization the former case corresponds to strongly interacting bosons with independent on spin interaction, and the latter case describes fermions. Throughout these notes we postulate the symmetry of the interaction coefficients: $J_j = J_{N-j}$, that is achieved by the spatially symmetric trapping potentials in the cold atoms realization. Hence, we only need one coefficient J_1 in the 3-particle case, and two coefficients J_1 and J_2 for the 4- and 5-particles cases. Additionally, we only focus on the situ-

ation when the ratio $J_1/J_2 \ll 1$.

7.2 Conditional state transfer

Our aim is to construct a scheme which would allow us to control state transfer through a spin chain as follows: For given values of interaction coefficients $\{J_i\}$, where $i = 1, \ldots, \frac{N-1}{2}$ for the odd N and $i = 1, \ldots, \frac{N}{2}$ for the even N, the fidelity of state transfer through the spin chain with $N_\uparrow = 1$ and $N_\downarrow = N - 1$ particles approaches unity (*perfect* state transfer), and for the spin chain with $N_\uparrow > 1$ and $N_\downarrow = N - N_\downarrow$ the transfer is "blocked", i.e. the fidelity of the transfer is much smaller than 1 (ideally, approaches zero). The control over spin transfer is achieved by manipulating the external magnetic field and the number of spin-up and spin-down particles in the spin chain. In order to achieve perfect state transfer in a $N_\uparrow = 1$ and $N_\downarrow = N - 1$ spin chain we build an effective three-level system. This system consists of state $|in\rangle$, which corresponds to the initial state of the system, state $|out\rangle$, which corresponds to the state to be read out, and the intermediate $\left|transfer\right\rangle$ state. For the $N_\uparrow = 1$ and $N_\downarrow = N - 1$ spin chain, the initial state of the system is $|in\rangle = |\uparrow\downarrow\downarrow \ldots \downarrow\rangle$, and the final state of the chain is $|out\rangle = |\downarrow\downarrow\downarrow \ldots \uparrow\rangle$. Due to the strong interaction between particles in the middle, $J_1/J_2 \ll 1$, we prediagonalize the block in the Hamiltonian which corresponds to the states with a spin-up in the middle, $\{|\downarrow\uparrow\downarrow \ldots \downarrow\downarrow\downarrow\rangle, |\downarrow\downarrow\uparrow \ldots \downarrow\downarrow\downarrow\rangle, \ldots, |\downarrow\downarrow\downarrow \ldots \uparrow\downarrow\downarrow\rangle, |\downarrow\downarrow\downarrow \ldots \downarrow\uparrow\downarrow\rangle\}$. The obtained eigenvalues of the prediagonalized block are strongly split with the difference being proportional to J_2. The state $\left|transfer\right\rangle$ is selected from the set of the eigenstates of the prediagonalized block. The condition of perfect state transfer is the "resonance" between the expectation values of the states $|in\rangle$, $|out\rangle$ and $\left|transfer\right\rangle$. This resonance can be achieved via manipulation of magnetic field. Fig. 7.1 depicts the approach schematically. If for the same values of the parameters (interaction coefficients J_i and magnetic field h_j) state transfer is blocked for $N_\uparrow > 1$ and $N_\downarrow = N - N_\uparrow$ then the conditional transfer is achieved, hence state transfer is perfect for one spin configuration and blocked for others.

In order to achieve conditional spin transfer we build an effective three-

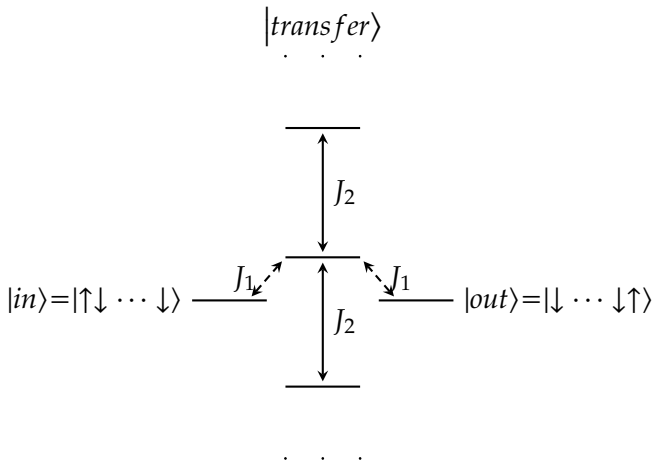

Figure 7.1: Schematic representation of spin states of the $N_\uparrow = 1$, $N_\downarrow > 1$ spin chain. Each level (horizontal line) depicts an expectation value of the Hamiltonian in one of the spin states. The solid vertical lines show gaps between levels. The dashed lines represent transitions between spin states.

level system. This system consists of state $|in\rangle$, which corresponds to the initial state of the system, state $|out\rangle$, which corresponds to the state to be read out, and the intermediate $|transfer\rangle$ state. The control over the spin transfer is achieved by manipulating magnetic field and the number of spin-up and spin-down particles in the spin chain. The idea is to determine parameters, so that for the $N_\uparrow = 1$ and $N_\downarrow = N - 1$ spin chain the initial state $|in\rangle = |\uparrow\downarrow\ldots\downarrow\rangle$ is evolved into $|out\rangle = |\downarrow\ldots\downarrow\uparrow\rangle$ with the fidelity, $F_{1,N-1} = \left|\langle\downarrow\ldots\downarrow\downarrow\uparrow| e^{-iH_s t} |\uparrow\downarrow\downarrow\ldots\downarrow\rangle\right|^2$, approaching unity. At the same time, for the spin chain $N_\uparrow > 1$ and $N_\downarrow > 1$ transfer should be blocked, meaning that the initial state does not change noticeably with time, i.e. $F_{N_\uparrow,N_\downarrow} = \left|\langle in| e^{-iH_s t} |in\rangle\right|^2 \to 1$. The schematic drawing for the $N_\uparrow = 1$, $N_\downarrow > 1$ spin chain is presented in Fig. 7.1. We utilize the fact that $J_1/J_2 \ll 1$, i.e. the particles at the edges of the chain are weakly coupled to the rest of the chain. The state $|transfer\rangle$ belongs to a set of the strongly coupled spin states. The off-diagonal matrix elements of the Hamiltonian for these states are proportional to J_2. Below we discuss this approach in more details and present the results for the special cases of $N = 3, 4$, and 5.

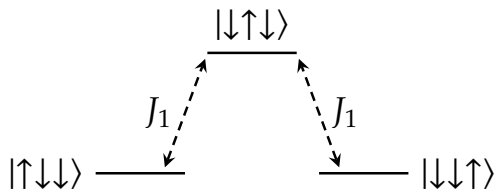

Figure 7.2: Schematic representation of the spin states for the $N_\uparrow = 1$, $N_\downarrow = 2$ spin chain. Each level (horizontal line) depicts to an expectation value of the Hamiltonian in one of the spin states. The solid vertical lines show gaps between levels. The dashed lines represent transitions between spin states.

7.3 $N = 3$ case

We start with the spin chain of one spin-up and two spin-down particles. Our goal is to transfer the initial state, $|\uparrow\downarrow\downarrow\rangle$, to the final state, $|\downarrow\downarrow\uparrow\rangle$, through the intermediate state, $|\downarrow\uparrow\downarrow\rangle$. In Fig. 7.2 we see the schematic diagram of the spin states. In the basis $\{\, |\uparrow\downarrow\downarrow\rangle, |\downarrow\uparrow\downarrow\rangle, |\downarrow\downarrow\uparrow\rangle \,\}$ the Hamiltonian can be written as the following matrix

$$H_s = \begin{pmatrix} -h & -J_1 & 0 \\ -J_1 & h + J_1(1 - \frac{2}{\kappa}) & -J_1 \\ 0 & -J_1 & -h \end{pmatrix}. \tag{7.4}$$

The eigenvalues of this Hamiltonian read

$$\lambda_1 = \frac{1}{2}J_1(1 - \frac{2}{\kappa}) - \sqrt{2J_1^2 + \left(h + \frac{1}{2}J_1\,(1 - 2/\kappa)\right)^2}, \tag{7.5a}$$

$$\lambda_2 = -h, \tag{7.5b}$$

$$\lambda_3 = \frac{1}{2}J_1(1 - \frac{2}{\kappa}) + \sqrt{2J_1^2 + \left(h + \frac{1}{2}J_1\,(1 - 2/\kappa)\right)^2}, \tag{7.5c}$$

and the corresponding non-normalized eigenvectors are

$$|\Psi_1\rangle = \{1, -\frac{1}{2J_1}\left[2h + J_1(1-\frac{2}{\kappa}) - \sqrt{2J_1^2 + \left(h + \frac{1}{2}J_1(1-2/\kappa)\right)^2}\right], 1\}, \tag{7.6a}$$

$$|\Psi_2\rangle = \{1, 0, -1\}, \tag{7.6b}$$

$$|\Psi_3\rangle = \{1, -\frac{1}{2J_1}\left[2h + J_1(1-\frac{2}{\kappa}) + \sqrt{2J_1^2 + \left(h + \frac{1}{2}J_1(1-2/\kappa)\right)^2}\right], 1\}. \tag{7.6c}$$

Let us start by looking at the conditions required to achieve perfect state transfer. We can expand the initial and final states in the basis of the eigenvectors from Eq. (7.6), i.e.,

$$|\uparrow\downarrow\downarrow\rangle = \sum_{k=1}^{N} a_k^{(1)} |\Psi_k\rangle, \tag{7.7a}$$

$$|\downarrow\downarrow\uparrow\rangle = \sum_{k=1}^{N} a_k^{(3)} |\Psi_k\rangle, \tag{7.7b}$$

where $a_k^{(i)}$ are the expansion coefficients, with index $i = 1, 2, 3$ denoting the expanded spin state. Since the Hamiltonian is a bisymmetric matrix the coefficients $a_k^{(1)}$ and $a_k^{(3)}$ are related as $a_k^{(1)} = (-1)^{k+1} a_k^{(3)}$ [Tao 2002, Nield 1994]. Then, applying the evolution operator $U(t) = e^{-iH_s t}$ to the initial state $|\downarrow\downarrow\uparrow\rangle = e^{-iH_s t_{out}} |\uparrow\downarrow\downarrow\rangle$ and expanding the spin states we obtain

$$\sum_{k=1}^{N} \left(e^{-i\lambda_k t_{out}} - (-1)^{k+1}\right) a_k^{(1)} |\Psi_k\rangle = 0. \tag{7.8}$$

To present our results we use the fidelity of transfer, F_{12}, which should approach unity for perfect state transfer. Then the conditions for perfect state transfer in this spin chain after the time interval t_{out} are

$$(\lambda_2 - \lambda_1) t_{out} = (2m_1 + 1)\pi, \tag{7.9a}$$

$$(\lambda_3 - \lambda_2) t_{out} = (2m_2 - 1)\pi. \tag{7.9b}$$

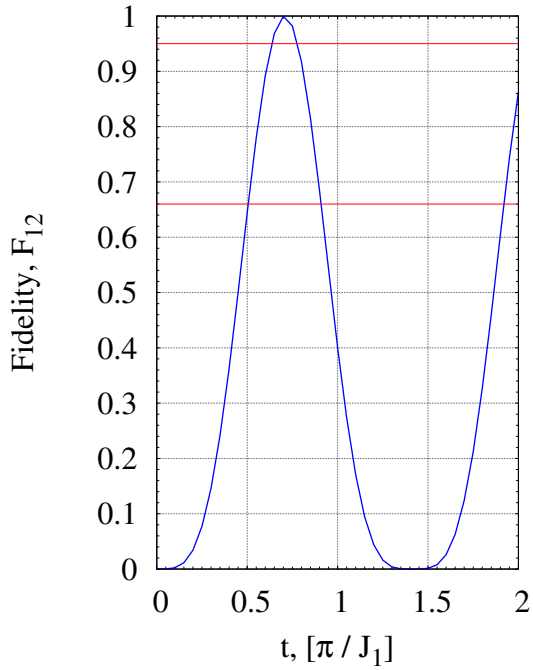

Figure 7.3: Fidelity of state transfer in the $N_\uparrow = 1$, $N_\downarrow = 2$ spin chain. The parameters are: $\kappa = 1$, $h = J_1/2$, $J_1 = 1$. The red horizontal lines correspond to values 0.66 and 0.95.

Here m_1 and m_2 are non-negative integers and, moreover, $m_2 > 0$, since we assume that $\lambda_1 < \lambda_2 < \lambda_3$. From these conditions we can find the value of magnetic field h for transfer to occur at minimal time, t_{min}. In this case $m_1 = 0$ and $m_2 = 1$ and we obtain

$$\frac{\lambda_2 - \lambda_1}{\lambda_3 - \lambda_2} = 1. \tag{7.10}$$

From this we find the magnetic field

$$h = -\frac{1}{2} J_1 \left(1 - \frac{2}{\kappa}\right). \tag{7.11}$$

For this value of h perfect transfer is achieved, as shown in Fig. 7.3 for $\kappa = 1$. The minimal time interval for state transfer is $t_{min} = \frac{\pi}{\lambda_2 - \lambda_1} = \frac{\pi}{\sqrt{2} J1}$.

If we now look back at the schematic picture, we notice that for magnetic

field $h = -\frac{1}{2}J_1(1 - \frac{2}{\kappa})$ the Hamiltonian expectation values of the initial, $|\uparrow\downarrow\downarrow\rangle$, and final, $|\downarrow\downarrow\uparrow\rangle$, states are equal to the expectation value of the intermediate state, $|\downarrow\uparrow\downarrow\rangle$. So perfect state transfer for the three-level system is achieved when the expectation values of the Hamiltonian are the same for $|in\rangle$, $|out\rangle$ and $\left|transfer\right\rangle$ states.

Now we consider the spin chain with $N_\uparrow = 2$ and $N_\downarrow = 1$. The idea is that, for the same value of the magnetic field, the Hamiltonian expectation values of the initial, $|\uparrow\uparrow\downarrow\rangle$, and final, $|\uparrow\downarrow\uparrow\rangle$, state will be out of resonance with the intermediate state and the state transfer will be blocked. However, this is only true if the transition matrix elements of the Hamiltonian are smaller than the energy gap between states, which is not the case for $N = 3$. In the figure 7.4 we show the "infidelity" of the initial state, $I_{21} = 1 - F_{21} = 1 - |\langle\uparrow\uparrow\downarrow| e^{-iH_s t} |\uparrow\uparrow\downarrow\rangle|^2$. This quantity shows how the initial state, $|\uparrow\uparrow\downarrow\rangle$, changes with time. In the case of blocked transfer, the infidelity should be close to zero during the time interval t_{min}, however, we see that the infidelity reaches 0.5, which means that the transfer is not blocked.

If we look again at the schematic picture we see that for the $N_\uparrow = 2$ and $N_\downarrow = 1$ configuration the energy gap between the non-interacting states is proportional to $J_1(1 - 2/\kappa)$ which is of the same order of magnitude as the transition matrix element. However, for $\kappa \to 0$ the energy gap approaches infinity and spin transfer is blocked. In this limit the $\sigma_z^j \sigma_z^{j+1}$ term exceeds all other terms in the Hamiltonian (7.3) and our Heisenberg model becomes the Ising model. Notice that for the same values of $\kappa \to 0$ and magnetic field $h = -\frac{J_1}{2}(1-2/\kappa)$ the fidelity of state transfer in the previously considered $N_\uparrow = 1$ and $N_\downarrow = 2$ spin chain still approaches unity after time interval t_{min}. To sum up, on the three-level system we see the main features of the conditional transfer idea. However, due to the strong interaction of the initial and final states with the intermediate state (which is of order J_1), the transfer for $N_\uparrow = 2$ and $N_\downarrow = 1$ is not fully blocked and the conditional transfer scheme doesn't work, except for the Ising model limit.

Below we show, that for the $N = 4$ and $N = 5$ cases it is possible to realize a quantum transistor scheme for any value of κ, except the very special $\kappa = 2$ case.

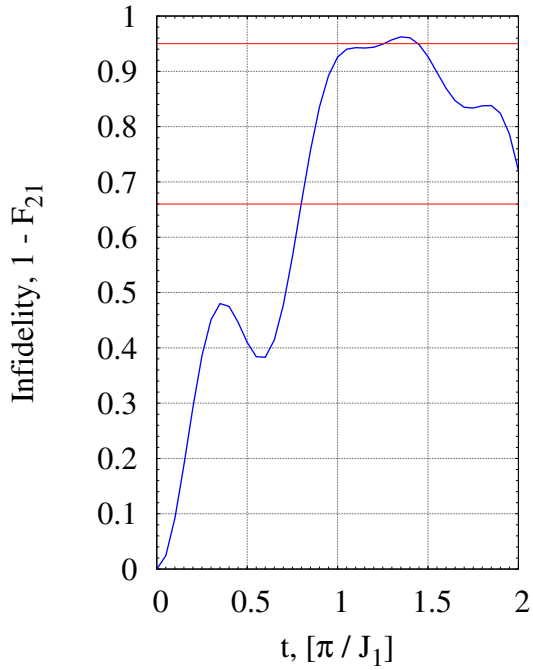

Figure 7.4: Infidelity, $1 - F$, of state transfer in the $N_\uparrow = 2$, $N_\downarrow = 1$ spin chain. The values of parameters are: $\kappa = 1$, $h = 1/2J_1$, $J_1 = 1$. The red horizontal lines correspond to values 0.66 and 0.95.

7.4 $N = 4$ case

We start our analysis with the $N_\uparrow = 1$ and $N_\downarrow = 3$ situation. The spin states basis is $\{|\uparrow\downarrow\downarrow\downarrow\rangle, |\downarrow\uparrow\downarrow\downarrow\rangle, |\downarrow\downarrow\uparrow\downarrow\rangle, |\downarrow\downarrow\downarrow\uparrow\rangle\}$. Our goal is to find such a value of the magnetic field that the fidelity of spin transfer will reach unity, i.e. $F_{13} \to 1$. In this system we have two different interaction coefficients, J_1 and J_2. The coefficient, J_1, defines the exchange interaction between sites 1 and 2 (or 3 and 4, by assumption) and the coefficient J_2 defines the interaction in the middle, between sites 2 and 3. The schematic figure of spin states is shown in Fig. 7.5. As was mentioned, we assume that $J_1/J_2 \ll 1$. The Hamiltonian for this system

is

$$H_s = \begin{pmatrix} -2h - \frac{1}{2}J_2(1-\frac{2}{\kappa}) & -J_1 & 0 & 0 \\ -J_1 & \frac{1}{2}J_2(1-\frac{2}{\kappa}) & -J_2 & 0 \\ 0 & -J_2 & \frac{1}{2}J_2(1-\frac{2}{\kappa}) & -J_1 \\ 0 & 0 & -J_1 & -2h - \frac{1}{2}J_2(1-\frac{2}{\kappa}) \end{pmatrix}. \tag{7.12}$$

The interaction between states $|\downarrow\uparrow\downarrow\downarrow\rangle$ and $|\downarrow\downarrow\uparrow\downarrow\rangle$ is the strongest in the system. To utilize this fact we pre-diagonalize the Hamiltonian. We find the eigenvalues and eigenvectors of the inner block $\begin{pmatrix} \frac{1}{2}J_2(1-\frac{2}{\kappa}) & -J_2 \\ -J_2 & \frac{1}{2}J_2(1-\frac{2}{\kappa}) \end{pmatrix}$. The eigenvalues of this matrix are $\lambda_+ = \frac{1}{2}J_2(1-\frac{2}{\kappa})-J_2$ and $\lambda_- = \frac{1}{2}J_2(1-\frac{2}{\kappa})+J_2$, and the eigenvectors are $|+\rangle = \frac{1}{\sqrt{2}}(|\uparrow\downarrow\rangle+|\downarrow\uparrow\rangle)$ and $|-\rangle = \frac{1}{\sqrt{2}}(|\uparrow\downarrow\rangle-|\downarrow\uparrow\rangle)$. Next, we choose a new basis to work with, $\left\{|\uparrow\downarrow\downarrow\downarrow\rangle, \frac{1}{\sqrt{2}}(|\downarrow\uparrow\downarrow\downarrow\rangle + |\downarrow\downarrow\uparrow\downarrow\rangle), \frac{1}{\sqrt{2}}(|\downarrow\uparrow\downarrow\downarrow\rangle - |\downarrow\downarrow\uparrow\downarrow\rangle), |\downarrow\downarrow\downarrow\uparrow\rangle\right\}$. We introduce a unitary transformation

$$O = \begin{pmatrix} 1 & 0 & 0 & 0 \\ 0 & \frac{1}{\sqrt{2}} & \frac{1}{\sqrt{2}} & 0 \\ 0 & \frac{1}{\sqrt{2}} & -\frac{1}{\sqrt{2}} & 0 \\ 0 & 0 & 0 & 1 \end{pmatrix}, \tag{7.13}$$

which we apply to the Hamiltonian from Eq. 7.12 and obtain

$$\widetilde{H} = \begin{pmatrix} -2h - \frac{1}{2}J_2(1-\frac{2}{\kappa}) & -\frac{1}{\sqrt{2}}J_1 & -\frac{1}{\sqrt{2}}J_1 & 0 \\ -\frac{1}{\sqrt{2}}J_1 & \lambda_+ & 0 & -\frac{1}{\sqrt{2}}J_1 \\ -\frac{1}{\sqrt{2}}J_1 & 0 & \lambda_- & \frac{1}{\sqrt{2}}J_1 \\ 0 & -\frac{1}{\sqrt{2}}J_1 & \frac{1}{\sqrt{2}}J_1 & -2h - \frac{1}{2}J_2(1-\frac{2}{\kappa}) \end{pmatrix}. \tag{7.14}$$

Now we can find the magnetic field needed to achieve perfect state transfer. We see that for small J_1 the Hamiltonian is almost diagonal. The eigenlevels of

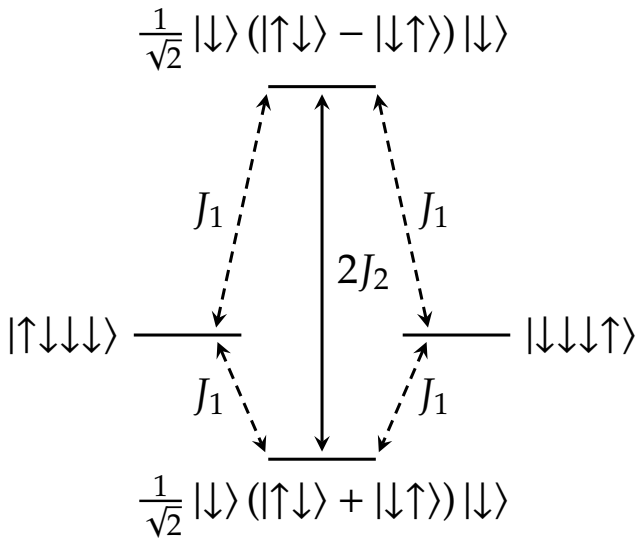

Figure 7.5: The schematic diagram of the spin states of the $N_\uparrow = 1$, $N_\downarrow = 3$ spin chain. The dashed lines represent transitions between states. The vertical solid line shows the width of the energy gap. Approximation $J_1/J_2 \ll 1$ is used. The value of magnetic field is arbitrary but such that the spin states are out of resonance. The condition for perfect state transfer is the resonance of the states $|\uparrow\downarrow\downarrow\downarrow\rangle$ and $|\downarrow\downarrow\downarrow\uparrow\rangle$ with the states $\frac{1}{\sqrt{2}}|\downarrow\rangle(|\uparrow\downarrow\rangle + |\downarrow\uparrow\rangle)|\downarrow\rangle$ or $\frac{1}{\sqrt{2}}|\downarrow\rangle(|\uparrow\downarrow\rangle - |\downarrow\uparrow\rangle)|\downarrow\rangle$
.

the Hamiltonian for $J_1 = 0$ are

$$\widetilde{\lambda}_1 = -\frac{1}{2}J_2\,(1 + 2/k)\,, \tag{7.15a}$$

$$\widetilde{\lambda}_2 = -\frac{1}{2}J_2\,(1 - 2/k) - 2h, \tag{7.15b}$$

$$\widetilde{\lambda}_3 = -\frac{1}{2}J_2\,(1 - 2/k) - 2h, \tag{7.15c}$$

$$\widetilde{\lambda}_4 = \frac{1}{2}J_2\,(3 - 2/k)\,. \tag{7.15d}$$

As we saw for the three-particle spin chain, perfect state transfer can be obtained if there are three levels in resonance to each other, i.e. either $\widetilde{\lambda}_1 = \widetilde{\lambda}_2 = \widetilde{\lambda}_3$ or $\widetilde{\lambda}_2 = \widetilde{\lambda}_3 = \widetilde{\lambda}_4$. There are two values of magnetic field to satisfy one of these conditions: $h_+ = \frac{1}{\kappa}J_2$ and $h_- = -J_2(1 - \frac{1}{\kappa})$. We see that for any value of κ it is possible to achieve perfect state transfer for this spin chain.

To show that perfect state transfer is indeed achieved we can use the same approach as we used in the three-spin case. The eigenvalues of the Hamiltonian are

$$\lambda_1 = -\frac{1}{2}J_2 - h - \sqrt{J_1^2 + \left(h - \frac{J_2}{\kappa}\right)^2}, \tag{7.16a}$$

$$\lambda_2 = \frac{1}{2}J_2 - h - \sqrt{J_1^2 + \left(h + J_2\left(1 - \frac{1}{\kappa}\right)\right)^2}, \tag{7.16b}$$

$$\lambda_3 = -\frac{1}{2}J_2 - h + \sqrt{J_1^2 + \left(h - \frac{J_2}{\kappa}\right)^2}, \tag{7.16c}$$

$$\lambda_4 = \frac{1}{2}J_2 - h + \sqrt{J_1^2 + \left(h + J_2\left(1 - \frac{1}{\kappa}\right)\right)^2}, \tag{7.16d}$$

and the corresponding non-normalized eigenvectors in the basis $\left\{|\uparrow\downarrow\downarrow\downarrow\rangle, |\downarrow\uparrow\downarrow\downarrow\rangle, |\downarrow\downarrow\uparrow\downarrow\rangle, |\downarrow\downarrow\downarrow\uparrow\rangle\right\}$ are

$$|\Psi_1\rangle = \left\{1, \frac{J_2 - h + \sqrt{J_1^2 + \left(h - \frac{J_2}{\kappa}\right)^2}}{J_1}, \frac{J_2 - h + \sqrt{J_1^2 + \left(h - \frac{J_2}{\kappa}\right)^2}}{J_1}, 1\right\}, \tag{7.17a}$$

$$|\Psi_2\rangle = \left\{1, \frac{J_1^2 + J_2\left(h + J_2(1 - \frac{1}{\kappa}) - \sqrt{J_1^2 + \left(h + J_2(1 - \frac{1}{\kappa})\right)^2}\right)}{J_1\left(h - \frac{J_2}{\kappa} + \sqrt{J_1^2 + \left(h + J_2(1 - \frac{1}{\kappa})\right)^2}\right)}, \right.$$
$$\left. \frac{h + J_2(1 - \frac{1}{\kappa}) - \sqrt{J_1^2 + \left(h + J_2(1 - \frac{1}{\kappa})\right)^2}}{J_1}, -1\right\}, \tag{7.17b}$$

$$|\Psi_3\rangle = \left\{1, \frac{J_2 - h - \sqrt{J_1^2 + \left(h - \frac{J_2}{\kappa}\right)^2}}{J_1}, \frac{J_2 - h - \sqrt{J_1^2 + \left(h - \frac{J_2}{\kappa}\right)^2}}{J_1}, 1\right\}, \tag{7.17c}$$

$$|\Psi_4\rangle = \left\{1, \frac{J_1^2 + J_2\left(h + J_2(1 - \frac{1}{\kappa}) + \sqrt{J_1^2 + \left(h + J_2(1 - \frac{1}{\kappa})\right)^2}\right)}{J_1\left(h - \frac{J_2}{\kappa} - \sqrt{J_1^2 + \left(h + J_2(1 - \frac{1}{\kappa})\right)^2}\right)}, \right.$$
$$\left. \frac{h + J_2(1 - \frac{1}{\kappa}) + \sqrt{J_1^2 + \left(h + J_2(1 - \frac{1}{\kappa})\right)^2}}{J_1}, -1\right\}. \tag{7.17d}$$

As before, we expand the initial and final states in the basis of eigenvectors of Hamiltonian (7.12):

$$|\uparrow\downarrow\downarrow\downarrow\rangle = \sum_{k=1}^{N} a_k^{(1)} |\Psi_k\rangle, \tag{7.18a}$$

$$|\downarrow\downarrow\downarrow\uparrow\rangle = \sum_{k=1}^{N} a_k^{(4)} |\Psi_k\rangle. \tag{7.18b}$$

Since the Hamiltonian is a bisymmetric matrix, the expansion coefficients $a_k^{(i)}$ are related as $a_1^{(1)} = a_1^{(4)}$, $a_2^{(1)} = -a_2^{(4)}$, $a_3^{(1)} = a_3^{(4)}$, $a_4^{(1)} = -a_4^{(4)}$Hence, the necessary

and sufficient conditions for state $|\uparrow\downarrow\downarrow\downarrow\rangle$ to evolve into state $|\downarrow\downarrow\downarrow\uparrow\rangle$ are

$$(\lambda_{k+1} - \lambda_k)t_{out} = \pi(2m_k + 1), \tag{7.19}$$

where m_k is a positive integer and t_out is time necessary for transfer to complete. We can use the values of magnetic field found previously to determine the fastest transfer time, $t_{min} = \frac{\pi}{\Delta\lambda}$, where $\Delta\lambda$ is the difference between the equidistant levels. For $h_+ = \frac{J_2}{\kappa}$ we obtain

$$\lambda_2 - \lambda_1 = J_1 + J_2 - \sqrt{J_1^2 + J_2^2} \approx J_1, \tag{7.20a}$$

$$\lambda_3 - \lambda_2 = J_1 - J_2 + \sqrt{J_1^2 + J_2^2} \approx J_1, \tag{7.20b}$$

$$\lambda_4 - \lambda_3 = -J_1 + J_2 + \sqrt{J_1^2 + J_2^2} \approx 2J_2 - J_1. \tag{7.20c}$$

We see that if $J_1/J_2 \ll 1$ the lowest three eigenlevels of the system are distributed equidistantly, with the energy difference $\Delta\lambda = J_1$, and the highest level lies far away from the others. That's why we can expect the perfect transfer to be achieved after time $t_{min} = \frac{\pi}{J_1}$. Now, for $h_- = -J_2(1 - \frac{1}{\kappa})$, the eigenlevel differences are

$$\lambda_2 - \lambda_1 = J_1 + J_2 + \sqrt{J_1^2 + J_2^2} \approx 2J_2 - J_1 \tag{7.21a}$$

$$\lambda_3 - \lambda_2 = J_1 - J_2 + \sqrt{J_1^2 + J_2^2} \approx J_1 \tag{7.21b}$$

$$\lambda_4 - \lambda_3 = J_1 + J_2 - \sqrt{J_1^2 + J_2^2} \approx J_1 \tag{7.21c}$$

and we see that this case is similar to the previous one. The highest three levels are equidistantly distributed and the lowest level is located much lower than the other three.

Let us consider an example with particular values $\kappa = 1$ and $h_- = -J_2(1-\frac{1}{\kappa}) = 0$. In this case the normalized eigenstates obtained from Eqs. (7.17) are

$$|\Psi_1\rangle = \frac{1}{2\sqrt{J_1^2 + J_2^2 + J_2\sqrt{J_1^2 + J_2^2}}}\left\{J_1, J_2 + \sqrt{J_1^2 + J_2^2}, J_2 + \sqrt{J_1^2 + J_2^2}, J_1\right\}, \quad (7.22a)$$

$$|\Psi_2\rangle = \frac{1}{2}\{1, 1, -1, -1\}, \quad (7.22b)$$

$$|\Psi_3\rangle = \frac{1}{2\sqrt{J_1^2 + J_2^2 - J_2\sqrt{J_1^2 + J_2^2}}}\left\{J_1, J_2 - \sqrt{J_1^2 + J_2^2}, J_2 - \sqrt{J_1^2 + J_2^2}, J_1\right\}, \quad (7.22c)$$

$$|\Psi_4\rangle = \frac{1}{2}\{1, -1, 1, -1\}, \quad (7.22d)$$

and the spin states expanded in this basis are

$$|\uparrow\downarrow\downarrow\downarrow\rangle = \frac{1}{2}\left\{\frac{J_1}{\sqrt{J_1^2 + J_2^2 + J_2\sqrt{J_1^2 + J_2^2}}}, 1, \frac{J_1}{\sqrt{J_1^2 + J_2^2 - J_2\sqrt{J_1^2 + J_2^2}}}, 1\right\}_\Psi, \quad (7.23a)$$

$$|\downarrow\uparrow\downarrow\downarrow\rangle = \frac{1}{2}\left\{\frac{J_2 + \sqrt{J_1^2 + J_2^2}}{\sqrt{J_1^2 + J_2^2 + J_2\sqrt{J_1^2 + J_2^2}}}, 1, \frac{J_2 - \sqrt{J_1^2 + J_2^2}}{\sqrt{J_1^2 + J_2^2 - J_2\sqrt{J_1^2 + J_2^2}}}, -1\right\}_\Psi, \quad (7.23b)$$

$$|\downarrow\downarrow\uparrow\downarrow\rangle = \frac{1}{2}\left\{\frac{J_2 + \sqrt{J_1^2 + J_2^2}}{\sqrt{J_1^2 + J_2^2 + J_2\sqrt{J_1^2 + J_2^2}}}, -1, \frac{J_2 - \sqrt{J_1^2 + J_2^2}}{\sqrt{J_1^2 + J_2^2 - J_2\sqrt{J_1^2 + J_2^2}}}, 1\right\}_\Psi, \quad (7.23c)$$

$$|\downarrow\downarrow\downarrow\uparrow\rangle = \frac{1}{2}\left\{\frac{J_1}{\sqrt{J_1^2 + J_2^2 + J_2\sqrt{J_1^2 + J_2^2}}}, -1, \frac{J_1}{\sqrt{J_1^2 + J_2^2 - J_2\sqrt{J_1^2 + J_2^2}}}, -1\right\}_\Psi. \quad (7.23d)$$

In the limit $J_1/J_2 \ll 1$ the expressions are simply

$$|\uparrow\downarrow\downarrow\downarrow\rangle \simeq \frac{1}{2}\left\{\frac{J_1}{\sqrt{2}J_2}, 1, \sqrt{2}, 1\right\}_\Psi, \tag{7.24a}$$

$$|\downarrow\uparrow\downarrow\downarrow\rangle \simeq \frac{1}{2}\left\{\sqrt{2}, 1, -\frac{J_1}{\sqrt{2}J_2}, -1\right\}_\Psi, \tag{7.24b}$$

$$|\downarrow\downarrow\uparrow\downarrow\rangle \simeq \frac{1}{2}\left\{\sqrt{2}, -1, -\frac{J_1}{\sqrt{2}J_2}, 1\right\}_\Psi, \tag{7.24c}$$

$$|\downarrow\downarrow\downarrow\uparrow\rangle \simeq \frac{1}{2}\left\{\frac{J_1}{\sqrt{2}J_2}, -1, \sqrt{2}, -1\right\}_\Psi. \tag{7.24d}$$

We see that for all spin states one of the coefficients of the expansion in the basis of eigenlevels is much smaller than all the others. Hence, it is fair to say that our system is effectively a three-level system.

In figure 7.6 we show the fidelity of state transfer for the both cases, since the results are completely identical. As for the $N_\uparrow = 1$, $N_\downarrow = 2$ spin chain we use $\kappa = 1$ for the figures. However, we had just proven that the values of magnetic field, obtained from the schematic picture, allow for perfect state transfer in the four-spin chain for any value of κ.

Now we continue to the $N_\uparrow = 2$, $N_\downarrow = 2$ case. The schematic diagram showing the spin states of the spin chain can be seen in Fig. 7.7. As we said before the spin in the middle works as a control parameter for state transfer. We start with initializing the spin chain with a spin-up in the middle (on the sites 2 and 3). By assumption, the exchange interaction between those two sites is the strongest in the system. The spin-up can be in one of the two states, $\frac{1}{\sqrt{2}}(|\uparrow\downarrow\rangle + |\downarrow\uparrow\rangle)$ or $\frac{1}{\sqrt{2}}(|\uparrow\downarrow\rangle - |\downarrow\uparrow\rangle)$. Then, to show that state transfer is blocked we set a spin-up on the site 1, so that the spin chain can be initialized in one of the two states, $|in+\rangle = \frac{1}{\sqrt{2}}|\uparrow\rangle(|\uparrow\downarrow\rangle + |\downarrow\uparrow\rangle)|\downarrow\rangle$ or $|in-\rangle = \frac{1}{\sqrt{2}}|\uparrow\rangle(|\uparrow\downarrow\rangle - |\downarrow\uparrow\rangle)|\downarrow\rangle$. We assume that for state state transfer to be successful the final states should be $|out+\rangle = \frac{1}{\sqrt{2}}|\downarrow\rangle(|\uparrow\downarrow\rangle + |\downarrow\uparrow\rangle)|\uparrow\rangle$ and $|out-\rangle = \frac{1}{\sqrt{2}}|\downarrow\rangle(|\uparrow\downarrow\rangle - |\downarrow\uparrow\rangle)|\uparrow\rangle$. These are the states with a spin-up on the site 4 and with the spin-up still located in the middle. The two intermediate states are: $|mid_1\rangle = |\uparrow\downarrow\downarrow\uparrow\rangle$ and $|mid_2\rangle = |\downarrow\uparrow\uparrow\downarrow\rangle$. In order for conditional transfer to work we need for the intermediate states to be out of the resonance with the initial and final states

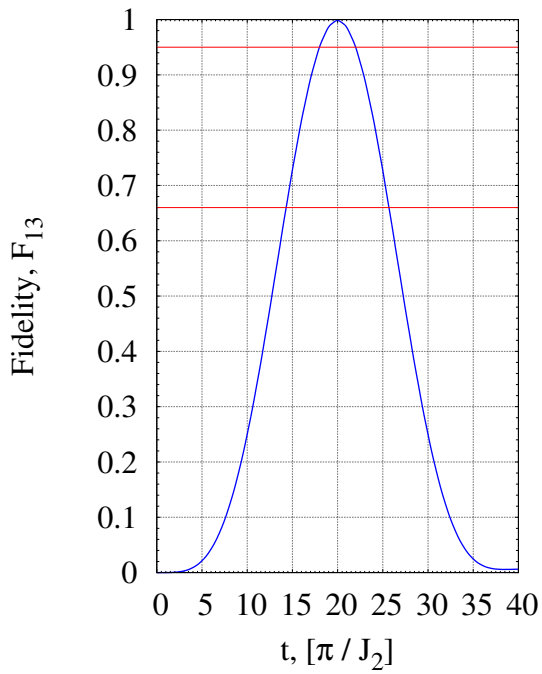

Figure 7.6: Fidelity of state transfer in the $N_\uparrow = 1$, $N_\downarrow = 3$ spin chain. The values of parameters are: $\kappa = 1$, $J_1 = 1$, $J_2 = 20$, $h = 0$ and $h = J_2$. Two curves for different values of h coincide (see the text). The red horizontal lines correspond to values 0.66 and 0.95.

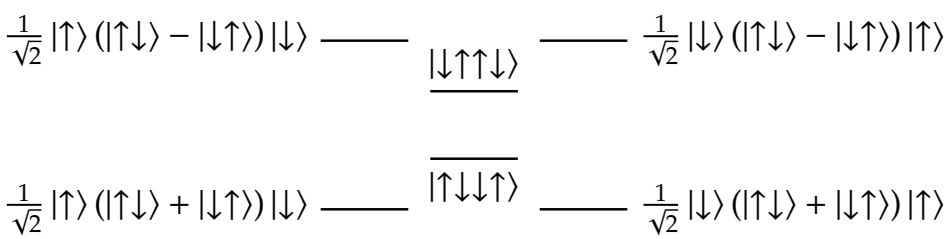

Figure 7.7: Schematic representation of diagonal elements of the prediagonalized Hamiltonian of the $N_\uparrow = 2$ and $N_\downarrow = 2$ spin chain. The left-hand side two levels represent the initial states, the right-hand side states represent the final states and the state in the middle correspond to state through which state transfer is realized.

for the values of the magnetic field for which perfect transfer is obtained in the $N_\uparrow = 1$, $N_\downarrow = 3$ spin chain. The Hamiltonian for the $N_\uparrow = 2$, $N_\downarrow = 2$ in the $\{|\uparrow\uparrow\downarrow\downarrow\rangle, |\uparrow\downarrow\uparrow\downarrow\rangle, |\uparrow\downarrow\downarrow\uparrow\rangle, |\downarrow\uparrow\uparrow\downarrow\rangle, |\downarrow\uparrow\downarrow\uparrow\rangle, |\downarrow\downarrow\uparrow\uparrow\rangle\}$ basis is

$$H_s = \begin{pmatrix} (-J_1' + \frac{1}{2}J_2') & -J_2 & 0 & 0 & 0 & 0 \\ -J_2 & (J_1' + \frac{1}{2}J_2') & -J_1 & -J_1 & 0 & 0 \\ 0 & -J_1 & (J_1' - \frac{1}{2}J_2') - 2h & 0 & -J_1 & 0 \\ 0 & -J_1 & 0 & (J_1' - \frac{1}{2}J_2') + 2h & -J_1 & 0 \\ 0 & 0 & -J_1 & -J_1 & (J_1' + \frac{1}{2}J_2') & -J_2 \\ 0 & 0 & 0 & 0 & -J_2 & (-J_1' + \frac{1}{2}J_2') \end{pmatrix}, \tag{7.25}$$

where we use shorthand $J_1' = J_1(1 - \frac{2}{\kappa})$ and $J_2' = J_2(1 - \frac{2}{\kappa})$. We now again prediagonalize the Hamiltonian and change the basis from $\Big\{|\uparrow\uparrow\downarrow\downarrow\rangle, |\uparrow\downarrow\uparrow\downarrow\rangle, |\uparrow\downarrow\downarrow\uparrow\rangle, |\downarrow\uparrow\uparrow\downarrow\rangle, |\downarrow\uparrow\downarrow\uparrow\rangle, |\downarrow\downarrow\uparrow\uparrow\rangle\Big\}$ to $\{|in+\rangle, |in-\rangle, |mid_1\rangle, |mid_2\rangle, |out+\rangle, |out-\rangle\}$. It can be achieved with the unitary transformation

$$O = \begin{pmatrix} \frac{1}{\sqrt{2}} & \frac{1}{\sqrt{2}} & 0 & 0 & 0 & 0 \\ \frac{1}{\sqrt{2}} & -\frac{1}{\sqrt{2}} & 0 & 0 & 0 & 0 \\ 0 & 0 & 1 & 0 & 0 & 0 \\ 0 & 0 & 0 & 1 & 0 & 0 \\ 0 & 0 & 0 & 0 & \frac{1}{\sqrt{2}} & \frac{1}{\sqrt{2}} \\ 0 & 0 & 0 & 0 & \frac{1}{\sqrt{2}} & -\frac{1}{\sqrt{2}} \end{pmatrix}. \tag{7.26}$$

Then the Hamiltonian transforms into

$$H = \begin{pmatrix} -\frac{1}{2}J_2(1 + \frac{2}{\kappa}) & -J_1(1 - \frac{2}{\kappa}) & -\frac{1}{\sqrt{2}}J_1 & -\frac{1}{\sqrt{2}}J_1 & 0 & 0 \\ -J_1(1 - \frac{2}{\kappa}) & \frac{1}{2}J_2(3 - \frac{2}{\kappa}) & \frac{1}{\sqrt{2}}J_1 & \frac{1}{\sqrt{2}}J_1 & 0 & 0 \\ -\frac{1}{\sqrt{2}}J_1 & \frac{1}{\sqrt{2}}J_1 & (J_1 - \frac{1}{2}J_2)(1 - \frac{2}{\kappa}) - 2h & 0 & -J_1 & 0 \\ -\frac{1}{\sqrt{2}}J_1 & \frac{1}{\sqrt{2}}J_1 & 0 & (J_1 - \frac{1}{2}J_2)(1 - \frac{2}{\kappa}) + 2h & -J_1 & 0 \\ 0 & 0 & -\frac{1}{\sqrt{2}}J_1 & -\frac{1}{\sqrt{2}}J_1 & \frac{1}{2}J_2(1 + \frac{2}{\kappa}) & J_1(1 - \frac{2}{\kappa}) \\ 0 & 0 & -\frac{1}{\sqrt{2}}J_1 & -\frac{1}{\sqrt{2}}J_1 & J_1(1 - \frac{2}{\kappa}) & \frac{1}{2}J_2(3 - \frac{2}{\kappa}) \end{pmatrix}. \tag{7.27}$$

As in the $N_\uparrow = 1$, $N_\downarrow = 3$ case, for zero J_1 the Hamiltonian is diagonal. The eigenvalues of the Hamiltonian in this case are shown in Tab. 7.1. We see that the values $\lambda^{in+} = \lambda^{out+}$ and $\lambda^{in-} = \lambda^{out-}$. For perfect state transfer to be blocked we need our initial state not to be in resonance with the states $|mid_1\rangle$

$\|in+\rangle$	$\lambda^{in+} = -\frac{J_2}{2}(1+\frac{2}{\kappa})$
$\|in-\rangle$	$\lambda^{in-} = \frac{J_2}{2}(3-\frac{2}{\kappa})$
$\|out+\rangle$	$\lambda^{out+} = -\frac{J_2}{2}(1+\frac{2}{\kappa})$
$\|out-\rangle$	$\lambda^{out-} = \frac{J_2}{2}(3-\frac{2}{\kappa})$
$\|mid_1\rangle$	$\lambda^{mid_1} = -2h - \frac{J_2}{2}(1-\frac{2}{\kappa})$
$\|mid_2\rangle$	$\lambda^{mid_2} = 2h - \frac{J_2}{2}(1-\frac{2}{\kappa})$

Table 7.1: The diagonal elements of the Hamiltonian in Eq. (7.27).

and $|mid_2\rangle$. Now let us see if it is possible for the values of magnetic field $h_+ = \frac{J_2}{\kappa}$ and $h_- = -J_2(1-\frac{1}{\kappa})$, for which perfect state transfer is achieved in the $N_\uparrow = 1$, $N_\downarrow = 3$ case. We see that for $h_+ = \frac{J_2}{\kappa}$ the expectation value $\lambda^{mid_1} = -\frac{J_2}{2}(1+\frac{2}{\kappa})$ and is equal to the energies $\lambda^{in+} = \lambda^{out+}$. That means that for this value of the magnetic field if we initialize the system in the state $|in+\rangle$ the transfer cannot be blocked, i.e. state $|in+\rangle$ leaks. However, if we initialize the system in the state $|in-\rangle$ then $\lambda^{in-} = \lambda^{out-} \neq \lambda^{mid_1}$ and $\lambda^{in-} = \lambda^{out-} \neq \lambda^{mid_2}$, so state transfer is blocked. In Fig. 7.8 we plot the "infidelities" of the initial states $|in+\rangle$ and $|in-\rangle$, i.e. the values $1 - F_{22}^{+/-} = 1 - \frac{1}{2}\langle\downarrow|(\langle\uparrow\downarrow| \pm \langle\downarrow\uparrow|)\langle\uparrow|e^{-iHt}|\downarrow\rangle(|\uparrow\downarrow\rangle \pm |\downarrow\uparrow\rangle)|\uparrow\rangle$, which show how the state evolves with time. We see that indeed to block state transfer the $N_\uparrow = 2$, $N_\downarrow = 2$ system with magnetic field $h_+ = \frac{J_2}{\kappa}$ should be initialized in the state $|in+\rangle$. For the value of the magnetic field $h_- = -J_2(1-\frac{1}{\kappa})$ the situation is in a way reversed. Here $\lambda^{mid_2} = \frac{J_2}{2}(3-\frac{2}{\kappa})$ is equal to λ^{in-} and λ^{out-}. So if we initialize the spin chain in the state $|in-\rangle$ the spin transfer is blocked and the conditional transfer is achieved. We present the corresponding result in Fig. 7.9 for $\kappa = 1$ and interaction coefficients $J_1/J_2 = \frac{1}{20}$.

7.4.1 The Heisenberg XX spin model, $\kappa = 2$

Let us consider the special case of $\kappa = 2$ in the four-spin chain. In the $N_\uparrow = 1$, $N_\downarrow = 3$ case the values of magnetic field to achieve the perfect spin transfer are $h_+ = \frac{J_2}{2}$ and $h_- = -\frac{J_2}{2}$. So, for this set-up the $\kappa = 2$ case does not differ much from the arbitrary κ case. However, if we look at the $N_\uparrow = 2$, $N_\downarrow = 2$ spin chain we notice that there always are energy levels in resonance which means that the spin transfer cannot be blocked. Let us look at the energies from table 7.1

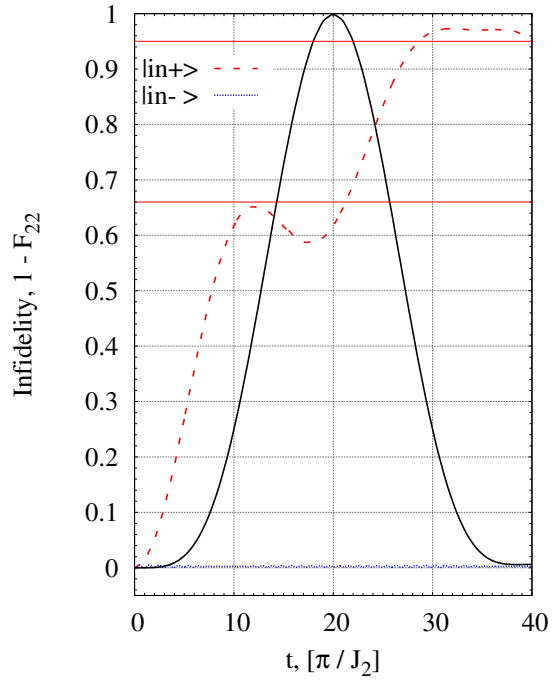

Figure 7.8: Infidelity of state transfer in the $N_\uparrow = 2$, $N_\downarrow = 2$ spin chain. The values of parameters are: $\kappa = 1$, $J_1 = 1$, $J_2 = 20$, $h = h_+ = J_2/\kappa = J_2$. The bold red curve corresponds to the transfer of the state $|in+\rangle$ and the blue curve corresponds to the transfer of the state $|in-\rangle$. The black curve shows the fidelity of state transfer in the $N_\uparrow = 1$, $N_\downarrow = 3$ spin chain for comparison. The red horizontal lines correspond to values 0.66 and 0.95.

for the case of $\kappa = 2$. Indeed the states $|mid_1\rangle$ and $|mid_2\rangle$ have the same energy with the *in* and *out* states for both values of the magnetic field. This means that whichever state we initialize our system in, we will always see the leakage of the initial state. In Fig. 7.10 we see that infidelities in the $N_\uparrow = 2$, $N_\downarrow = 2$ spin chain coincide, which proves that state transfer cannot be blocked in this case.

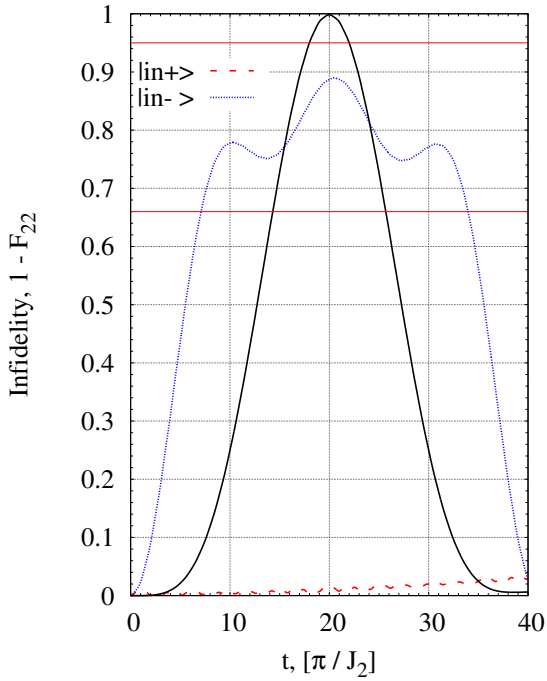

Figure 7.9: Infidelity of state transfer in the $N_\uparrow = 2$, $N_\downarrow = 2$ spin chain. The values of parameters are: $\kappa = 1$, $J_1 = 1$, $J_2 = 20$, $h = h_- = -J_2(1 - 1/\kappa) = 0$. The bold red curve corresponds to the transfer of the state $|in+\rangle$ and the blue curve corresponds to the transfer of the state $|in-\rangle$. The black curve shows the fidelity of state transfer in the $N_\uparrow = 1$, $N_\downarrow = 3$ spin chain for comparison. The red horizontal lines correspond to values 0.66 and 0.95.

$\|in+\rangle$	$\lambda^{in+} = -J_2$
$\|in-\rangle$	$\lambda^{in-} = J_2$
$\|out+\rangle$	$\lambda^{out+} = -J_2$
$\|out-\rangle$	$\lambda^{out-} = J_2$
$\|mid_1\rangle$	$\lambda^{mid_1} = -2h$
$\|mid_2\rangle$	$\lambda^{mid_2} = 2h.$

Table 7.2: The diagonal elements of the Hamiltonian in Eq. (7.27) with $\kappa = 2$.

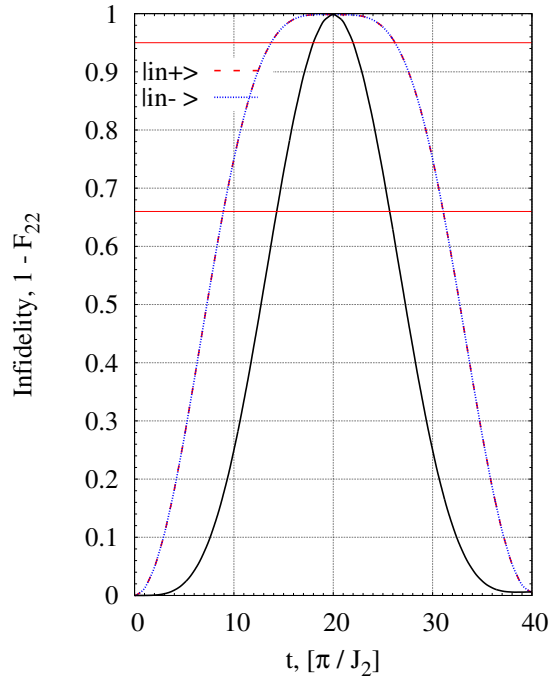

Figure 7.10: Infidelity of state transfer in the $N_\uparrow = 2$, $N_\downarrow = 2$ spin chain. The values of parameters are: $\kappa = 2$, $J_1 = 1$, $J_2 = 20$, $h_+ = J_2/2$. The value $h_- = -J_2/2$ gives identical results. The bold red curve corresponds to the transfer of the state $|in+\rangle$ and the blue curve corresponds to the transfer of the state $|in-\rangle$. As we see both curves coincide. The black curve shows the fidelity of state transfer in the $N_\uparrow = 1$, $N_\downarrow = 3$ spin chain for comparison. The red horizontal lines correspond to values 0.66 and 0.95.

7.5 $N = 5$ case

The five-spin chain does not differ much in principle from four-spin chain. So in the spirit of previous sections we start with looking for values of magnetic field, such that perfect state transfer is achieved in a $N_\uparrow = 1$, $N_\downarrow = 4$ spin chain. The spin states basis is $\{|\uparrow\downarrow\downarrow\downarrow\downarrow\rangle, |\downarrow\uparrow\downarrow\downarrow\downarrow\rangle, |\downarrow\downarrow\uparrow\downarrow\downarrow\rangle, |\downarrow\downarrow\downarrow\uparrow\downarrow\rangle, |\downarrow\downarrow\downarrow\downarrow\uparrow\rangle\}$. Our goal is to find such a value of the magnetic field in the middle that the fidelity of the spin transfer will reach unity, i.e. $F_{14} = \langle\downarrow\downarrow\downarrow\downarrow\uparrow| e^{-iH_s t} |\uparrow\downarrow\downarrow\downarrow\downarrow\rangle|^2 \to 1$. Since we postulate the symmetry of the confining potential, we have only two values of interaction coefficients: J_1 and J_2, with the same condition $J_1/J_2 \ll 1$. The

major difference between previous cases and five-spin chain is that magnetic field in the middle of the chain might not be the same on the different sites. In this section we use the following assumption for the value of magnetic field on site, h_i, where $i = 1, \ldots, 5$: $h_1 = h_5 = 0$, $h_2 = h_4 = h'$, and $h_3 = h$.

The Hamiltonian for this system is

$$H = \begin{pmatrix} -2h' - h - J_2(1-\frac{2}{\kappa}) & -J_1 & 0 & 0 & 0 \\ -J_1 & -h & -J_2 & 0 & 0 \\ 0 & -J_2 & h - 2h' + J_2(1-\frac{2}{\kappa}) - J_1(1-\frac{2}{\kappa}) & -J_2 & 0 \\ 0 & 0 & -J_2 & -h & -J_1 \\ 0 & 0 & 0 & -J_1 & -2h' - h - J_2(1-\frac{2}{\kappa}) \end{pmatrix}. \tag{7.28}$$

We see that the states $|\downarrow\uparrow\downarrow\downarrow\downarrow\rangle, |\downarrow\downarrow\uparrow\downarrow\downarrow\rangle, |\downarrow\downarrow\downarrow\uparrow\downarrow\rangle$ interact the strongest in the system and so we once again prediagonalize the Hamiltonian and switch to a new basis. To find the new basis we diagonalize the matrix

$$\begin{pmatrix} -h & -J_2 & 0 \\ -J_2 & h - 2h' + (J_2 - J_1)(1-\frac{2}{\kappa}) & -J_2 \\ 0 & -J_2 & -h \end{pmatrix}$$

and find its eigenvalues and eigenvectors. Introducing notation $\Delta = h' - \frac{1}{2}(J_2 - J_1)\left(1 - \frac{2}{\kappa}\right)$ we write eigenvalues as

$$\lambda_+ = -\Delta + \sqrt{2J_2^2 + (h-\Delta)^2}, \tag{7.29a}$$

$$\lambda_0 = -h, \tag{7.29b}$$

$$\lambda_- = -\Delta - \sqrt{2J_2^2 + (h-\Delta)^2}, \tag{7.29c}$$

and the corresponding non-normalized eigenvectors in the basis $\{|\uparrow\downarrow\downarrow\rangle, |\downarrow\uparrow\downarrow\rangle, |\downarrow\downarrow\uparrow\rangle\}$

are

$$|\Psi_+\rangle = \frac{1}{\sqrt{2J_2^2 + (h+\lambda_+)^2}}\{J_2, -(h+\lambda_+), J_2\}, \tag{7.30a}$$

$$|\Psi_0\rangle = \frac{1}{\sqrt{2}}\{1, 0, -1\}, \tag{7.30b}$$

$$|\Psi_-\rangle = \frac{1}{\sqrt{2J_2^2 + (h+\lambda_-)^2}}\{J_2, -(h+\lambda_-), J_2\}. \tag{7.30c}$$

Then we introduce a new basis $\{|\uparrow\downarrow\downarrow\downarrow\downarrow\rangle, |\downarrow\rangle|\Psi_+\rangle|\downarrow\rangle, |\downarrow\rangle|\Psi_0\rangle|\downarrow\rangle, |\downarrow\rangle|\Psi_-\rangle|\downarrow\rangle, |\downarrow\downarrow\downarrow\downarrow\uparrow\rangle\}$ and a uniform transformation

$$U = \begin{pmatrix} 1 & 0 & 0 & 0 & 0 \\ 0 & \frac{J_2}{\sqrt{2J_2^2+(h+\lambda_+)^2}} & -\frac{h+\lambda_+}{\sqrt{2J_2^2+(h+\lambda_+)^2}} & \frac{J_2}{\sqrt{2J_2^2+2(h+\lambda_+)^2}} & 0 \\ 0 & \frac{1}{\sqrt{2}} & 0 & -\frac{1}{\sqrt{2}} & 0 \\ 0 & \frac{J_2}{\sqrt{2J_2^2+(h+\lambda_-)^2}} & -\frac{h+\lambda_-}{\sqrt{2J_2^2+(h+\lambda_-)^2}} & \frac{J_2}{\sqrt{2J_2^2+2(h+\lambda_-)^2}} & 0 \\ 0 & 0 & 0 & 0 & 1 \end{pmatrix}. \tag{7.31}$$

As in previous cases the transformed Hamiltonian is diagonal in the approximation $J_1/J_2 \ll 1$

$$\widetilde{H} = \begin{pmatrix} -2h' - h - J_2(1-\frac{2}{\kappa}) & 0 & 0 & 0 & 0 \\ 0 & \lambda_+ & 0 & 0 & 0 \\ 0 & 0 & \lambda_0 & 0 & 0 \\ 0 & 0 & 0 & \lambda_- & 0 \\ 0 & 0 & 0 & 0 & -2h' - h - J_2(1-\frac{2}{\kappa}) \end{pmatrix}. \tag{7.32}$$

To achieve perfect state transfer we find the values of magnetic field so that one of the values λ_+, λ_- or λ_0 is equal to $-2h' - h - J_2(1-\frac{2}{\kappa})$. From condition $-2h' - h - J_2(1-\frac{2}{\kappa}) = \lambda_0$ we find that fidelity of state transfer approaches unity for $h' = -\frac{1}{2}J_2(1-\frac{2}{\kappa})$ and any value of magnetic field in the middle of the spin chain, h. In this case quantum state transfer goes via the state with energy λ_0.

The conditions $-2h' - h - J_2(1 - \frac{2}{\kappa}) = \lambda_\pm$ give the following expression

$$h' = \frac{J_2^2}{2(h + J_2(1 - \frac{2}{\kappa}))} - \frac{1}{2}J_2(1 - \frac{2}{\kappa}). \tag{7.33}$$

We see that the value h cannot be equal to $-J_2(1 - \frac{2}{\kappa})$ for the denominator goes to zero in this case. For this relation between the values of magnetic field quantum state transfer occurs through the states $\lambda_\pm$, depending on the value of the parameter κ. In Fig. 7.11 we plot fidelities of state transfer in the $N_\uparrow = 1$, $N_\downarrow = 4$ for different values of magnetic field, with $\kappa = 1$, $J_1 = 1$, and $J_2 = 20$. Here the *green* curve corresponds to the values $h = -J_2(1 - \frac{2}{\kappa})$ and $h' = -\frac{1}{2}J_2(1 - \frac{2}{\kappa})$, the *blue* curve corresponds to the values $h = 0$ and $h' = -\frac{1}{2}J_2(1 - \frac{2}{\kappa})$, and the *black* curve corresponds to to the values $h = -2J_2(1 - \frac{2}{\kappa})$ and $h' = -J_2\frac{(\kappa-1)^2+1}{\kappa-2}$. We see that the black curve does not reach the fidelity $F > 0.9$, when the green and blue ones do, with the green curve approaching unity. This is due to the interference between levels $\lambda_\pm$ and λ_0. In any case, we show that it is possible to achieve perfect state transfer with the initial state $|\uparrow\downarrow\downarrow\downarrow\downarrow\rangle$ propagating through the state $|\downarrow\rangle|\Psi_0\rangle|\downarrow\rangle$. In order to block quantum state transfer we apply the same idea as in the four-spin chain. However, in the five-spin case we have two spins as controls of the transfer. Let us begin with the $N_\uparrow = 2$, $N_\downarrow = 3$ spin chain. The spin states basis for this spin chain is: $\Big\{|\uparrow\uparrow\downarrow\downarrow\downarrow\rangle, |\uparrow\downarrow\uparrow\downarrow\downarrow\rangle, |\uparrow\downarrow\downarrow\uparrow\downarrow\rangle, |\uparrow\downarrow\downarrow\downarrow\uparrow\rangle, |\downarrow\uparrow\uparrow\downarrow\downarrow\rangle, |\downarrow\uparrow\downarrow\uparrow\downarrow\rangle, |\downarrow\uparrow\downarrow\downarrow\uparrow\rangle, |\downarrow\downarrow\uparrow\uparrow\downarrow\rangle, |\downarrow\downarrow\uparrow\downarrow\uparrow\rangle, |\downarrow\downarrow\downarrow\uparrow\uparrow\rangle\Big\}$. The Hamiltonian in this basis reads (we denote $J_1' \equiv J_1(1 - 2/\kappa)$ and $J_2' \equiv J_2(1 - 2/\kappa)$ for brevity)

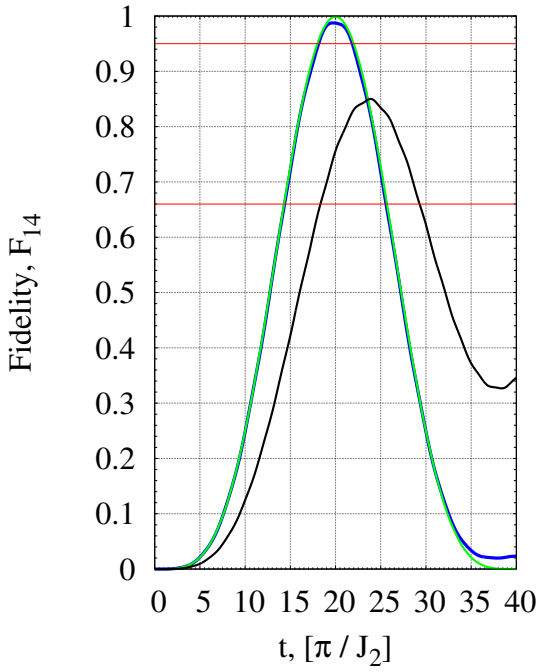

Figure 7.11: Fidelity of state transfer in the $N_\uparrow = 1$, $N_\downarrow = 4$ spin chain. The *green* curve corresponds to the values $h = -J_2(1 - \frac{2}{\kappa})$ and $h' = -\frac{1}{2}J_2(1 - \frac{2}{\kappa})$, the *blue* curve corresponds to the values $h = 0$ and $h' = -\frac{1}{2}J_2(1 - \frac{2}{\kappa})$, and the *black* curve corresponds to to the values $h = -2J_2(1 - \frac{2}{\kappa})$ and $h' = -J_2\frac{(\kappa-1)^2+1}{\kappa-2}$. For all curves $J_1 = 1$, $J_2 = 20$ and $\kappa = 1$. The red horizontal lines correspond to values 0.66 and 0.95.

$$H = \begin{pmatrix} -J_1' & -J_2 & 0 & 0 & 0 & 0 & 0 & 0 & 0 & 0 \\ -J_2 & 2h - 2h' - J_2' & -J_2 & 0 & -J_1 & 0 & 0 & 0 & 0 & 0 \\ 0 & -J_2 & J_1' & -J_1 & 0 & -J_1 & 0 & 0 & 0 & 0 \\ 0 & 0 & -J_1 & -2h' + J_1' - J_2' & 0 & 0 & -J_1 & 0 & 0 & 0 \\ 0 & -J_1 & 0 & 0 & 2h & -J_2 & 0 & 0 & 0 & 0 \\ 0 & 0 & -J_1 & 0 & -J_2 & 2h' + J_1' + J_2' & -J_1 & -J_2 & 0 & 0 \\ 0 & 0 & 0 & -J_1 & 0 & -J_1 & J_1' & 0 & -J_2 & 0 \\ 0 & 0 & 0 & 0 & 0 & -J_2 & 0 & 2h & -J_1 & 0 \\ 0 & 0 & 0 & 0 & 0 & 0 & -J_2 & -J_1 & 2h - 2h' + J_2' & -J_1 \\ 0 & 0 & 0 & 0 & 0 & 0 & 0 & 0 & -J_1 & -J_1' \end{pmatrix}, \tag{7.34}$$

where we subtracted h from the diagonal. As in previous cases we use exercise the ratio $J_1/J_2 \ll 1$ and introduce new basis:

$$|l_+\rangle = \frac{1}{\sqrt{2J_2^2 + (h+\lambda_+)^2}} |\uparrow\rangle \left[J_2 |\uparrow\downarrow\downarrow\rangle - (h+\lambda_+) |\downarrow\uparrow\downarrow\rangle + J_2 |\downarrow\downarrow\uparrow\rangle\right] |\downarrow\rangle\,, \tag{7.35a}$$

$$|l_0\rangle = \frac{1}{\sqrt{2}} |\uparrow\rangle \left[|\uparrow\downarrow\downarrow\rangle - |\downarrow\downarrow\uparrow\rangle\right] |\downarrow\rangle\,, \tag{7.35b}$$

$$|l_-\rangle = \frac{1}{\sqrt{2J_2^2 + (h+\lambda_-)^2}} |\uparrow\rangle \left[J_2 |\uparrow\downarrow\downarrow\rangle - (h+\lambda_-) |\downarrow\uparrow\downarrow\rangle + J_2 |\downarrow\downarrow\uparrow\rangle\right] |\downarrow\rangle\,, \tag{7.35c}$$

$$|r_+\rangle = \frac{1}{\sqrt{2J_2^2 + (h+\lambda_+)^2}} |\downarrow\rangle \left[J_2 |\uparrow\downarrow\downarrow\rangle - (h+\lambda_+) |\downarrow\uparrow\downarrow\rangle + J_2 |\downarrow\downarrow\uparrow\rangle\right] |\uparrow\rangle\,, \tag{7.35d}$$

$$|r_0\rangle = \frac{1}{\sqrt{2}} |\downarrow\rangle \left[|\uparrow\downarrow\downarrow\rangle - |\downarrow\downarrow\uparrow\rangle\right] |\uparrow\rangle\,, \tag{7.35e}$$

$$|r_-\rangle = \frac{1}{\sqrt{2J_2^2 + (h+\lambda_-)^2}} |\downarrow\rangle \left[J_2 |\uparrow\downarrow\downarrow\rangle - (h+\lambda_-) |\downarrow\uparrow\downarrow\rangle + J_2 |\downarrow\downarrow\uparrow\rangle\right] |\uparrow\rangle\,, \tag{7.35f}$$

$$|m_+\rangle = \frac{1}{\sqrt{2J_2^2 + (h+\lambda'_+)^2}} |\downarrow\rangle \left[J_2 |\uparrow\uparrow\downarrow\rangle - (h+\lambda'_+) |\uparrow\downarrow\uparrow\rangle + J_2 |\downarrow\uparrow\uparrow\rangle\right] |\downarrow\rangle\,, \tag{7.35g}$$

$$|m_0\rangle = \frac{1}{\sqrt{2}} |\downarrow\rangle \left[|\uparrow\uparrow\downarrow\rangle - |\downarrow\uparrow\uparrow\rangle\right] |\downarrow\rangle\,, \tag{7.35h}$$

$$|m_-\rangle = \frac{1}{\sqrt{2J_2^2 + (h+\lambda'_-)^2}} |\downarrow\rangle \left[J_2 |\uparrow\uparrow\downarrow\rangle - (h+\lambda'_-) |\uparrow\downarrow\uparrow\rangle + J_2 |\downarrow\uparrow\uparrow\rangle\right] |\downarrow\rangle\,, \tag{7.35i}$$

where

$$\lambda_+ = -h' + \frac{1}{2}J_2' + \sqrt{2J_2^2 + \left(h - h' + \frac{1}{2}J_2'\right)^2}, \tag{7.36a}$$

$$\lambda_- = -h' + \frac{1}{2}J_2' - \sqrt{2J_2^2 + \left(h - h' + \frac{1}{2}J_2'\right)^2}, \tag{7.36b}$$

$$\lambda_+' = h' + \frac{1}{2}J_2' + \sqrt{2J_2^2 + \left(h' - h - \frac{1}{2}J_2'\right)^2}, \tag{7.36c}$$

$$\lambda_-' = h' + \frac{1}{2}J_2' - \sqrt{2J_2^2 + \left(h - h' - \frac{1}{2}J_2'\right)^2}. \tag{7.36d}$$

As in the $N_\uparrow = 2$, $N_\downarrow = 2$ case there are several states we can initialize the spin chain in. They are the new basis states with one spin-up located in the middle (sites $2-3$) and the other spin-up located at the site 1 in accordance with our spin transistor idea. In Fig. (7.12) we show the infidelities of state transfer in the $N_\uparrow = 2$, $N_\downarrow = 3$ spin chain for all the initial states, $|l_0\rangle$ and $|l_\pm\rangle$ for the inhomogeneous magnetic field which allows perfect state transfer to be achieved in the $N_\uparrow = 1$, $N_\downarrow = 3$ spin chain. We choose the values $h = -J_2(1 - \frac{2}{\kappa})$ and $h' = -\frac{1}{2}J_2(1 - \frac{2}{\kappa})$ since as we saw the state transfer achieves the best fidelity values. We can clearly see that if the spin chain is initialized in the state $|l_0\rangle$ it is not being preserved with time. It signifies that state transfer is not blocked in this case and, hence, we cannot use the state $|l_0\rangle$ as an initial state of the $N_\uparrow = 2$, $N_\downarrow = 3$ spin chain for the quantum transistor idea to work. However, the two other states $|l_\pm\rangle$ are suitable for this goal. Fig. 7.12 shows that the infidelities of these states do not exceed 10% which means that if the spin chain is initialize in one of these two states then state transfer would be blocked. The small oscillations of the infidelities in Fig. 7.12 are due to interference between the states.

To summarize, from the $N_\uparrow = 2$, $N_\downarrow = 3$ spin chain we see that the quantum transistor concept can be also realized in a five-spin chain and in contrast with the $N_\uparrow = 2$, $N_\downarrow = 2$ spin chain we have two initial states to initialize our system in to block state transfer.

Let us consider now the $N_\uparrow = 3$, $N_\downarrow = 2$ spin chain, with two spin-up lo-

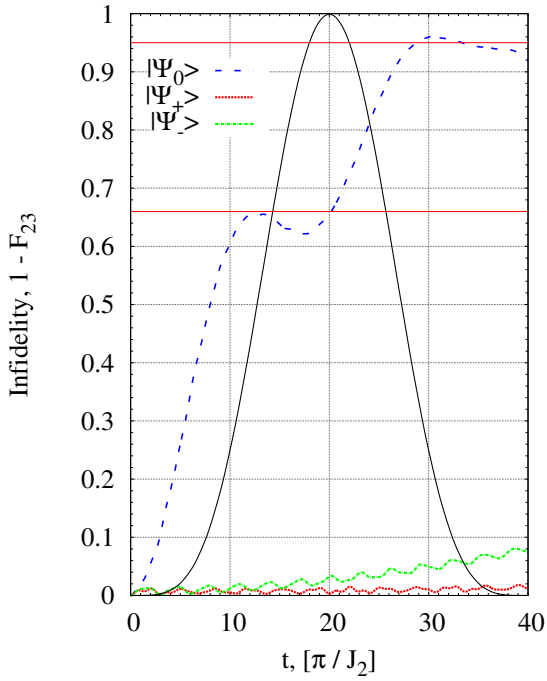

Figure 7.12: Fidelity of state transfer in the $N_\uparrow = 2$, $N_\downarrow = 3$ spin chain. The curves correspond to different initial states in the middle block (see the text): the *blue solid* curve corresponds to the state Ψ_0, the *red dashed* curve corresponds to the state Ψ_+ and the *green dashed and dotted* curve corresponds to to the state Ψ_-. For all curves $J_1 = 1$, $J_2 = 20$ and $\kappa = 1$.The values of magnetic field are $h = -J_2(1 - \frac{2}{\kappa}) = 20$ and $h' = -\frac{1}{2}J_2(1 - \frac{2}{\kappa}) = 10$. The red horizontal lines correspond to values 0.66 and 0.95.

cated in the middle. The spin states basis for this system is $\{|\uparrow\uparrow\uparrow\downarrow\downarrow\rangle, |\uparrow\uparrow\downarrow\uparrow\downarrow\rangle, |\uparrow\uparrow\downarrow\downarrow\uparrow\rangle, |\uparrow\downarrow\uparrow\uparrow\downarrow\rangle, |\uparrow\downarrow\uparrow\downarrow\uparrow\rangle, |\uparrow\downarrow\downarrow\uparrow\uparrow\rangle, |\downarrow\uparrow\uparrow\uparrow\downarrow\rangle, |\downarrow\uparrow\uparrow\downarrow\uparrow\rangle, |\downarrow\uparrow\downarrow\uparrow\uparrow\rangle, |\downarrow\downarrow\uparrow\uparrow\uparrow\rangle\}$. Then the Hamiltonian for this system differs from the Hamiltonian in Eq. (7.34) for the $N_\uparrow = 2$, $N_\downarrow = 3$ only by the opposite sign for the magnetic field values. We utilize the same approach as before and choose a new basis such that for $J_1 = 0$ the Hamiltonian is diagonal. As for the $N_\uparrow = 2$, $N_\downarrow = 3$ there are three states the system can be initialized in. In Fig. 7.13 we show the infidelities for all three states for $h = -J_2(1 - \frac{2}{\kappa})$ and $h' = -\frac{1}{2}J_2(1 - \frac{2}{\kappa})$ don't exceed 15%, i.e. all three initial states can be used to block state transfer in a $N_\uparrow = 3$, $N_\downarrow = 2$ spin chain. In general, the $N_\uparrow = 3$, $N_\downarrow = 2$ case is very similar to the $N_\uparrow = 2$, $N_\downarrow$ one.

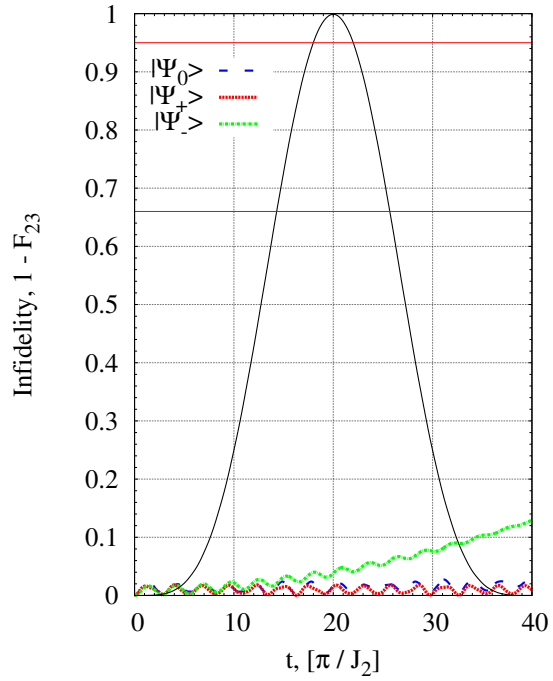

Figure 7.13: Fidelity of state transfer in the $N_\uparrow = 3$, $N_\downarrow = 2$ spin chain. The curves correspond to different initial states in the middle block (see the text): the *blue solid* curve corresponds to the state Ψ_0, the *red dashed* curve corresponds to the state Ψ_+ and the *green dashed and dotted* curve corresponds to to the state Ψ_-. For all curves $J_1 = 1$, $J_2 = 20$ and $\kappa = 1$.The values of magnetic field are $h = -J_2(1 - \frac{2}{\kappa}) = 20$ and $h' = -\frac{1}{2}J_2(1 - \frac{2}{\kappa}) = 10$. The red horizontal lines correspond to values 0.66 and 0.95.

However, it provides one more state to initialize the spin chain in and so can be used to control state transfer in a five-spin chain more easily, since there is no need to choose a specific state to initialize the system.

7.6 Realization in cold atoms set-ups

In this Section we present a confining 1D potential of a specific shape that allows one to obtain the exchange interaction coefficients J_j such that the ratio $J_1/J_2 \ll 1$ is fulfilled. As was mentioned in Chapter 6 the strongly-interacting two-component atoms in one-dimensional confinement can be mapped into

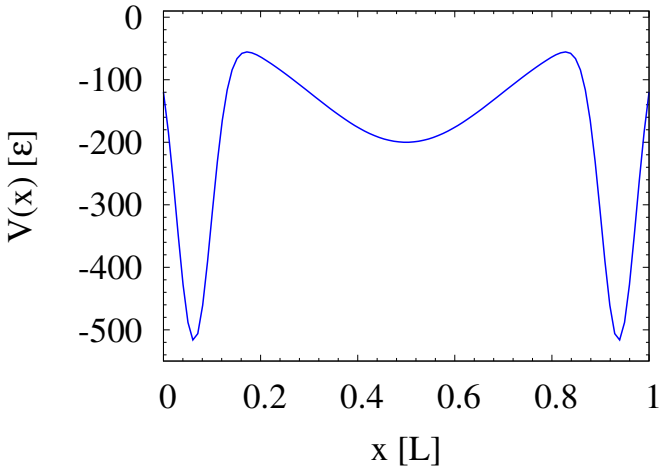

Figure 7.14: The shape of the potential $V(x)$ in Eq. (7.37). The values of parameters are $V_0 = 500$ and $U = 200$ in the units of energy.

the Heisenberg XXZ spin model. The exchange coefficients J_i are defined by the shape of the 1D potential which means that one can search for such a potential that the ratio $J_1/J_2 \ll 1$ is obtained.

In our calculations we used an external confinement – a box – in which the potential is located. Thus, the length of the box L is the natural unit in our calculations. We find that the exchange coefficients ratio J_1/J_2 can be realized via the potential $V(x)$ which reads

$$V(x) = -V_0 \exp\left(-A\,(x-x_0)^2\right) - U \exp\left(-B\,(x-x_1)^2\right) - V_0 \exp\left(-A\,(x-x_2)^2\right), \tag{7.37}$$

where V_0 and U are measured in the units of energy of the box, $\varepsilon = \frac{\hbar^2}{mL^2}$; the shifts in the Gaussians are $x_0 = \frac{L}{16}$, $x_1 = \frac{L}{2}$, $x_2 = \frac{15L}{16}$; and the constants $A = \frac{384}{L^2}$ and $B = \frac{64}{5L^2}$.

The shape of the potential for values $V_0 = 500$ and $U = 200$ is shown in the figure 7.14. The potential is a three-well potential with the wells on the edges being very deep compared to the well in the middle. In Fig. 7.15 we show the ratio of coefficients J_2/J_1 as function of the parameter U in the potential in Eq. (7.37). We see that the ratio reaches rather large values, for example

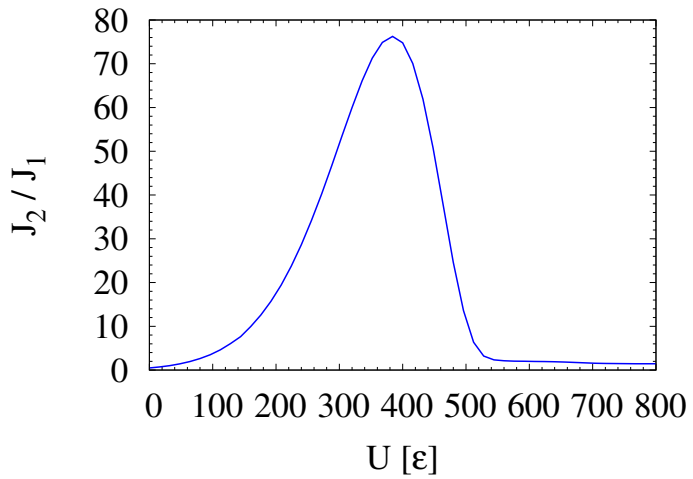

Figure 7.15: The interaction coefficients ratio J_2/J_1 as a function of the parameter U in the potential in Eq. (7.37).

$J_2/J_1 > 10$ for the values of U from 150 to 550. It means that the potential in Eq. (7.37) with these values of U can be used to realize conditional state transfer.

CHAPTER 8

Summary

This dissertation studied spin-1/2 particles in two different systems: 1) spin-orbit coupled particles in the harmonic trapping potential, 2) one-dimensional spin chains and state transfer therein. The first setup was analyzed in chapters 3, 4 and 5, and the second system was investigated in chapter 7.

First System

In chapter 3 we studied the single-particle energy levels of a spin-orbit coupled particle moving in a deformed harmonic potential. We saw that the resulting spectrum strongly depends on the interplay between the deformation of the trap, the strength of the spin-orbit coupling and the strength of the external magnetic field.

In chapter 4 we investigated the effects of the zero-range interparticle interaction for N-body systems trapped in a harmonic potential with spin-orbit coupling and external magnetic field. We implemented the Hartree-Fock method to include the interaction and witnessed that the Hartree-Fock single-particle energy levels are shifted compared to the energy levels in Chapter 3, but otherwise their behavior is very similar. We also showed that for not too large values of the interaction strength, the energy spectrum can be approximated very well with the help of perturbation theory.

In chapter 5 we implemented the so-called unfolding of the spectrum in order to investigate the quantum signatures of chaos. It is known that these signatures, in particular the nearest neighbor energy levels spacing following Wigner-Brody distribution, can emerge in spectra with avoided crossings and certain symmetries. The single-particle energy spectra we obtained in chapters 3-4 meet these conditions. Indeed, we showed that for specific values of

parameters the quantum signatures of chaos can be seen in both systems.

Second System

In chapter 7 investigated spin chains of 3, 4 and 5 particles and showed that for specific values of magnetic field applied to the middle of the chain perfect state transfer can be achieved. Moreover, we saw that in the $N_\uparrow = 2$, $N_\downarrow = 2$ spin chains state transfer can be blocked for the same values of magnetic field. The similar blocking cannot be realized in the three-spin chain, except for the Ising model limit, but can be implemented in the five-spin chain for both $N_\uparrow = 2$, $N_\downarrow = 3$ and $N_\uparrow = 3$, $N_\downarrow = 2$ configurations. All these results were obtained in the assumption that the values of the exchange coefficients J_i in the middle are much larger than on the edges, i.e. for the four-spin chain $J_1/J_2 \ll 1$, where we assume that $J_1 = J_3$.

Bibliography

[Abramowitz 1965] Milton Abramowitz and Irene A. Stegun, editeurs. Handbook of Mathematical Functions with Formulas, Graphs and Mathematical Tables. Dover Publications, Inc., New York, 1965.

[Aidelsburger 2011] M. Aidelsburger, M. Atala, S. Nascimbène, S. Trotzky, Y.-A. Chen and I. Bloch. *Experimental Realization of Strong Effective Magnetic Fields in an Optical Lattice*. Phys. Rev. Lett., vol. 107, page 255301, Dec 2011.

[Anderson 1995] M H Anderson, J R Ensher, M R Matthews, C E Wieman and E A Cornell. *Observation of bose-einstein condensation in a dilute atomic vapor.* Science, vol. 269, no. 5221, pages 198–201, July 1995.

[Bernevig 2013] B. Andrei Bernevig and Taylor L. Hughes. Topological Insulators and Topological Superconductors. Princeton University Press, 2013.

[Berry 1977] M. V. Berry and M. Tabor. *Level Clustering in the Regular Spectrum*. Proceedings of the Royal Society of London A: Mathematical, Physical and Engineering Sciences, vol. 356, no. 1686, pages 375–394, 1977.

[Blinov 2004] B B Blinov, D L Moehring, L-M Duan and C Monroe. *Observation of entanglement between a single trapped atom and a single photon.* Nature, vol. 428, no. 6979, pages 153–7, March 2004.

[Bloch 2008] Immanuel Bloch, Jean Dalibard and Wilhelm Zwerger. *Many-body physics with ultracold gases*. Reviews of Modern Physics, vol. 80, no. 3, pages 885–964, July 2008.

[Bloch 2012] Immanuel Bloch, Jean Dalibard and Sylvain Nascimbene. *Quantum simulations with ultracold quantum gases*. Nature Physics, vol. 8, no. 4, pages 267–276, April 2012.

[Bohigas 1984] O. Bohigas, M. J. Giannoni and C. Schmit. *Characterization of Chaotic Quantum Spectra and Universality of Level Fluctuation Laws*. Phys. Rev. Lett., vol. 52, pages 1–4, Jan 1984.

[Bose 2008] Sougato Bose. *Quantum Communication through Spin Chain Dynamics: an Introductory Overview*. Contemporary Physics, Volume 48, Issue 1 January 2007, pages 13 - 30, February 2008.

[BRACK 1972] M. BRACK, JENS DAMGAARD, A. S. JENSEN, H. C. PAULI, V. M. STRUTINSKY and C. Y. WONG. *Funny Hills: The Shell-Correction Approach to Nuclear Shell Effects and Its Applications to the Fission Process*. Rev. Mod. Phys., vol. 44, pages 320–405, Apr 1972.

[Bradley 1995] C.C. Bradley, C.A. Sackett, J.J. Tollett and R.G. Hulet. *Evidence of Bose-Einstein condensation in an atomic gas with attractive interactions*. Phys. Rev. Lett., vol. 75, no. 9, page 1687, August 1995.

[Brody 1981] T. A. Brody, J. Flores, J. B. French, P. A. Mello, A. Pandey and S. S. M. Wong. *Random-matrix physics: spectrum and strength fluctuations*. Rev. Mod. Phys., vol. 53, pages 385–479, Jul 1981.

[Bychkov 1984] Yu A Bychkov and E I Rashba. *Oscillatory effects and the magnetic susceptibility of carriers in inversion layers*. Journal of Physics C: Solid State Physics, vol. 17, no. 33, page 6039, 1984.

[Cheuk 2012] Lawrence W. Cheuk, Ariel T. Sommer, Zoran Hadzibabic, Tarik Yefsah, Waseem S. Bakr and Martin W. Zwierlein. *Spin-Injection Spectroscopy of a Spin-Orbit Coupled Fermi Gas*. Phys. Rev. Lett. 109, 095302 (2012), May 2012.

[Chin 2004] C. Chin, M. Bartenstein, A. Altmeyer, S. Riedl, S. Jochim, J. Hecker Denschlag and R. Grimm. *Observation of the Pairing Gap in a Strongly Interacting Fermi Gas*. Science, vol. 305, no. 5687, pages 1128–1130, 2004.

[Christandl 2004] Matthias Christandl, Nilanjana Datta, Artur Ekert and Andrew J. Landahl. *Perfect State Transfer in Quantum Spin Networks*. Phys. Rev. Lett., vol. 92, page 187902, May 2004.

[Cirac 1997] J. I. Cirac, P. Zoller, H. J. Kimble and H. Mabuchi. *Quantum State Transfer and Entanglement Distribution among Distant Nodes in a Quantum Network*. Phys. Rev. Lett., vol. 78, pages 3221–3224, Apr 1997.

[Dalibard 2011] Jean Dalibard, Fabrice Gerbier, Gediminas Juzeliunas and Patrik Öhberg. *Artificial gauge potentials for neutral atoms*. Rev. Mod. Phys. 83, 1523 (2011), September 2011.

[Davis 1995] K. B. Davis, M. O. Mewes, M. R. Andrews, N. J. van Druten, D. S. Durfee, D. M. Kurn and W. Ketterle. *Bose-Einstein Condensation in a Gas of Sodium Atoms*. Phys. Rev. Lett., vol. 75, no. 22, pages 3969–3973, November 1995.

[DeMarco 1999] B. DeMarco and D. S. Jin. *Onset of Fermi Degeneracy in a Trapped Atomic Gas*. Science, vol. 285, no. 5434, pages 1703–1706, 1999.

[Deuretzbacher 2014] F. Deuretzbacher, D. Becker, J. Bjerlin, S. M. Reimann and L. Santos. *Quantum magnetism without lattices in strongly interacting one-dimensional spinor gases*. Phys. Rev. A 90, 013611 (2014), July 2014.

[Dresselhaus 1955] G. Dresselhaus. *Spin-Orbit Coupling Effects in Zinc Blende Structures*. Phys. Rev., vol. 100, pages 580–586, Oct 1955.

[Duan 2001] L M Duan, M D Lukin, J I Cirac and P Zoller. *Long-distance quantum communication with atomic ensembles and linear optics.* Nature, vol. 414, no. 6862, pages 413–8, November 2001.

[Duan 2010] L.-M. Duan and C. Monroe. *Colloquium : Quantum networks with trapped ions*. Rev. Mod. Phys., vol. 82, pages 1209–1224, Apr 2010.

[Feynman 1982] Richard Phillips Feynman. *Simulating physics with computers*. International Journal of Theoretical Physics, vol. 21, no. 6, pages 467–488, June 1982.

[Fritz 2010] Haake Fritz. Quantum Signatures of Chaos. Springer, 2010.

[Galassi 2009] M. Galassi, J. Davies, J. Theiler, B. Gough, G. Jungman, P. Alken, M. Booth and F. Rossi. GNU Scientific Library Reference Manual. Network Theory Ltd., third édition, 2009.

[Galitski 2013] Victor Galitski and Ian B. Spielman. *Spin-orbit coupling in quantum gases*. Nature 494, 49-54 (2013), December 2013.

[Ghosh 2011] Sudeep Kumar Ghosh, Jayantha P. Vyasanakere and Vijay B. Shenoy. *Trapped fermions in a synthetic non-Abelian gauge field*. Physical Review A, 84, 053629 (2011), September 2011.

[Goldman 2014] N Goldman, G JuzeliÅ«nas, P Öhberg and I B Spielman. *Light-induced gauge fields for ultracold atoms.* Rep Prog Phys, vol. 77, no. 12, page 126401, December 2014.

[Greiner 2002] Markus Greiner, Olaf Mandel, Tilman Esslinger, Theodor W. Hansch and Immanuel Bloch. *Quantum phase transition from a superfluid to a Mott insulator in a gas of ultracold atoms*. Nature, vol. 415, no. 6867, pages 39–44, January 2002.

[Hasan 2010] M. Z. Hasan and C. L. Kane. *Topological Insulators*. Rev.Mod.Phys.82:3045,2010, November 2010.

[Hu 2012a] Hui Hu and Xia-Ji Liu. *Critical temperature of a Rashba spin-orbit coupled Bose gas in harmonic traps*. Phys. Rev. A 85, 013619 (2012), January 2012.

[Hu 2012b] Hui Hu, B. Ramachandhran, Han Pu and Xia-Ji Liu. *Spin-Orbit Coupled Weakly Interacting Bose-Einstein Condensates in Harmonic Traps*. Phys. Rev. Lett., vol. 108, page 010402, Jan 2012.

[Hu 2013] Haiping Hu and Shu Chen. *Mapping trapped atomic gas with spin-orbit coupling to quantum Rabi-like model*, February 2013.

[Huang 2015] Lianghui Huang, Zengming Meng, Pengjun Wang, Peng Peng, Shao-Liang Zhang, Liangchao Chen, Donghao Li, Qi Zhou and Jing Zhang. *Experimental realization of a two-dimensional synthetic spin-orbit coupling in ultracold Fermi gases*, June 2015.

[KAY 2010] ALASTAIR KAY. *PERFECT, EFFICIENT, STATE TRANSFER AND ITS APPLICATION AS A CONSTRUCTIVE TOOL*. International Journal of Quantum Information, vol. 08, no. 04, pages 641–676, 2010.

[Ketterle 2008] Wolfgang Ketterle and Martin W. Zwierlein. *Making, probing and understanding ultracold Fermi gases*. Nuovo Cimento Rivista, January 2008.

[Kinoshita 2004] Toshiya Kinoshita, Trevor Wenger and David S Weiss. *Observation of a one-dimensional Tonks-Girardeau gas.* Science, vol. 305, no. 5687, pages 1125–8, August 2004.

[Kinoshita 2006] Toshiya Kinoshita, Trevor Wenger and David S Weiss. *A quantum Newton's cradle.* Nature, vol. 440, no. 7086, pages 900–3, April 2006.

[Lambropoulos 2007] Peter Lambropoulos and David Petrosyan. Fundamentals of Quantum Optics and Quantum Information. Springer, 2007.

[Landau 1981] L. D. Landau and L. M. Lifshitz. Quantum Mechanics Non-Relativistic Theory, Third Edition: Volume 3. Butterworth-Heinemann, 3 édition, January 1981.

[Levinsen 2015] Jesper Levinsen, Pietro Massignan, Georg M. Bruun and Meera M. Parish. *Strong-coupling ansatz for the one-dimensional Fermi gas in a harmonic potential*. Science Advances 1, e1500197 (2015), July 2015.

[Lewenstein 2012] Maciej Lewenstein, Anna Sanpera and Verònica Ahufinger. Ultracold Atoms in Optical Lattices: Simulating Quantum Many-Body Systems. Oxford University Press, 2012.

[Lin 2011] Y-J Lin, K Jiménez-García and I B Spielman. *Spin-orbit-coupled Bose-Einstein condensates.* Nature, vol. 471, no. 7336, pages 83–6, March 2011.

[Liu 2014] Xiong-Jun Liu, K. T. Law and T. K. Ng. *Realization of 2D Spin-Orbit Interaction and Exotic Topological Orders in Cold Atoms*. Phys. Rev. Lett., vol. 112, page 086401, Feb 2014.

[Loft 2015] N. J. S. Loft, L. B. Kristensen, A. E. Thomsen and N. T. Zinner. *Comparing models for the ground state energy of a trapped one-dimensional Fermi gas with a single impurity*, August 2015.

[Marchukov 2013] O. V. Marchukov, A. G. Volosniev, D. V. Fedorov, A. S. Jensen and N. T. Zinner. *Spectral Gaps of Spin-orbit Coupled Particles in Deformed Traps*. J. Phys. B: At. Mol. Opt. Phys. 46 (2013) 134012, June 2013.

[Marchukov 2014a] O. V. Marchukov, A. G. Volosniev, D. V. Fedorov, A. S. Jensen and N. T. Zinner. *Statistical properties of spectra in harmonically trapped spin-orbit coupled systems*. J. Phys. B: At. Mol. Opt. Phys. 47 (2014) 195303, September 2014.

[Marchukov 2014b] Oleksandr V. Marchukov, Artem G. Volosniev, Dmitri V. Fedorov, Aksel S. Jensen and Nikolaj T. Zinner. *Spin-Orbit Coupling in Deformed Harmonic Traps*, January 2014.

[Marchukov 2015a] O. V. Marchukov, E. H. Eriksen, J. M. Midtgaard, A. A. S. Kalaee, D. V. Fedorov, A. S. Jensen and N. T. Zinner. *Computation of local exchange coefficients in strongly interacting one-dimensional few-body systems: local density approximation and exact results*, August 2015.

[Marchukov 2015b] O. V. Marchukov, D. V. Fedorov, A. S. Jensen, A. G. Volosniev and N. T. Zinner. *Repulsively interacting fermions in a two-dimensional deformed trap with spin-orbit coupling*. European Physical Journal D, 69, 73 (2015), March 2015.

[Moore 1998] G.E. Moore*et al.* *Cramming more components onto integrated circuits*. Proceedings of the IEEE, vol. 86, no. 1, pages 82–85, 1998.

[Moritz 2003] Henning Moritz, Thilo Stöferle, Michael Köhl and Tilman Esslinger. *Exciting collective oscillations in a trapped 1D gas.* Phys. Rev. Lett., vol. 91, no. 25, page 250402, December 2003.

[Murmann 2015a] Simon Murmann, Andrea Bergschneider, Vincent M. Klinkhamer, Gerhard Zürn, Thomas Lompe and Selim Jochim. *Two Fermions in a double well: Exploring a fundamental building block of the Hubbard model*. Phys. Rev. Lett. 114, 080402 (2015), February 2015.

[Murmann 2015b] Simon Murmann, Frank Deuretzbacher, Gerhard Zürn, Johannes Bjerlin, Stephanie M. Reimann, Luis Santos, Thomas Lompe and Selim Jochim. *Antiferromagnetic Heisenberg spin chain of few cold atoms in a one-dimensional trap*, July 2015.

[Nield 1994] D. A. Nield. *Odd-Even Factorization Results for Eigenvalue Problems.* SIAM Review, vol. 36, no. 4, pages 649–651, 1994.

[Olshanii 2001] Maxim Olshanii and Ludovic Pricoupenko. *Rigorous Approach to the Problem of Ultraviolet Divergencies in Dilute Bose Gases*. Phys. Rev. Lett., vol. 88, page 010402, Dec 2001.

[Paredes 2004] Belén Paredes, Artur Widera, Valentin Murg, Olaf Mandel, Simon Fölling, Ignacio Cirac, Gora V Shlyapnikov, Theodor W Hänsch and Immanuel Bloch. *Tonks-Girardeau gas of ultracold atoms in an optical lattice.* Nature, vol. 429, no. 6989, pages 277–81, May 2004.

[Rashba 1960] E. I. Rashba. *Properties of semiconductors with an extremum loop .1. Cyclotron and combinational resonance in a magnetic field perpendicular to the plane of the loop*. Sov. Phys. Solid. State, no. 2, page 1109, 1960.

[Reichl 2004] Linda Reichl. The Transition to Chaos: Conservative Classical Systems and Quantum Manifestations. Springer, second édition, 2004.

[Reimann 2002] S. M. Reimann and M. Manninen. *Electronic structure of quantum dots*. Rev. Mod. Phys., vol. 74, page 1238, 2002.

[Sakhr 2005] Jamal Sakhr and John M Nieminen. *Poisson-to-Wigner crossover transition in the nearest-neighbor statistics of random points on fractals.* Phys Rev E Stat Nonlin Soft Matter Phys, vol. 72, no. 4 Pt 2, page 045204, October 2005.

[Sakurai 1994] J. J. Sakurai. Modern Quantum Mechanics. Addison-Wesley, New York, Revised ed édition, 1994.

[Santos 2010] Lea F. Santos and Marcos Rigol. *Onset of quantum chaos in one-dimensional bosonic and fermionic systems and its relation to thermalization*. Phys. Rev. E 81, 036206 (2010), March 2010.

[Schreck 2001] F. Schreck, L. Khaykovich, K. L. Corwin, G. Ferrari, T. Bourdel, J. Cubizolles and C. Salomon. *A quasi-pure Bose-Einstein condensate immersed in a Fermi sea*. Phys. Rev. Lett. 87, 080403 (2001), July 2001.

[Siemens 1993] Philip J. Siemens and Aksel S. Jensen. Elements of Nuclei: Many-Body Physics with the Strong Interaction. Allan Wylde, 1993.

[Sinha 2011] Subhasis Sinha, Rejish Nath and Luis Santos. *Trapped two-dimensional condensates with synthetic spin-orbit coupling.* Phys. Rev. Lett., vol. 107, no. 27, page 270401, December 2011.

[Stöferle 2004] Thilo Stöferle, Henning Moritz, Christian Schori, Michael Köhl and Tilman Esslinger. *Transition from a strongly interacting 1D superfluid to a Mott insulator*. Phys. Rev. Lett. 92, 130403 (2004), April 2004.

[Stute 2013] A. Stute, B. Casabone, B. Brandstätter, K. Friebe, T. E. Northup and R. Blatt. *Quantum-state transfer from an ion to a photon*, January 2013.

[Tao 2002] David Tao and Mark Yasuda. *A Spectral Characterization of Generalized Real Symmetric Centrosymmetric and Generalized Real Symmetric Skew-Centrosymmetric Matrices.* SIAM J. Matrix Analysis Applications, vol. 23, no. 3, pages 885–895, 2002.

[Truscott 2001] Andrew G. Truscott, Kevin E. Strecker, William I. McAlexander, Guthrie B. Partridge and Randall G. Hulet. *Observation of Fermi Pressure in a Gas of Trapped Atoms*. Science, vol. 291, no. 5513, pages 2570–2572, March 2001.

[Valiente 2012] Manuel Valiente. *Tan's distributions and Fermi-Huang pseudopotential in momentum space*. Phys. Rev. A, vol. 85, page 014701, Jan 2012.

[Volosniev 2015a] A. G. Volosniev, D. V. Fedorov, A. S. Jensen, M. Valiente and N. T. Zinner. *Strongly interacting confined quantum systems in one dimension*. Nature Communications 5, 5300 (2014), May 2015.

[Volosniev 2015b] A. G. Volosniev, D. Petrosyan, M. Valiente, D. V. Fedorov, A. S. Jensen and N. T. Zinner. *Engineering the dynamics of effective spin-chain models for strongly interacting atomic gases*. Phys. Rev. A, vol. 91, page 023620, Feb 2015.

[Volosniev 2015c] Artem G. Volosniev, Dmitri V. Fedorov, Aksel S. Jensen, Nikolaj T. Zinner and Manuel Valiente. *Multicomponent Strongly Interacting Few-Fermion Systems in One Dimension*. Few-Body Systems, Volume 55, Issue 8-10, pp 839-842 2014, April 2015.

[Vyasanakere 2012] Jayantha P Vyasanakere and Vijay B Shenoy. *Rashbons: properties and their significance*. New Journal of Physics, vol. 14, no. 4, page 043041, 2012.

[Wang 2012] Pengjun Wang, Zeng-Qiang Yu, Zhengkun Fu, Jiao Miao, Lianghui Huang, Shijie Chai, Hui Zhai and Jing Zhang. *Spin-Orbit Coupled Degenerate Fermi Gases*. Phys. Rev. Lett., vol. 109, page 095301, Aug 2012.

[Weinberg 2013] Steven Weinberg. Lectures on Quantum Mechanics. Cambridge University Press, 2013.

[Winkler 2003] Roland Winkler. Spin–Orbit Coupling Effects in Two-Dimensional Electron and Hole Systems. Springer-Verlag, 2003.

[Zhai 2011] Hui Zhai. *Spin-Orbit Coupled Quantum Gases*. Int. J. Mod. Phys. B 26, 1230001 (2012), October 2011.

[Zhang 2012] Jin-Yi Zhang, Si-Cong Ji, Zhu Chen, Long Zhang, Zhi-Dong Du, Bo Yan, Ge-Sheng Pan, Bo Zhao, You-Jin Deng, Hui Zhai, Shuai Chen

and Jian-Wei Pan. *Collective Dipole Oscillations of a Spin-Orbit Coupled Bose-Einstein Condensate*. Phys. Rev. Lett., vol. 109, page 115301, Sep 2012.

[Zinner 2014] N. T. Zinner, A. G. Volosniev, D. V. Fedorov, A. S. Jensen and M. Valiente. *Fractional energy states of strongly-interacting bosons in one dimension*. EPL 107 (2014) 60003, September 2014.

[Zürn 2013a] G. Zürn, F. Serwane, T. Lompe, A. N. Wenz, M. G. Ries, J. E. Bohn and S. Jochim. *Fermionization of two distinguishable fermions*. Phys. Rev. Lett. 108, 075303 (2012), July 2013.

[Zürn 2013b] G. Zürn, A. N. Wenz, S. Murmann, A. Bergschneider, T. Lompe and S. Jochim. *Pairing in Few-Fermion Systems with Attractive Interactions*. Phys. Rev. Lett., vol. 111, page 175302, Oct 2013.

[Zwierlein 2005] M. W. Zwierlein, J. R. Abo-Shaeer, A. Schirotzek, C. H. Schunck and W. Ketterle. *Vortices and Superfluidity in a Strongly Interacting Fermi Gas*. Nature 435, 1047-1051 (2005), May 2005.